Title

STUDY OF OPTICAL PUMPING TRANSIENTS IN RUBIDIUM-87 AND APPLICATION TO DISORIENTATION CROSS SECTIONS

Author

Yellin, Joseph.

Publication Date

1965-07-09

UCRL-16241

University of California

Ernest O. Lawrence Radiation Laboratory

STUDY OF OPTICAL PUMPING TRANSIENTS IN RUBIDIUM-87 AND APPLICATION TO DISORIENTATION CROSS SECTIONS

Berkeley, California

DISCLAIMER

Research and Development

UCRL-16241

UNIVERSITY OF CALIFORNIA

Lawrence Radiation Laboratory
Berkeley, California

AEC Contract No. W-7405-eng-48

STUDY OF OPTICAL PUMPING TRANSIENTS IN RUBIDIUM-87 AND APPLICATION TO DISORIENTATION CROSS SECTIONS

Joseph Yellin

(Ph. D. Thesis)

July 9, 1965

STUDY OF OPTICAL PUMPING TRANSIENTS IN RUBIDIUM-87 AND APPLICATION TO DISORIENTATION CROSS SECTIONS

Contents

STUDY OF OPTICAL PUMPING TRANSIENTS IN RUBIDIUM-87 AND APPLICATION TO DISORIENTATION CROSS SECTIONS

Joseph Yellin

Lawrence Radiation Laboratory
University of California
Berkeley, California

July 9, 1965

ABSTRACT

The shapes of optical pumping transients in Rb^{87} with and without buffer gas have been studied in detail and shown to be expressible as a sum of two exponentials when the pumping occurs in the presence of a buffer gas and a single exponential when no buffer gas is present. These results are shown to agree with a phenomenological model of optical pumping for which a single relaxation time is assumed. It is shown that from a study of the transient structure of the optical pumping signal as a function of buffer-gas density, information can be obtained about the reorientation of a polarized rubidium atom as a result of buffer-gas collisions. From such a study an effective cross section, σ_{eff}, for disorientation of a polarized Rb^{87} atom in the excited state through collisions with He, Ne, and Ar has been determined. This effective cross section is related to the cross section for disorienting a polarized Rb^{87} atom in the $5^2P_{1/2}$ state, $\sigma_{1/2,\,1/2}$, and to the cross section for transfer of excitation of the Rb^{87} atom from the $5^2P_{1/2}$ state to the $5^2P_{3/2}$, $\sigma_{1/2,\,3/2}$, by $\sigma_{eff} = \sigma_{1/2,\,1/2} + \sigma_{1/2,\,3/2}$. Using recently measured values of $\sigma_{1/2,\,3/2}$ we have deduced $\sigma_{1/2,\,1/2}$. The cross sections are: $\sigma_{1/2,\,1/2}$(Rb-He) = $1.5(0.8)\times10^{-17}$ cm^2, $\sigma_{1/2,\,1/2}$(Rb-Ne) = $4.4(2.2)\times10^{-17}$ cm^2, and $\sigma_{1/2,\,1/2}$(Rb-Ar) = $2.5(1.8)\times10^{-16}$ cm^2.

It is also shown that a method due to Dehmelt may be used for the accurate determination of ground-state relaxation times, provided that the exponential components of the pumping transient are carefully separated. This method has been applied to the measurement of ground-state relaxation times for Rb^{87} and Cs. The experimental technique is particularly suitable for the measurements of short relaxation times ($\approx$ 1 msec). Cross sections for disorientation of the ground state of Rb^{87} and Cs ($^2S_{1/2}$) through collisions with Ne, Ar, Kr, and Xe have been determined from the relaxation times and the results are compared with independent measurements. The measured ground-state disorientation cross sections are: $\sigma(Rb^{87}\text{-Ne}) = 1.0(0.3)\times10^{-22}\,cm^2$, $\sigma(Rb^{87}\text{-Ar}) = 3.3(1.0)\times10^{-22}\,cm^2$, $\sigma(Rb^{87}\text{-Kr}) = 3.0(0.5)\times10^{-20}\,cm^2$, $\sigma(Rb^{87}\text{-Xe}) = 1.8(0.3)\times10^{-19}\,cm^2$, $\sigma(Cs\text{-Ar}) = 1.2(0.2)\times10^{-22}\,cm^2$, and $\sigma(Cs\text{-Kr}) = 1.9(0.2)\times10^{-20}\,cm^2$.

I. INTRODUCTION

The development of optical pumping techniques, particularly as applied to optical-double resonance, has spurred new interest in collision-induced relaxation of oriented excited states. This interest is partly because optical pumping techniques often necessitate the employment of a foreign gas (e.g., a buffer gas) whose role must be clearly understood for the proper interpretation of experimental results, and partly because optical orientation affords a new technique for studying disorienting collisions for which a good theoretical treatment appears to be lacking. The problem was treated by Bender[1] on the basis of a Van der Wall interaction and more recently by James Jordan,[2] who calculated the cross section for the process $Rb(P_{1/2}) \rightleftarrows Rb(P_{3/2})$ by assuming, in addition to the Van der Wall force, an interaction involving the quadrupole moment of the $P_{3/2}$ state, i.e., the matrix element $\langle P_{1/2}|Q|P_{3/2}\rangle$ where Q is the quadrupole moment of the $P_{3/2}$ state is considered. This model predicts cross sections several orders of magnitude larger than measured for Rb. Thus relaxation within an excited state by collisions is of interest for its own sake apart from its practical application.

Our purpose is to explore a new technique for the observation of collision-induced mixing in an excited state and to apply this method to the $5^2P_{1/2}$ state of Rb^{87}. The experimental techniques introduced are also suitable for the measurement of ground-state relaxation times, particularly short relaxation times such as those of alkalis diffusing in the heavy noble gases, krypton and xenon. There is presently disagreement among published values of ground-state disorientation cross sections for the alkalis. Therefore, our secondary objective is to remeasure the ground-state disorientation cross sections for Rb and Cs diffusing in the noble gases. The Franzen technique employed in many previous measurements has been limited by mechanical difficulties to relaxation times no shorter than about 10 msec, whereas relaxation times encountered for an alkali in krypton or xenon is of

the order of 1 msec. Our selection of Rb^{87} for the excited-state experiment was due to its low nuclear spin (which simplifies the analysis), as well as to the availability of Rb interference filters and a stable Rb resonance lamp. Similar considerations apply to the ground-state measurements.

The technique we used is discussed in detail in Sec. III, and is based on an analysis of the structure of the pumping transient signals. That is, when optical pumping is allowed to proceed, the transparency of the vapor pumped changes in a manner that depends on the degree of orientation of the $5^2P_{1/2}$ intermediate state as well as on the amount of ground-state orientation. Thus, if the light coming through the vapor is monitored, the effect of the excited-state orientation can be observed. The transient optical pumping signal is expressible as a sum of exponentials with simple decay constants if it is assumed that the ground-state relaxation process can be described by a spin relaxation time. Experimentally, one observes a signal which in general is a sum of only two exponentials, except in the extreme case of no buffer gas (no reorientation of the excited state) for which one exponential is observed. These experimental signals are in excellent agreement with the predicted signals when the finite resolution of the detection system is taken into account. By measuring the relative amplitudes of the exponentials or their decay rates as a function of buffer-gas pressure, one can get a measure of the degree of mixing in the excited state. Because the amplitude ratio is more sensitive to mixing in the excited state, our cross sections for disorienting the $5^2P_{1/2}$ state of Rb^{87} are based on a study of the relative abundance of the two exponentials that form the signal.

II. THEORY OF OPTICAL PUMPING TRANSIENTS

We propose to measure the cross section for disorienting an alkali atom in its excited state ($P_{1/2}$) through collision with a noble-gas atom by means of the effect which such collisions (alkali-noble gas) have on the pumping transients. It is necessary, therefore, to have some quantitative expression for the pumping transients. We begin with a simple, often quoted, example. For a review of the principles and techniques of optical pumping, see the review article by Skratskii and Izyumova.[3]

A. Two-Level System

Suppose an alkali with zero nuclear spin is irradiated with right circular polarized D_1 light ($nS_{1/2} \rightarrow nP_{1/2}$). Since the selection rule involved is $\Delta m = +1$, it is clear that transitions are induced only from the ground-state level $m = -1/2$ to the $m = +1/2$ level of the excited state. If, as is usual in optical pumping experiments, the emission line is much broader than the adsorption line so that we may assume the spectral density (light intensity per unit frequency interval) to be constant over the absorption line, the transition probability is proportional to the square of a Clebsch-Gordan coefficient, $C(\frac{1}{2}\ 1\ \frac{1}{2}\ ;\ -\frac{1}{2}\ 1\ \frac{1}{2})$.[4] The excited atom may decay to either the $m = -1/2$ or $m = +1/2$ level of the ground state with a probability proportional, respectively, to $\left|C(\frac{1}{2}\ 1\ \frac{1}{2};\ \frac{1}{2}\ -1\ -\frac{1}{2})\right|^2$ and $\left|C(\frac{1}{2}\ 1\ \frac{1}{2};\ \frac{1}{2}\ 0\ \frac{1}{2})\right|^2$. If A_{ij} is the rate at which an atom in ground-state level i is transferred to ground-state level j as a result of absorption and subsequent emission, a_{ik} is the rate of absorption from ground-state sublevel i to excited state sublevel k, and e_{kj} is the emission on probability, then[5]

$$A_{ij} = \sum_k a_{ik}\, e_{kj}\,.$$

For the case at hand $a_{ik} \propto \left|C(\frac{1}{2}\ 1\ \frac{1}{2}\ ;\ i\ u\ k)\right|^2$ with $i, k = \pm 1/2$, and $\mu = -1,\ 0,\ 1$ (vector transition). The actual transition rates are $a_{ik} = \sigma_0 I_0 \left|C(\frac{1}{2}\ 1\ \frac{1}{2};\ i\ \mu\ k)\right|^2$ for absorption and $e_{ik} = a_{ik}/\sigma_0 I_0$, where σ_0 is the cross section for light absorption at the center of the

emission line and I_0 is the photon flux at the center of the emission line (which we assume to be much broader than the absorption line). From Table II-1 we find $A_{-\frac{1}{2}\frac{1}{2}} = (2/3)\,\sigma_0 I_0$, $A_{-\frac{1}{2}-\frac{1}{2}} = A_{\frac{1}{2}-\frac{1}{2}} = 0$.

Table II-1. Transition probabilities for the two-level system.

	m	$-\frac{1}{2}$	$\frac{1}{2}$	m	$-\frac{1}{2}$	$\frac{1}{2}$
m	$-\frac{1}{2}$	1/3	2/3	$-\frac{1}{2}$	4/3	0
	$\frac{1}{2}$	2/3	1/3	$\frac{1}{2}$	2/3	0
		$a_{ik}/\sigma_0 I_0$			$A_{ik}/\sigma_0 I_0$ for $\Delta m = +1$	
					with $\sum_k A_{ik} = 2\sigma_0 I_0$	

Thus the rate at which the $m = -\frac{1}{2}$ level of the ground state is depleting is $A_{-\frac{1}{2}\frac{1}{2}} = 2/3\ \sigma_0 I_0$. We may then write $\frac{dn_{-1/2}}{dt} = -\frac{2}{3}\sigma_0 I_0 n_{-\frac{1}{2}}$ for the rate equation governing the density of the $m = -\frac{1}{2}$ ground-state level in the absence of other processes which compete with the light in establishing an equilibrium. But in fact, there are always present ground-state relaxation processes (collisions with walls and foreign gases, and spin exchange) which tend to restore the Boltzmann distribution among the atomic levels. It is found experimentally that these thermalizing collisions can be expressed by a relaxation time T_1 so that in the absence of the pumping light $\frac{dn_{-1/2}}{dt} = +\frac{1}{2T_1} n_{+1/2} - \frac{1}{2T_1} n_{-1/2} = \frac{1}{2T_1} n - \frac{1}{2T_1} n_{-1/2} - \frac{1}{2T_1} n_{-1/2} = -\frac{1}{T_1} n_{-1/2} + \frac{n}{2T_1}$ where $n = n_{-1/2} + n_{1/2}$. Combining the relaxation rate with the pumping rate we get $dn_{-1/2}/dt = -\frac{2}{3}\sigma_0 I n_{-1/2} - \frac{1}{T_1} n_{-1/2} + \frac{n}{2T_1}$. The solution to this equation is

$$n_{-\frac{1}{2}} = \frac{n}{2}\left(1 - \frac{1/T_1}{\frac{2}{3}\sigma_0 I_0 + \frac{1}{T_1}} \exp\left[-\left(\frac{2}{3}\sigma_0 I_0 + \frac{1}{T_1}\right)t\right]\right) + \frac{n}{2}\,\frac{1/T_1}{\frac{2}{3}\sigma_0 I_0 + \frac{1}{T_1}}, \qquad (1)$$

assuming $n_{-\frac{1}{2}}(0) = \frac{n}{2}$; this assumption is justified because the Zeeman splitting is very small compared with the thermal energy for the kind of fields employed (≈ 1 gauss). That is, $H\mu_0/kT << 1$ so that

$\frac{n_{-1/2}}{n_{+1/2}} = \exp(-2\mu_0 H/kT) \approx 1$. We can interpret $\frac{2}{3}\sigma_0 I_0$ as the reciprocal of the pumping speed of the light source, and write $n_{-\frac{1}{2}} = \frac{n}{2}\left(1 - \frac{1/T_1}{(1/\tau)+(1/T_1)}\right) \exp\left[-\left(\frac{1}{\tau} + \frac{1}{T_1}\right)t\right] + \frac{n}{2} \frac{1/T_1}{(1/\tau) + (1/T_1)}$ where $\tau^{-1} = \frac{2}{3}\sigma_0 I_0$. Implicit in this derivation is the assumption that the excited atom remains in the $m = +\frac{1}{2}$ sublevel until emission occurs. But this is not always a good assumption. In optical pumping experiments one often employs a noble gas to inhibit diffusion of the polarized atoms to the walls so as to increase the relaxation time T_1. The excited atom may then be perturbed by collisions with the noble-gas atoms so that transitions may be induced to the $m = +\frac{1}{2}$ level. We now consider the effect of such perturbations.

If the excited state is completely mixed, that is, if the excited atom may be found with equal probability in either of its sublevels prior to emission, then it is evident that emission will occur with equal probability to either of the ground-state sublevels. It then follows that

$$\frac{dn_{-1/2}}{dt} = -\left(\frac{1}{2}\sigma_0 I_0 + \frac{1}{T_1}\right) n_{-\frac{1}{2}} + \frac{n}{2T_1} \quad \text{and}$$

$$n_{-\frac{1}{2}} = \frac{n}{2}\left(1 - \frac{1/T_1}{\frac{1}{2}\sigma_0 I_0 + \frac{1}{T_1}}\right) \exp\left[\left(\frac{1}{2}\sigma_0 I_0 + \frac{1}{T_1}\right)\right] + \frac{n}{2} \frac{1/T_1}{\frac{1}{2}\sigma_0 I_0 + \frac{1}{T_1}} \qquad (2)$$

The difference between this result and the previous case is that here the pumping time is $\left(\frac{1}{2}\sigma_0 I_0\right)^{-1}$, whereas previously it was $\left(\frac{2}{3}\sigma_0 I_0\right)^{-1}$. Between these two extreme cases of complete mixing and no mixing in the excited state we expect to have for the pumping time τ

$$\left(\frac{2}{3}\sigma_0 I_0\right)^{-1} < \tau < \left(\frac{1}{2}\sigma_0 I_0\right)^{-1} .$$

Now let a be the probability that the excited state is mixed. We might then expect for the pumping rate $\frac{1}{\tau} = a\left(\frac{1}{2}\sigma_0 I_0\right) + (1-a)\left(\frac{2}{3}\sigma_0 I_0\right)$. Furthermore, we can relate a to the cross section for disorientation in the excited state, σ_{eff}, by $1 - a = \exp(-N\sigma_{eff}\bar{v}t)$, where N is the density of the buffer-gas atoms, $\bar{v}$ the mean relative velocity for

alkali-noble gas collisions, and t the lifetime of the excited state. Thus if we know the product $\sigma_0 I_0$ and the lifetime of the excited state t, we can obtain the cross section σ_{eff}. The relaxation time T_1 can be eliminated from the experimentally observed quantity, $\frac{1}{\tau} + \frac{1}{T_1} = \frac{1}{\tau_e}$ by measuring this quantity as a function of light intensity and extrapolating to zero light intensity. The intercept on the $1/\tau_e$ axis is T_1^{-1}. Other methods, such as Franzen's,[6] may also be employed to obtain T_1. We now consider the feasibility of such an experiment.

A little reflection shows that an experiment to measure α is (at best) marginal. This is evident when we note that

$$\frac{\frac{1}{\tau}(\text{no mixing}) - \frac{1}{\tau}(\text{complete mixing})}{\frac{1}{2}[\frac{1}{\tau}(\text{no mixing}) + \frac{1}{\tau}(\text{complete mixing})]} = \frac{\frac{2}{3} - \frac{1}{2}}{\frac{1}{2}(\frac{2}{3} + \frac{1}{2})} = \frac{\frac{1}{6}}{\frac{7}{12}} = \frac{2}{7}$$

or about 30%. From this follows that a measurement of α is very sensitive to errors in $1/\tau_e$ and $\sigma_0 I_0$. We see in Sec. IV that it is possible to measure $1/\tau_e$ to $\approx 1\%$, but measuring $\sigma_0 I_0$ to even 10% is difficult. Fortunately, the complications brought about by the existence of the nuclear spin are such as to make α more accessible to measurement. We shall see, for example, that the difference between the pumping rates for the two extreme cases considered in the last paragraph is three times as great for an alkali with nuclear spin $I = 3/2$.

The neglect of the nuclear spin in the above treatment has led to an oversimplification, that of having to consider only two levels in the ground state of the alkali, $^2S_{1/2}$, and in the resonance state, $^2P_{1/2}$. Actually the nuclear spin I has a profound effect on the optical properties of the atom. The reason for this is that the electronic angular momentum $\underset{\sim}{J}$ is coupled to the nuclear spin $\underset{\sim}{I}$ so that neither one is rigorously a good quantum number. It is therefore not possible to describe the optical properties of the atom strictly in terms of the electronic angular momentum states; instead, we have a new quantum number $\underset{\sim}{F} = \underset{\sim}{I} + \underset{\sim}{J}$. There are $2I + 1$ or $2J + 1$ F states according to whether $I < J$ or $I > J$, respectively, and for each F state there are $2F + 1$ Zeeman sublevels. Thus the ground state of a spin 3/2 alkali is split into two hyperfine levels, $F = 1$ and $F = 2$, with a total of

eight Zeeman sublevels. A similar result holds for the $^2P_{1/2}$ state. The polarization state of the alkali is described not by two but by eight coupled first-order differential equations which we now set up and solve.

B. Inclusion of Nuclear Spin in the Rate Equations

The rate equations for an alkali of spin 3/2 for the extreme cases of complete mixing and no mixing in $P_{1/2}$ were first solved by Franzen and Emslie,[7] but unfortunately they did not obtain an analytic solution to the problem, only a numerical solution for a particular value of the parameter which enters the equations. As we need the solution for a wide variety of conditions, we will do well to obtain a general solution for arbitrary nuclear spin. For the case in which the excited state is completely mixed, an analytic solution can be obtained without too much difficulty;[8] we treat only this case and give the important results for the other extreme case, that of no mixing in the excited state.

Consider first the physics of the situation. We have an ensemble of alkali atoms distributed in n ground-state sublevels according to the Boltzmann distribution.[9] Again, we can ignore the Boltzmann factors and take the populations as equal initially, for $N_i/N_i = e^{-\Delta E/kT}$ where $\Delta E = g_F \mu_0 H_0$ for adjacent levels, and $g_F \approx \frac{g_j}{2I+1}$, so that if $\Delta E/kT << 1$ for $I = 0$ it is certainly also true for $I \neq 0$. Irradiate the ensemble with right circular polarized D_1 resonance light so that $\Delta m_F = +1$, and assume the excited state to be completely mixed. The last assumption means that emission occurs to each of the ground-state sublevels with equal probability and this in turn means that the transition rates A_{ij} are determined entirely by the absorption rate r_i. To get an approximate answer we temporarily lift the constraint $\Sigma N_i = \text{const}$. We then see each level depleting at a rate $r_i N_i$ as a result of absorption; some fraction of this depletion ($\frac{1}{8} r_i N_i$) will go into each other level. We can infer from this that approximately $N_i = -a_i e^{-\frac{7}{8} r_i t} + \sum_{j \neq i} a_j e^{-r_j t} + \text{const}$. The result of the constraint is

to adjust the rates r_i and constants a_i so that $\sum n_i = \text{const.}$ Although the adjustments can be determined by perturbation technique, we need not do so as an exact solution is possible. We can go a step further at this point and show that the result just obtained is indeed a good one. The coupled equations, neglecting for the moment relaxation, are $\frac{dn_i}{dt} = -\sum_{\substack{j \\ j\neq i}} A_{ij} n_i + \sum_{\substack{j \\ j\neq i}} A_{ji} n_j$ where $A_{ij} \propto r_i$ for $i \neq j$. In fact the proportionality constant is merely $1/n$ where n is the number of levels. This follows from the complete mixing assumption that requires each level to spill over into each other level at $1/n$ times its absorption rate. Thus we have

$$\frac{dn_i}{dt} = -n_i \sum_{\substack{j \\ j\neq i}} \frac{r_i}{n} + \sum_{j\neq i} \frac{r_j}{n} n_j , \tag{3}$$

or, since

$$\sum_{\substack{j=1 \\ j\neq i}}^{n} r_i = (n-1)\, r_i,$$

$$\frac{dn_i}{dt} = -\frac{(n-1)}{n} r_i n_i + \sum_{\substack{j=1 \\ j\neq i}}^{n} \frac{r_j}{n} n_j + \frac{1}{nT_1} . \tag{4}$$

We observe that the diagonal terms are dominant [e.g., for Rb^{87}, Rb^{85}, and Cs^{133}, n is respectively 8, 12, and 16 whereas $(r_j)_{max} = 2$].

It will be convenient from now on to talk not of the population n_i but of the occupation probability $p_i = n_i / \sum n_i$. Also, instead of using transition rates a_{ij} it si easier for us to work with the relative transition probabilities w_{ij}. The latter are related to the former by $a_{ij} = w_{ij}\beta_0$ where β_0 is the average light-absorption probability per time and per unit frequency. From its definition, $\beta_0 = \frac{1}{n} \sum_{i,j}^{n} a_{ij}$ where a_{ij} are the transition rates previously defined. We can also relate β_0 to the light intensity per unit frequency interval through the classical result,[10]

$$\beta_0 = \int_0^\infty I_\nu \sigma_\nu d\nu = I_0 \int \sigma_\nu d\nu = \frac{\pi e^2}{mc} f I_0, \qquad (5)$$

assuming I_ν to be flat over the absorption line and equal to I_0. Here σ_ν is the cross section for light absorption at frequency ν, and f is the oscillator strength of the resonance line. Finally, instead of the transition rates $A_{ik} = \sum_j a_{ij} a_{jk}$ we now have $b_{ik} = \sum_j w_{ij} w_{jk}$. The rate equations for the occupation probabilities in the absence of relaxation may now be written

$$\dot{p}_k = - p_k \sum_{\substack{j \\ j \neq k}} b_{kj} + \sum_{j \neq k} b_{jk} p_j . \qquad (6)$$

It is found experimentally that the effect of relaxation can be described phenomenologically by a relaxation time T_1 so that in the absence of the pumping light $\dot{p}_k = - (p_k / T_1) + (1/nT_1)$. Combining the relaxation and pumping equations, we get the complete rate equation

$$\dot{p}_k = - p_k \left(\frac{1}{T_1} + \sum_{\substack{j \\ j \neq k}} b_{kj} \right) + \sum_{\substack{i \\ i \neq k}} b_{ik} p_i + \frac{1}{nT_1} , \qquad (7)$$

where T_1 is in units of β_0^{-1}. To simplify the notation, let $B_{ij} = b_{ij}$ for $i \neq k$ and $B_{kk} = - \left(\frac{1}{T} + \sum_{\substack{j \\ j \neq k}} b_{kj} \right)$; then

$$\dot{p}_k = \sum_j B_{ij} p_j + \frac{1}{nT_1} . \qquad (8)$$

The solution to this system is straightforward and the details are left for Appendic C. The result is

$$p_k = \sum a_i \alpha_{ki} e^{- \lambda_i t} - \frac{1}{nT_1} \sum_j B_{kj}^{-1} , \qquad (9)$$

where λ_i are the eigenvalues of the secular determinant $\det(B_{ij} - \lambda\delta_{ij}) = 0$, a_{ki} is the kth component of the ith eigenvector of B_{ij}, B_{ij}^{-1} is the matrix inverse to B_{ij}, and a_i is determined by the initial conditions. Thus far the solution is general and applies regardless of the degree of mixing. We now digress for a moment to consider the transition probabilities b_{ij}.

C. Transition Probabilities

Before calculating b_{ij}, we need the transition probabilities w_{ij}. As absorption (emission) is of the vector type, we have

$$w_{ij} \propto \sum_{\mu} \left|\left\langle i \left| Y_{\mu}^{1} \right| j \right\rangle\right|^2$$

where Y^1 is the spherical tensor of rank 1. The matrix element $\left\langle i \left| Y_{\mu}^{1} \right| j \right\rangle^{\mu}$ is most easily evaluated by means of the Wigner-Eckart theorem;[11] note first that the transition takes place through the interaction of the electric field of the radiation field with the electronic coordinates so that Y_{μ}^{1} operates only on the J space, i.e., $Y_{\mu}^{1} = Y_{\mu}^{1}(\Omega_J)$. The theorem then states

$$\left\langle F' m'_F J' I' \left| Y_{\mu}^{1}(\Omega_J) \right| F m_F J I \right\rangle = (-1)^{I+1-J-F'} \delta_{I'I} C(F \,|\, F'; m_F \mu m'_F)$$
$$\times [(2J'+1)(2F+1)]^{1/2} W(JFJ'F'; I1) \left\langle J' \left|\left| Y^{1}(\Omega_J) \right|\right| J \right\rangle$$

where $W(JFJ'F'; I1)$ is a Racah coefficient[11] and $\left\langle J' \left|\left| Y_{\mu}^{1}(\Omega_J) \right|\right| J \right\rangle$ is the reduced matrix element of $Y_{\mu}^{1}(\Omega_J)$. We need not be concerned with the latter since we are after the relative transition probabilities only. The Racah coefficients, Clebsch-Gordan coefficients, and the w_{ij} are tabulated in Appendix A for several values of the nuclear spin I. Tables II-2 and II-3 give the B_{ij} for $I = 3/2$ for the two extreme cases of mixing and no mixing in the excited state. We must consider one other case, that of electron randomization in the excited state, before continuing with the solution of the rate equations.

Table II-2. Matrix coefficients B_{ij} for I = 3/2 assuming no reorientation in the P state.

Initial State		F' = 1			F' = 2				
		-1	0	1	-2	-1	0	1	2
Final State									
F = 1	-1	$-\frac{11}{24}-\rho$	0	0	1/4	1/8	0	0	0
	0	1/12	$-\frac{19}{24}-\rho$	0	1/4	1/4	5/24	0	0
	1	1/24	5/24	$-\frac{3}{4}-\rho$	0	1/8	5/24	1/4	0
F = 2	-2	0	0	0	$-\frac{7}{6}-\rho$	0	0	0	0
	-1	1/8	0	0	5/12	$-\frac{9}{8}-\rho$	0	0	0
	0	1/2	5/24	0	1/4	1/4	$-\frac{19}{24}-\rho$	0	0
	1	1/8	1/8	1/4	0	3/8	1/8	$-\frac{15}{12}-\rho$	0
	2	0	1/4	1/2	0	0	1/4	1/6	$-\rho$

Table II-3. Transition probabilities B_{ij} for I = 3/2, assuming complete reorientation of the P state.

Initial State		F' = 1			F' = 2				
		-1	0	1	-2	-1	0	1	2
Final State									
F = 1	-1	$-\frac{7}{16}-\rho$	1/8	3/16	1/4	3/16	1/8	1/16	0
	0	1/16	$-\frac{7}{8}-\rho$	3/16	1/4	3/16	1/8	1/16	0
	1	1/16	1/8	$-\frac{21}{16}-\rho$	1/4	3/16	1/8	1/16	0
F = 2	-2	1/16	1/8	3/16	$-\frac{7}{4}-\rho$	3/16	1/8	1/16	0
	-1	1/16	1/8	3/16	1/4	$-\frac{21}{16}-\rho$	1/8	1/16	0
	0	1/16	1/8	3/16	1/4	3/16	$-\frac{7}{8}-\rho$	1/16	0
	1	1/16	1/8	3/16	1/4	3/16	1/8	$-\frac{7}{16}$	0
	2	1/16	1/8	3/16	1/4	3/16	1/8	1/16	$-\rho$

It has been suggested that at high buffer-gas pressures the nucleus may not partake in the relaxation of the excited state which then involves electron flip only (a similar situation applies in the ground state). The argument is that if we are dealing with a dipole perturbation then the transition rate is proportional to $1/\tau_c$ where τ_c is a correlation time.[12] For high buffer-gas pressures the correlation time is of the same order as the alkali—buffer-gas interaction time (or $\approx 10^{-12}$ sec) whereas the precessional frequency of the nucleus in the hyperfine field is $\nu_{HF} << 10^{12}$/sec. For example, the hyperfine splitting in the $5^2P_{1/2}$ state of Rb^{87} is 81×10^8 cp/sec.[13] The nucleus does not have time to respond to the perturbation. We can calculate the transition rates b_{ij} with this in mind.

If $w(Fm_F;\ F'm'_F)$ is the transition probability due to absorption or spontaneous emission and $S(Fm_F;F'm'_F)$ the transition probability due to electron flip in the $P_{1/2}$ state, than the total transition probability for going from ground state Fm_F to ground state $F'm'_F$ is

$$b(Fm_F;F'm'_F) = \sum_{\substack{F'''m_F''' \\ F''m_F''}} w(Fm_F;F'''m_F''')\,S(F'''m_F''';F''m_F'')\,w(F''m_F'';F'm'_F).$$

As the $w(Fm_F;F'm'_F) = w_{ij}$ have already been calculated we need only find the transition probabilities due to spin flip, we decompose the $|F,m\rangle$ states in a Clebsch-Gordan series

$$|Fm_F\rangle = \sum_{m_J m_I} C(FIJ;m_F m_I m_J)\,|Im_I\rangle\,|Jm_J\rangle$$

and solve for the simple product states $|Im_I\rangle\,|Jm_J\rangle$. We then consider what happens to each $|Fm_F\rangle$ under an electron flip by replacing the products $|Im_I\rangle\,|Jm_J\rangle$ with $|Im_I\rangle\,|Jm_J\pm1\rangle$. Thus, for Rb^{87}

$$
\begin{aligned}
|22\rangle &= \left|\tfrac{3}{2}\ \tfrac{3}{2}\right\rangle \left|\tfrac{1}{2}\ \tfrac{1}{2}\right\rangle \\
|21\rangle &= \tfrac{1}{2}\left|\tfrac{3}{2}\ \tfrac{3}{2}\right\rangle \left|\tfrac{1}{2}\ -\tfrac{1}{2}\right\rangle + \sqrt{3/4}\ \left|\tfrac{3}{2}\ \tfrac{1}{2}\right\rangle \left|\tfrac{1}{2}\ \tfrac{1}{2}\right\rangle \\
|20\rangle &= \frac{1}{\sqrt{2}}\left|\tfrac{3}{2}\ -\tfrac{1}{2}\right\rangle \left|\tfrac{1}{2}\ \tfrac{1}{2}\right\rangle + \frac{1}{\sqrt{2}}\left|\tfrac{3}{2}\ \tfrac{1}{2}\ -\tfrac{1}{2}\right\rangle \\
|2\text{-}1\rangle &= \sqrt{3/4}\left|\tfrac{3}{2}\ -\tfrac{1}{2}\right\rangle \left|\tfrac{1}{2}\ -\tfrac{1}{2}\right\rangle + \tfrac{1}{2}\left|\tfrac{3}{2}\ -\tfrac{3}{2}\right\rangle \left|\tfrac{1}{2}\ \tfrac{1}{2}\right\rangle \\
|2\text{-}2\rangle &= \left|\tfrac{3}{2}\ -\tfrac{3}{2}\right\rangle \left|\tfrac{1}{2}\ -\tfrac{1}{2}\right\rangle \\
|1\ 1\rangle &= -\tfrac{1}{2}\left|\tfrac{3}{2}\ \tfrac{1}{2}\right\rangle \left|\tfrac{1}{2}\ \tfrac{1}{2}\right\rangle + \sqrt{3/4}\ \left|\tfrac{3}{2}\ \tfrac{3}{2}\right\rangle \left|\tfrac{1}{2}\ -\tfrac{1}{2}\right\rangle \\
|1\ 0\rangle &= \frac{1}{\sqrt{2}}\left|\tfrac{3}{2}\ \tfrac{1}{2}\right\rangle \left|\tfrac{1}{2}\ -\tfrac{1}{2}\right\rangle - \frac{1}{\sqrt{2}}\left|\tfrac{3}{2}\ -\tfrac{1}{2}\right\rangle \left|\tfrac{1}{2}\ \tfrac{1}{2}\right\rangle \\
|1\text{-}1\rangle &= \tfrac{1}{2}\left|\tfrac{3}{2}\ -\tfrac{1}{2}\right\rangle \left|\tfrac{1}{2}\ -\tfrac{1}{2}\right\rangle - \sqrt{3/4}\ \left|\tfrac{3}{2}\ -\tfrac{3}{2}\right\rangle \left|\tfrac{1}{2}\ \tfrac{1}{2}\right\rangle
\end{aligned}
$$

and solving these for the products $|Im_I\rangle |Jm_J\rangle$ we get,

$$
\begin{aligned}
\left|\tfrac{3}{2}\ \tfrac{3}{2}\right\rangle \left|\tfrac{1}{2}\ \tfrac{1}{2}\right\rangle &= |2\ 2\rangle \\
\left|\tfrac{3}{2}\ \tfrac{3}{2}\right\rangle \left|\tfrac{1}{2}\ -\tfrac{1}{2}\right\rangle &= \tfrac{1}{2}\left[|2\ 1\rangle + \sqrt{3}\,|1\ 1\rangle\right] \\
\left|\tfrac{3}{2}\ \tfrac{1}{2}\right\rangle \left|\tfrac{1}{2}\ \tfrac{1}{2}\right\rangle &= \tfrac{1}{2}\left[\sqrt{3}\,|2\ 1\rangle - |1\ 1\rangle\right] \\
\left|\tfrac{3}{2}\ \tfrac{1}{2}\right\rangle \left|\tfrac{1}{2}\ -\tfrac{1}{2}\right\rangle &= \frac{1}{\sqrt{2}}\left(|2\ 0\rangle + |1\ 0\rangle\right) \\
\left|\tfrac{3}{2}\ -\tfrac{1}{2}\right\rangle \left|\tfrac{1}{2}\ \tfrac{1}{2}\right\rangle &= \frac{1}{\sqrt{2}}\left(|2\ 0\rangle - |1\ 0\rangle\right) \\
\left|\tfrac{3}{2}\ -\tfrac{1}{2}\right\rangle \left|\tfrac{1}{2}\ \tfrac{1}{2}\right\rangle &= \tfrac{1}{2}\left(|2\ -1\rangle - \sqrt{3}\,|1\ -1\rangle\right) \\
\left|\tfrac{3}{2}\ -\tfrac{1}{2}\right\rangle \left|\tfrac{1}{2}\ -\tfrac{1}{2}\right\rangle &= \tfrac{1}{2}\left(\sqrt{3}\,|2\ -1\rangle + |1\ -1\rangle\right) \\
\left|\tfrac{3}{2}\ -\tfrac{3}{2}\right\rangle \left|\tfrac{1}{2}\ -\tfrac{1}{2}\right\rangle &= |2\ -2\rangle\ .
\end{aligned}
$$

The probability that an atom in some initial level $|Fm_F\rangle$ in the $P_{1/2}$ state will end up in any other level of the $P_{1/2}$ state can now be obtained and is summarized in Table II-4. With the aid of this table plus the tabulations of w_{ij} we obtain the transition rates b_{ij} for the case in which an electron flip only occurs in the $P_{1/2}$ state. These are given in Table II-5. We return now to the solution, focusing our attention on the case of complete mixing in the excited state.

Table II-4. Transition probabilities due to electron flip S(ij; i'j').

		m_F							
		F = 1			F = 2				
		-1	0	1	-2	-1	0	1	2
	m'_F								
F' = 1	-1		1/8		3/4		1/8		
	0	1/8		1/8		3/8		3/8	
	1		1/8				1/8		3/4
F' = 2	-2	3/4				1/4			
	-1		3/8		1/4		3/8		
	0	1/8		1/8		3/8		3/8	
	1		3/8				3/8		1/4
	2			3/4				1/4	

Table II-5. Transition probability B_{ij} assuming electron randomization in $P_{1/2}$ state.

Initial State		F = 1			F = 2				
	m'_F	-1	0	1	-2	-1	0	1	2
Final State	m_F								
F = 1	-1	$-\frac{43}{96}-\rho$	5/96	0	11/16	5/32	5/96	0	0
	0	5/48	$-\frac{43}{48}-\rho$	3/16	1/8	5/16	5/48	1/16	0
	1	5/96	23/96	$-\frac{21}{16}-\rho$	1/16	5/32	23/96	1/16	0
F = 2	-2	1/16	0	0	$-\frac{19}{12}-\rho$	3/16	0	0	0
	-1	1/32	5/32	0	19/48	$-\frac{45}{32}-\rho$	5/32	0	0
	0	5/48	5/48	3/16	1/8	5/16	$-\frac{43}{48}-\rho$	1/16	0
	1	1/32	7/32	5/16	3/16	3/32	7/32	$-\frac{19}{48}-\rho$	0
	2	1/16	1/8	5/8	0	3/16	1/8	5/24	$-\rho$

D. Solution of the Rate Equations for the Case of Complete Mixing in the Excited State

With the aid of the tabulated values of w_{ij} and the definition of the relative absorption probabilities $r_i = \sum_j w_{ij}$, we see by inspection of B_{ij} that for complete mixing $B_{ij} = r_j/n$, $i \neq j$, and $B_{ii} = -\frac{n-1}{n} r_i - \frac{1}{T_1}$. This result was previously deduced. Furthermore, we note that $r_{n-i} = r_i$ and r_i is related to the nuclear spin (for $J = 1/2$) through $r_i = \frac{2i}{2I+1}$, $i = 1, 2, \cdots, 2I+1$. Combining these results with the fact that the number of levels n is equal to $2(2I+1)$, we arrive at the following explicit form for B_{ij} for any nuclear spin

$$B_{ij} = \frac{j}{(2I+1)^2} \qquad j = 1, 2, \cdots, 2I+1, \text{ and } i \neq j$$

$$B_{in-j} = B_{ij} \qquad B_{kk} = -\frac{2(2I+1) - 1}{2(2I+1)^2}(2k) - \frac{1}{T_1}.$$

(complete mixing)

Because of these simple properties it is possible to expand $\det(B_{ij} - \lambda\delta_{ij})$ for arbitrary nuclear spin (and arbitrary J) and obtain

$$f(\lambda) = 0 = 1 - \frac{1}{2I+1} \sum_{i=1}^{n} \frac{r_i}{r_i - \lambda} \quad \text{(complete mixing).} \qquad (10)$$

This last result localizes the eigenvalues λ_i in the intervals (r_i, r_{i+1}) so that they can be obtained easily with a few Newtonian iterations, $\lambda_n = \lambda_{n-1} - \frac{f(\lambda_{n-1})}{f'(\lambda_{n-1})}$, taking for λ_0 any number in the intervals (r_i, r_{i+1}). We do not, however, have to find $n = (2I+1)2$ eigenvalues but only $(2I+1)/2$ eigenvalues, as the constraints $r_{n-i} = r_i$ and $\sum p_i = 1$ halve the number of equations. In fact, from $r_{n-i} = r_i$ it follows immediately that $p_{n-i} = p_i$. The further relation $r_{\frac{n}{2}-i} + r_i = 2$ halve again the number of eigenvalues that need be found. Table II-6 lists the decay constants and amplitudes for $I = 3/2$ for the case of complete mixing in the excited state, as well as similar results for no reorientation and electron randomization in the $P_{1/2}$ state. The amplitudes of the exponential for the absorption probability can also be deduced; but

Table II-6. Optical pumping transients for the three cases considered and a $\rho = 0.05$. To get the decay rates exclusive of the relaxation time T_1, subtract ρ from λ. Note that is in units of β_0^{-1} and that the a corresponding to $\lambda=0$ is merely $\beta(\infty)$.

No mixing		Complete mixing		Electron randomization	
λ	a	λ	a	λ	a
1.216667	-2.020556	1.942488	0.039861	1.869354	0.022742
1.197667	2.377703	1.330116	0.082752	1.518020	0.100491
0.485667	-0.226161	0.769884	0.142969	1.365126	0.043672
0.633333	0.082448	0.157512	0.491584	0.775675	0.116138
0.332871	0.953700	0.000000	0.242834	0.451748	-0.053015
0.933796	-0.315940			0.257577	0.614776
0.000000	0.148806			0.000000	0.155196

inasmuch as these depend on $1/\beta_0 T_1$ in no simple way, they are left for the computer. We turn now to a consideration of the relative absorption probability per unit time per atom which we designate by β/β_0, and to the polarization of the absorbing alkali vapor.

The absorption probability per unit time, $\beta(t)$, is given by $\beta(t) = (\sum r_i p_i)\beta_0$ where the quantities are as previously defined. Explicitly, using the solution we have obtained for p_i, we get

$$\beta(t) = \beta_0 \sum_i r_i \left\{ \sum a_k \alpha_{ik} e^{-\lambda_k t} - \frac{1}{nT_1\beta_0} \sum_j B_{ij}^{-1} \right\} \tag{11}$$

from which we immediately get the equilibrium value of the relative absorption probability per atom $\frac{\beta(\infty)}{\beta_0}$; it is $\frac{\beta(\infty)}{\beta_0} = -\frac{1}{nT_1\beta_0} \sum_{i,j} r_i B_{ij}^{-1}$. This result is a basis for estimating the optical thickness of the absorbing vapor. The experimental method utilizing the above result as well as a discussion of the limitations of this technique is discussed in Sec. IV. By definition, the polarization of an atom is $P = \sum_i m_i p_i$, where m_i is the m value of the ith state. From the equilibrium populations $p_i(\infty) = -\frac{1}{nT_1\beta_0} \sum_j B_{ij}^{-1}$ we obtain for the equilibrium polarization

$$P(\infty) = -\frac{1}{nT_1\beta_0} \sum_{i,j} m_i B_{ij}^{-1} . \tag{12}$$

In the general case one would expect partial mixing in the P state. To handle this case exactly one would have to know the details of the interaction. In the absence of such knowledge we assume that the mixing occurs in a uniform fashion, that is, that collisions will connect an atom in some m level of the $P_{1/2}$ state with any other level of the P state with equal probability. This assumption allows us to define a mixing parameter α in such a way that

$$\frac{dp_k}{dt} = \alpha \sum_i (B_{ki})_{CM} p_i + (1-\alpha) \sum_i (B_{ki})_{NM} p_i + \frac{\rho}{n}, \tag{13}$$

where $(B_{ki})_{CM}$ is the transition probability with complete mixing of the P state assumed, and $(B_{ki})_{NM}$ is the transition probability with no reorientation of the $P_{1/2}$ state assumed. We might also try replacing $(B_{ki})_{CM}$ with $(B_{ki})_{er}$, where er stands for electron randomization, and see which of these two possibilities best describes the data. Now α is the probability that the P state is mixed uniformly in the one case and is mixed through electron randomization in the $P_{1/2}$ state in the second case. We define α as follows: Let N be the total number of atoms in the $P_{1/2}$ state and N* the number of atoms that have not been reoriented; then

$$\frac{dN^*}{dt} = -(\sigma_{1/2,\,1/2}\bar{nv} + \sigma_{1/2,\,3/2}\bar{nv})N^* \qquad (14)$$

where $\sigma_{1/2,\,1/2}$ is the cross section for mixing the $P_{1/2}$ state, $\sigma_{1/2,3/2}$ cross section for transfer[14] of excitation from the $P_{1/2}$ to the $P_{3/2}$ state, and n is the buffer-gas density. If we integrate (14) and average it over the lifetim of the $P_{1/2}$ state ($\tau_{1/2}$ = lifetime of the $P_{1/2}$ state), then

$$\frac{N^*(\tau_{1/2})}{N} = \exp[-(\sigma_{1/2}+\sigma_{3/2})\bar{nv}\,\tau_{1/2}],$$

and the average fractional number of reoriented atoms is

$$1 - \frac{N^*(\tau_{1/2})}{N} \equiv \alpha. \qquad (15)$$

Equation (13) were solved for different values of α and ρ for the case of uniform relaxation as well as electron randomization in the $P_{1/2}$ state, but before the resulting signal is compared with experiment it is profitable to investigate the approximate form of the signal and to consider the consequence of signal averaging.

E. Two-Exponential Approximation

If we examine the decay rates exclusive of ρ for complete mixing in the P state (λ - 0.05 in Table II-6), we see two striking features: the smallest decay rate (0.108) accounts for a major portion of the signal, and this decay rate is smaller by at least a factor of 7 from each of the other decay rates that are very close to each other by comparison. We might expect that because of the close proximity of the lifetimes of the faster decaying exponentials, these exponentials would be garbled in any real situation and some avergae exponential would only be observed. One would then expect the signal to consist of two exponentials, one of which would be identical with the dominant exponential of the exact theoretical signal and the second of which would be some average of the remainder of the theoretical signal. As the average exponential would depend somewhat on the fineness of the averaging, it would be desirable to average the theoretical signal in a manner that simulates the experimental averaging. Since each of the exponentials is of the form $e^{-(\lambda+\rho)t}$ there is reason to expect the average to be of this form.

To test the reasonableness of the two-exponential approximation of the signal, the theoretical signals were averaged over the experimental sampling time and fitted to a two-exponential form by the least squares method. We obtained exceedingly good results. The two-exponential fits deviate by less than 1 part in 10^4. Similar remarks can be made for the case of electron randomization and for higher nuclear-spin values—e.g., I = 5/2, 7/2—except that as I increases, the lifetime of the dominant exponential becomes less distinguishable from the other lifetimes of the signal and may thus be sensitive to averaging.

It is not obvious what kind of simplification, if any, can be achieved for the case that the $P_{1/2}$ state is not reoriented. But the lifetimes of the signal do not differ by a great deal from each other, and as the amplitudes are both positive and negative in sign we might anticipate some cancellation. In fact, a remarkable thing happens. The signal in this case is effectively singly exponential, to a high degree of accuracy, with a lifetime expressible as $1/\tau = 0.35\,\beta_0 + (1/T_1)$.

This is precisely the form observed in a wall-coated cell having no buffer gas (e.g., see Fig. V-1). No physical reason for this simplification is offered. We might expect that the observed signal in general will consist of two exponentials going to one exponential in the limit of no reorientation in the P state. Theoretical signals for different values of ρ and α were fitted to two exponentials and the results shown in Figs. II-1 to II-3. These results will be needed in Sec. V where we interpret the data.

F. Numerical Solutions of the Rate Equations for Rb^{87}

A Fortran II computer program was written to solve the population equations on an IBM 7094 and obtained $\beta(t)/\beta_0$ over a wide variety of conditions. Representative solutions are given graphically in Figs. II-4 to II-7. Quantities computed included the lifetimes and amplitudes of the exponentials in $\beta(t)$ for different values of ρ and α, with both complete mixing and electron randomization in the $P_{1/2}$ state considered. In Table II-6 we show the decay constants for the Rb^{87} pumping signals and the amplitudes for a particular value of ρ, for the three cases: no mixing in the excited state, complete mixing in the excited state, and electron randomization in the excited state. Two other quantities computed were the equilibrium value of $\beta(t)/\beta_0$--i.e., $\beta(\infty)/\beta_0$--and the equilibrium polarization $P(\infty)$. These are presented in Figs. II-8 and II-19 for the three cases considered. The equilibrium signal ($\propto 1 - \beta(\infty)/\beta_0$) changes rapidly with ρ for small values of ρ, but approaches 0 slowly and asymptotically for large values of ρ. Perhaps the most interesting result thus far is that the equilibrium signal for the case of electron randomization in the $P_{1/2}$ state differs only slightly from the case of no reorientation in the $P_{1/2}$ state. This suggests an interesting experiment to test whether relaxation in the $P_{1/2}$ state is uniform or involves only the electronic spin. One could monitor the light through the absorption cell as buffer gas is added to the cell beginning with an evacuated cell. Allowing for changes in the relaxation time, a small fractional decrease in signal would favor electron randomization whereas a large fractional decrease in signal would favor uniform relaxation.

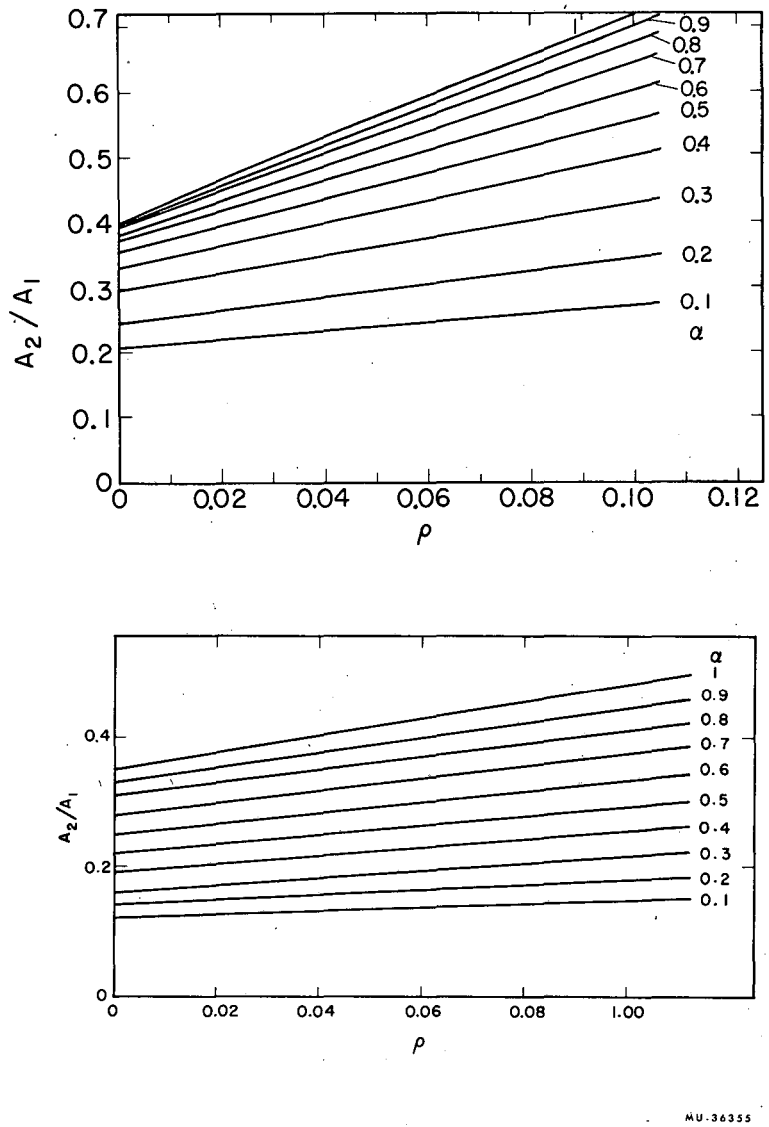

Fig. II-1. Result of fitting theoretical signals to a two-exponential form. Shown are the amplitude ratios A_2/A_1 as a function of ρ and α, with uniform mixing assumed in the P state. The curves shown were computed for a $\beta_0 = 0.5$ and a 1-msec sampling interval. For values of $\rho > 0.1$ the curves deviate from straight lines.

Fig. II-2. Same as II-10, but with electron randomization assumed in the $P_{1/2}$ state.

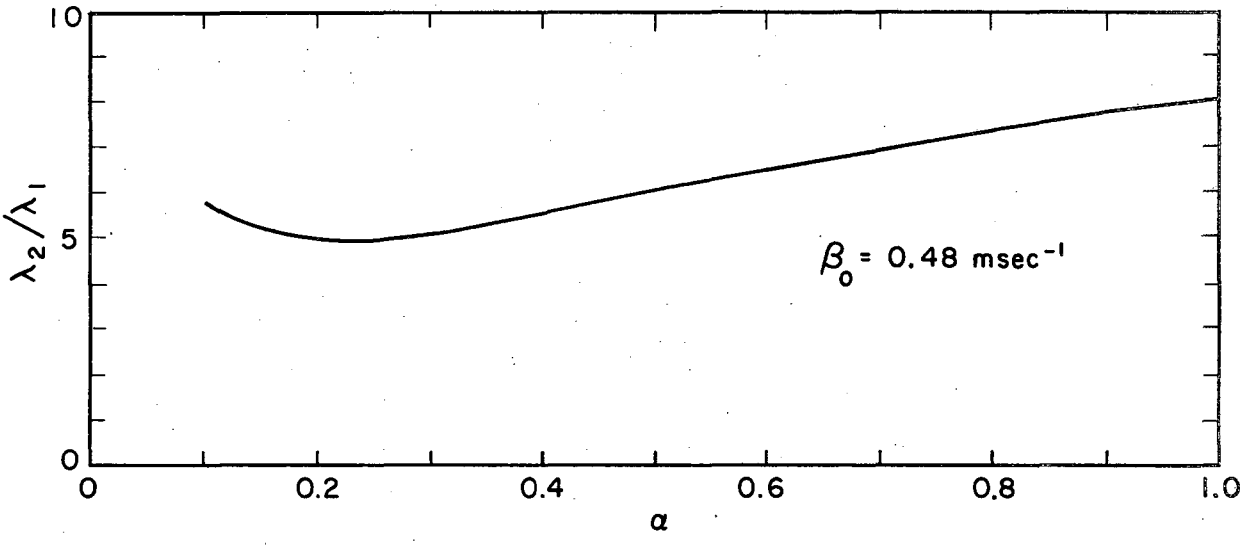

Fig. II-3. Decay-constant ratio λ_2/λ_1 for uniform relaxation.

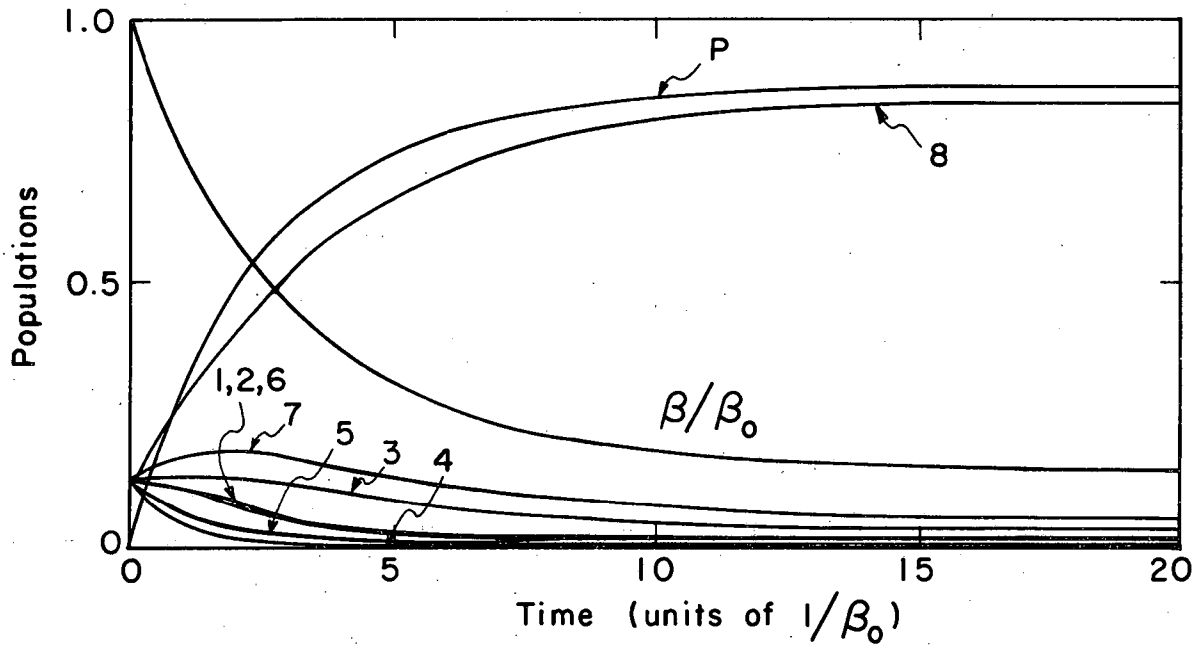

MU-36432

Fig. II-4. Populations of the Zeeman sublevels of the ground state of Rb^{87} when the incident light (D_1) is right circularly polarized and with no reorientation of the $P_{1/2}$ state assumed. Also shown are the absorption probability β/β_0 and the polarization P. The calculations are for a $\rho = 0.05$.

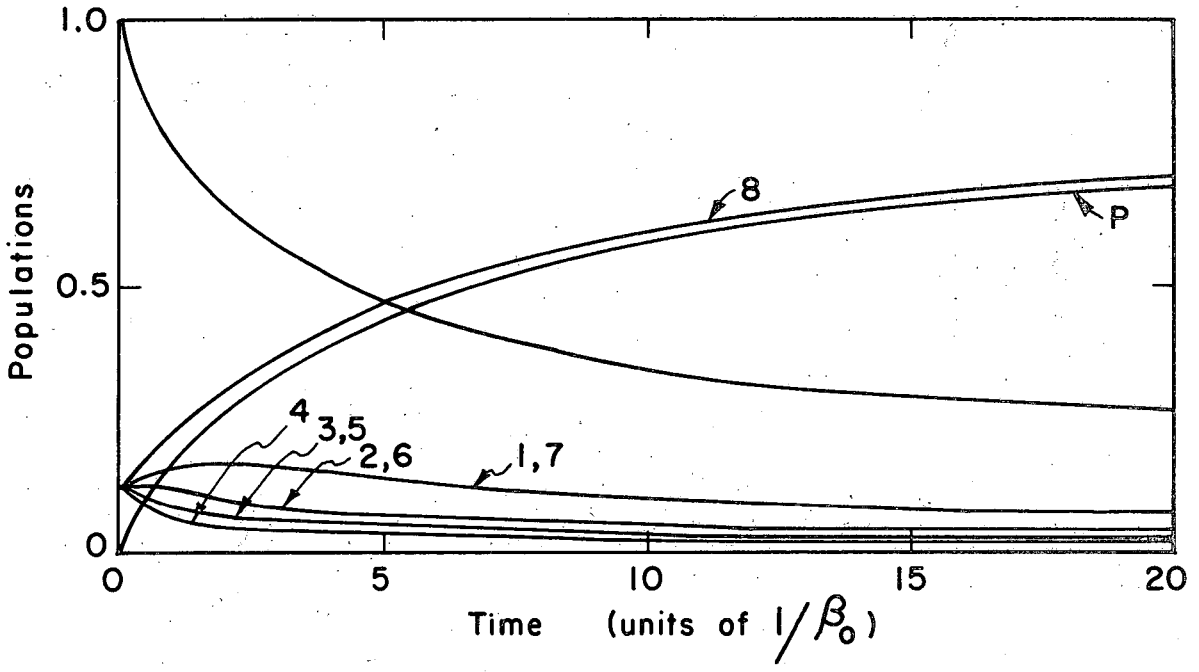

Fig. II-5. Same as II-4, except complete mixing in the P state.

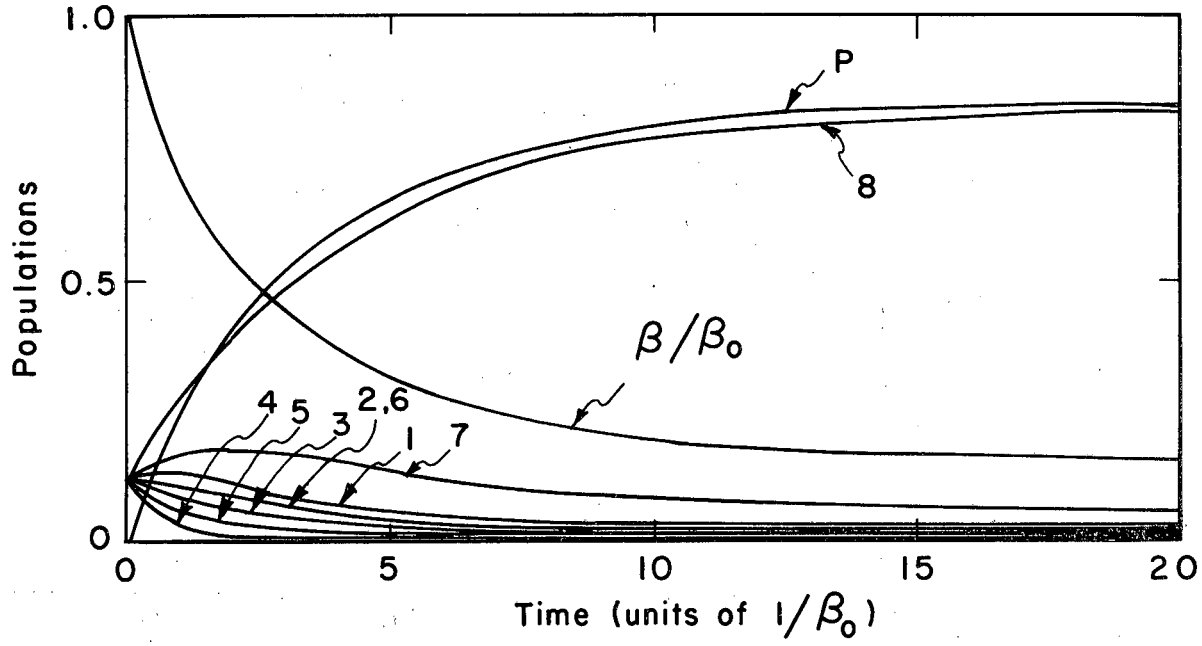

MU-36391

Fig. II-6. Same as II-4, except electron randomization in the $P_{1/2}$ state.

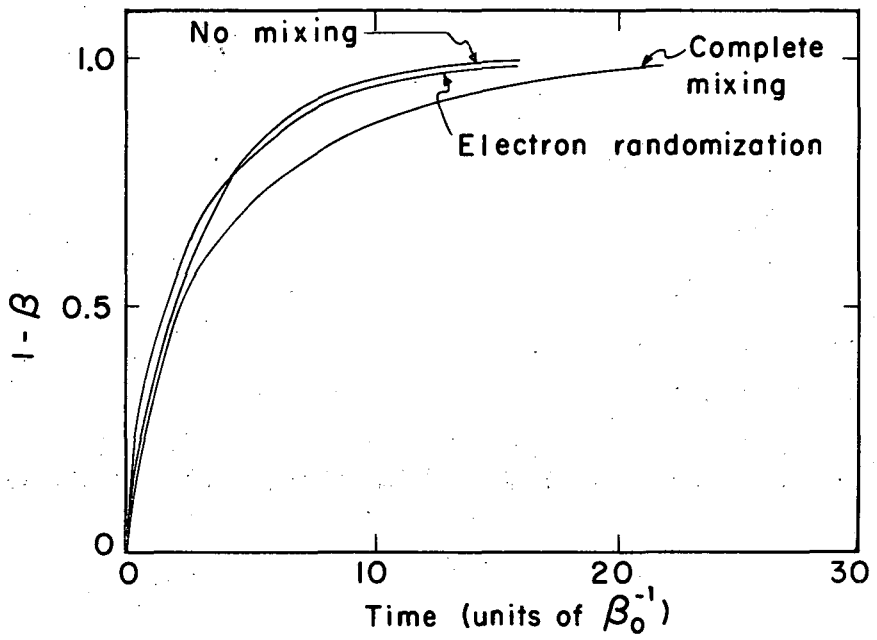

MU-36375

Fig. II-7. Dynamic signal for the three cases considered in Figs. II-4, II-5, and II-6.

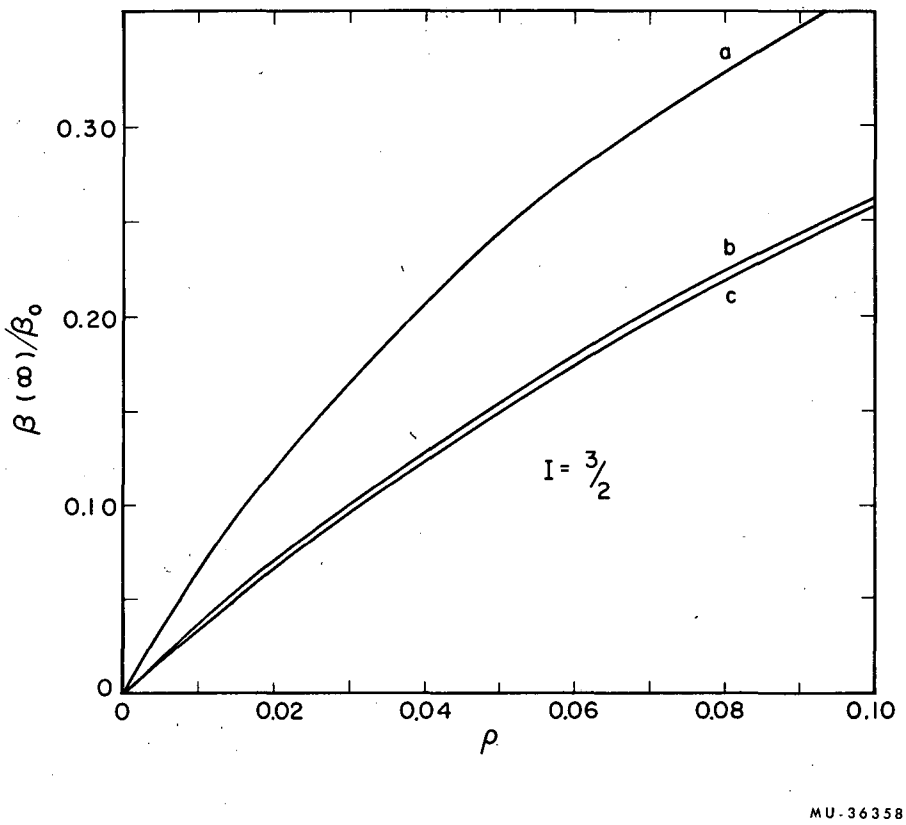

Fig. II-8. Equilibrium absorption probability $\beta(\infty)/\beta_0$ for Rb^{87} optically pumped with circularly polarized D_1 light. Curve a, complete disorientation in $P_{1/2}$ state. Curve b, electron randomization in $P_{1/2}$ state. Curve c, no disorientation in $P_{1/2}$ state.

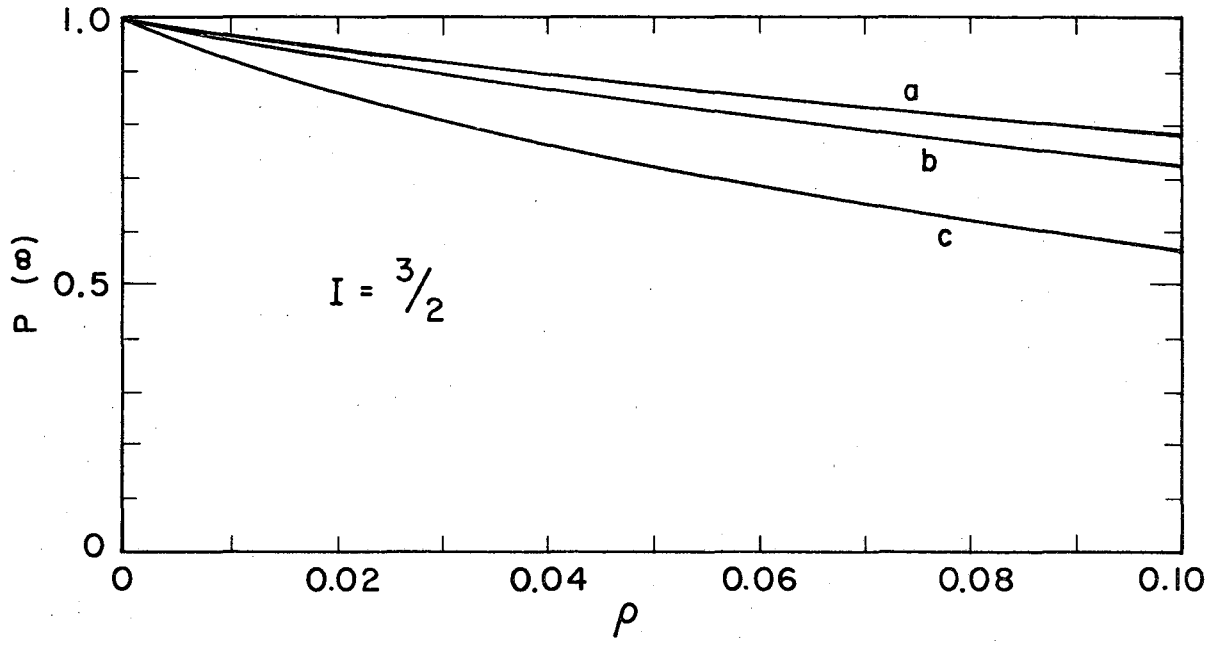

MU-36376

Fig. II-9. Equilibrium polarization of Rb^{87} optically pumped with circularly polarized D_1 light. Curve a, no orientation. Curve b, electron randomization. Curve c, complete mixing.

It is of interest to calculate the electronic and nuclear polarizations for the various cases considered. This is done in Appendix B where similar though less extensive results are also presented for Rb^{85} and Cs^{133}. The results for Rb^{87} are presented in Fig. II-10.

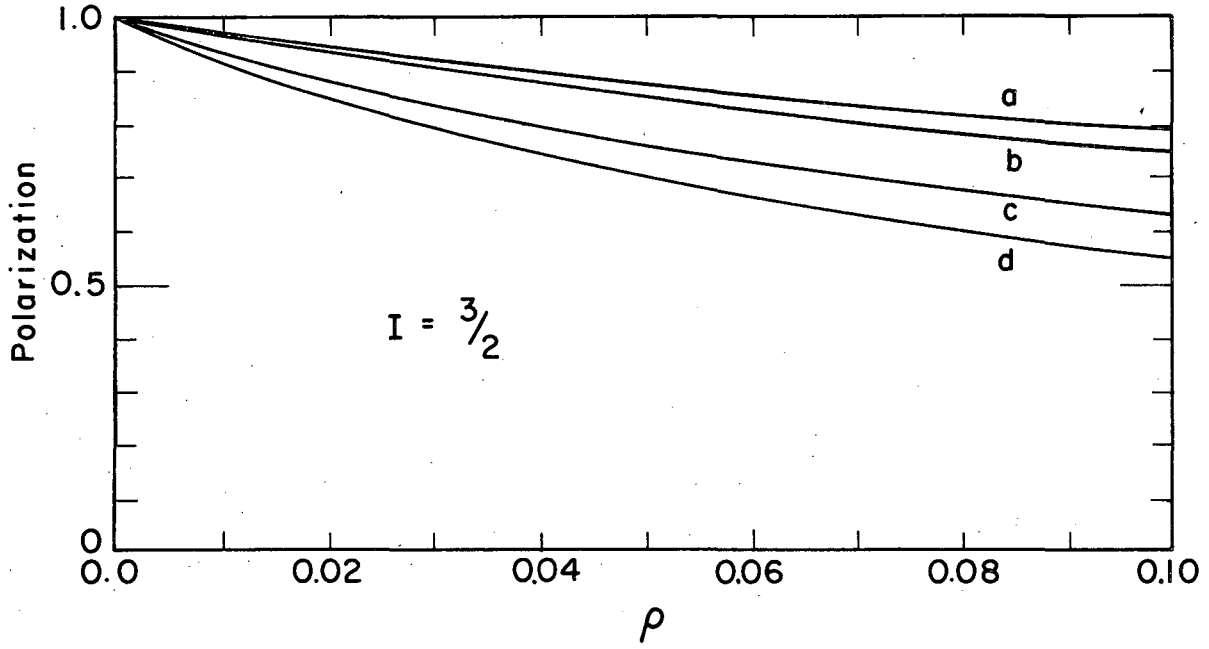

Fig. II-10. Electronic and nuclear polarizations corresponding to Fig. II-9. Curve a, nuclear polarization (no mixing). Curve b, electronic polarization (no mixing). Curve c, electronic polarization (complete mixing). Curve d, nuclear polarization (complete mixing).

III. EXPERIMENTAL METHOD

Circularly polarized D_1 resonance radiation ($5^2P_{1/2} \rightarrow 5^2S_{1/2}$) from an enriched Rb^{87} resonance lamp was made incident on an enriched optically thin Rb^{87} absorption cell containing a buffer gas such as Ne. Due to unequal absorption rates by the ground-state Zeeman levels and spontaneous emission, the ground state of the Rb^{87} atom becomes oriented as selective absorption ($\Delta m = \pm 1$) followed by nearly isotropic emission eventually leads the atom into the nonabsorbing level ($m_F = F_{max}$ for right circularly polarized light and $m_F = -F_{max}$ for left circularly polarized light). The transparency of the Rb^{87} vapor therefore increases under this "optical pumping" action so that the intensity of the D_1 light coming through the absorption cell increases. This increase in intensity is registered by a silicon solar-cell detector whose output is a faithful reproduction of the electronic-spin polarization, as the transparency of the vapor is proportional to the electronic-spin polarization for an optically thin absorption cell.

After some amplification the signal is digitized by a voltage-to-frequency converter and stored in the memory of a pulse-height analyzer which is operating in time mode as a multichannel scalar, henceforth abbreviated as mcs. The mcs performs a gross count for a fixed interval of time and stores the result in one of its channels (storage location), then advances to the next channel where it stores the gross count of the next time interval. The counts accumulated in successive intervals of time are stored in successive channels; each channel always corresponds to the same time interval in the evolution of the signal; that is, the signal is synchronized with the switching of the channels, the nth channel being active at time $n\Delta t$ after optical pumping commences if Δt is the count-time per channel. In this way the accumulated signal increases linearly with the number of optical pumping transient signals observed, while the noise, to the extent that it is random, increases as the square root of the number of transients.

A very large signal-to-noise ratio is built up in this way, making possible a detailed analysis of the optical pumping transient signals. Figure III-1 illustrates the data-accumulation scheme.

The pumping transients were generated by pulsing an rf source at the Larmor precession frequency. Magnetic-field inhomogeneities and power broadening insured that the Zeeman levels overlapped so that the rf field equalized the Zeeman populations within each hyperfine state, provided the rf field was intense enough. Sufficient time was allowed between transients for the hyperfine states to relax thermally before the rf was turned off and pumping was allowed to proceed.[15] Signals were observed for different values of buffer-gas pressure, and for each value of the buffer-gas pressure a number of measurements were made at different values of the light intensity. The digital output of the mcs was then fitted to the predicted two-exponential form by the least-squares method, and from the variation of the pumping times with light intensity the ground-state relaxation times, T_1, were obtained. Moreover, for the speical case of zero buffer-gas pressure, the average light-absorption rate per atom, β_0, was also obtained. The mixing parameter α was then determined from the ratio of the amplitudes of the exponential components of the signal, A_2/A_1, in conjunction with $\rho = 1/\beta_0 T_1$; from the variation of α with buffer-gas density the effective cross section $\sigma_{eff} = \sigma_{1/2,\,1/2} + \sigma_{1/2,\,3/2}$ for disorientation of the 5^2P state of Rb^{87} was obtained. Cross sections for disorientation of a polarized Rb^{87} atom in the ground state $5^2S_{1/2}$ were obtained from the variation of T_1 with buffer-gas density according to the diffusion theory of Franzen[6] (see Appendix E).

A block diagram of the experimental arrangement is shown in Fig. III-2. The magnetic field H_0($\approx$ 1 gauss) is not necessary for optical pumping; however, any magnetic field, $H_\perp$, perpendicular to the axis of quantization (defined by the direction of the beam of light) will disorient the atoms to a degree that depends on the ratio $H_\perp / H_{||}$, where $H_{||}$ is the component parallel to the light beam. As it is

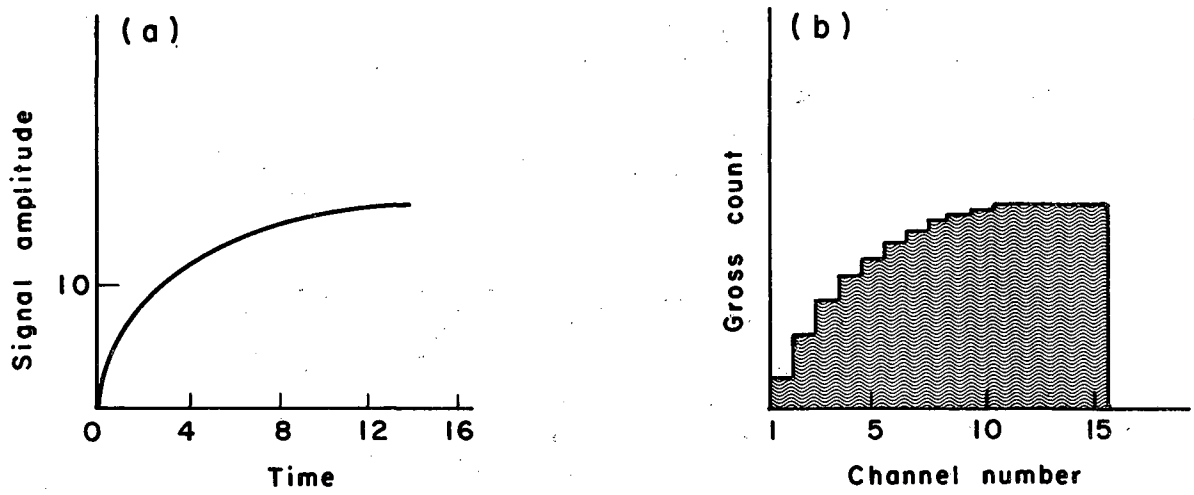

Fig. III-1. If V(t) is the signal amplitude in (a), then the height of the nth column in (b) is $N = \int_{m-1}^{m} V(t)\, f\, dt$, where f is the proportionality between voltage and frequency.

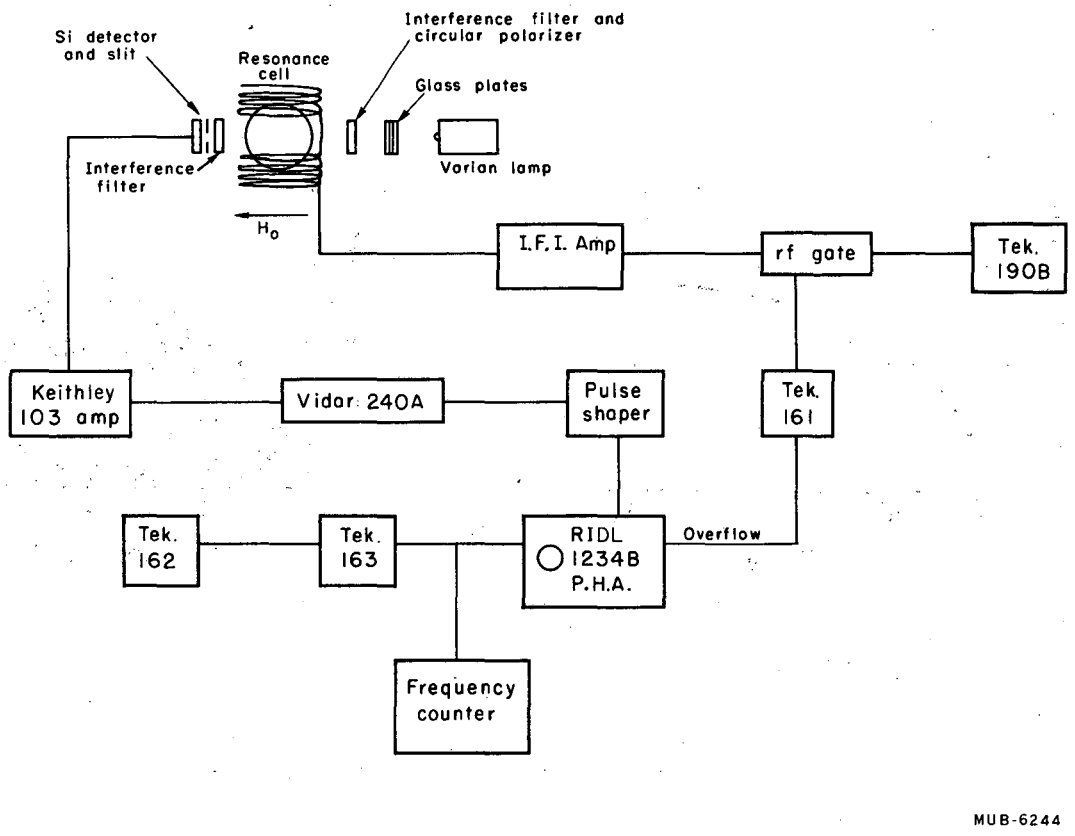

Fig. III-2. Block diagram of experiment.

difficult to eliminate local fields present in the laboratory the experiment was performed in an $H_0' \gg H_\perp$ that pointed in the direction of the light beam. As the resultant field was then very nearly parallel to the light beam, the effect of off-axis fields was minimized.

IV. EXPERIMENT

A. Procedure

In Sec. IV. A, we discuss the procedure used in obtaining data, with the experimental apparatus and the analysis of the data described in Secs. IV. B and V. We have seen in Sec. II that the interpretation of the pumping signals necessitates knowledge of the parameter $\rho = 1/\beta_0 T_1$, where β_0 is the average light-absorption probability per atom per unit time and T_1 is the ground-state relaxation time. Without this value of ρ, the experimental ratio A_2/A_1 cannot be related to theory except in the extreme case of such high light intensity that $\rho \approx 0$, in which case A_2/A_1 is independent of ρ. However, this case is not encountered in this experiment. The determination of β_0 and T_1 was based on two reasonable assumptions: (a) that the absorption line (in the absence of pressure broadening) is much narrower than the emission line, so that $\beta_0 \propto I$ where I is the light intensity; and (b) that the excited state is unperturbed in the absence of a buffer gas (wall collisions are of no consequence since they occur in a time of the order of 10^{-4} sec, whereas the radiative lifetime of the P state is $\approx 10^{-8}$ sec).

1. Determination of β_0 in the Absence of Buffer Gas

It is shown in Sec. II that if the P state of Rb^{87} is not reoriented, the pumping signal consists of a single exponential with decay constant $\lambda = 0.35\,\beta_0 + 1/T$. Experimentally, we observe that pumping transients in evacuated cells are, without exception, singly exponential, this supports the hypothesis that the P state is not perturbed in the absence of buffer gas. It is reasonable then to equate the observed decay rate λ_e to the theoretical one and eliminate $1/T_1$. The procedure is to measure pumping times as a function of light intensity in the evacuated cell (the same cell that will then be used for cross-section measurements) and plot the reciprocal of the pumping times against the light intensity. A straight line is obtained (because $\beta_0 \propto I$) whose slope m equals $0.35\,\beta_0$ (and whose intercept is $1/T_1$). Such a measurement eliminates the relaxation time directly. Since the wall relaxation rate in an evacuated

Pyrex cell (> 1000/sec) is greater than the pumping rate of the resonance lamp used (≈ 250/sec), it was essential to coat the wall to increase the wall-collision relaxation time so that the pumping signal was not dominated by wall relaxation. Otherwise, the signal would be insensitive to the light intensity and in any case be so small as to make its measurement impractical (see Figs. II-8 and II-9). The type wall coating used was $(C_{40}H_{82})_X$ and has the commercial name "Paraflint."[16]

The experimental arrangement was the same as that shown in Fig. III-2. Pumping transients were accumulated in the mcs for different values of the light intensity, and the digital output plotted on semilog graph paper. The lifetimes, τ, of the transients were determined from the slopes of the straight lines and their reciprocals plotted against the light intensity I. Since the transients are single exponentials, it is not necessary to do a least-squares analysis nor to obtain the kind of statistics needed for a multiply exponential function. A typical determination of β_0 is exemplified by Fig. V-1. When buffer gas is added to the absorption cell, Lorentz broadening of the absorption line results, so that values of β_0 obtained with zero buffer-gas pressure have to be corrected for finite pressure. Such a correction is discussed when we intercept the data(Sec. V).

2. Measurement of Light Intensity

A schematic diagram of the arrangement used to measure I is shown in Fig. IV-1. The output of the detector, digitized by the V-to-f, was stored in the mcs. The integration time (10 sec) and number of measurements (5 to 10) were sufficient to uncover drifts or long-term fluctuations. The 10-sec integration time was rather arbitrary, although the total observation interval (50 to 100 sec) was necessary to uncover instabilities of significant duration. Light-intensity measurements were made before and after observation of each pumping transient and the average of these measurements computed.

3. Measurement of T_1 in Cells having a Buffer Gas

The ground-state relaxation times were measured by the Dehmelt technique[17] at the same time as the amplitude ratio A_2/A_1. Before the Dehmelt technique could be used for the measurement of T, the two

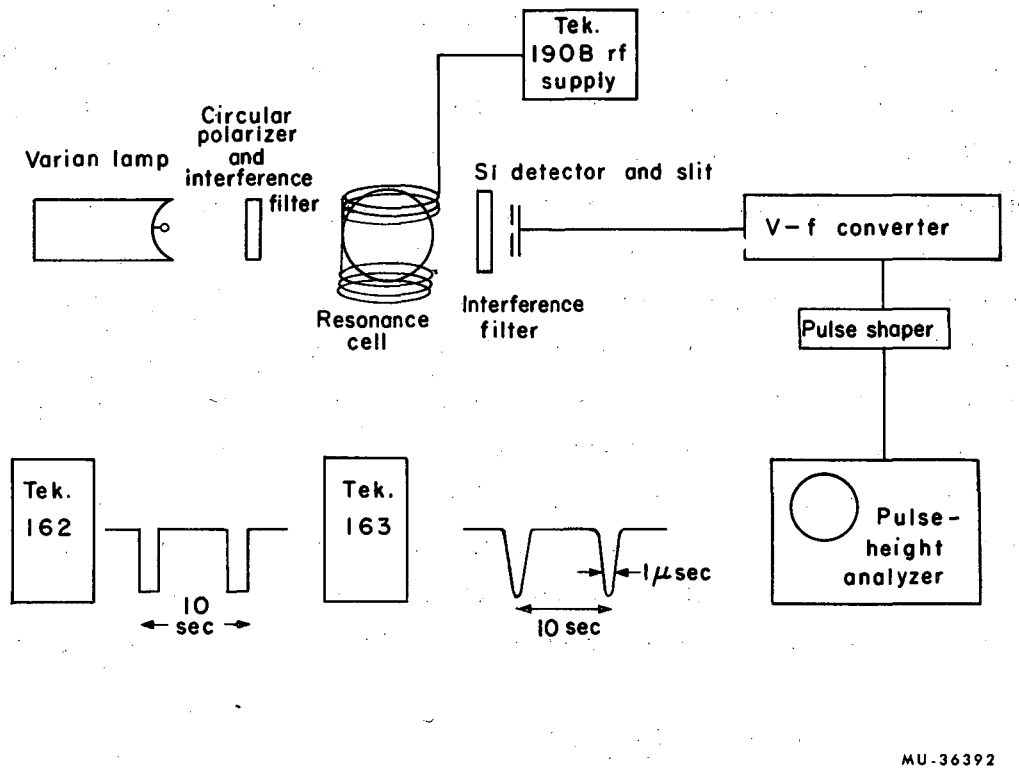

Fig. IV-1. Arrangement for measuring light intensity and absorption.

exponentials that comprise the signal had to be separated.[18] This separation is accomplished first graphically. The graphical results serve as starting points for a least-squares analysis. One of the outcomes of this analysis is the lifetime of the long-lived exponential τ_1; the reciprocal of this lifetime was plotted against the light intensity and extrapolated to zero light intensity to yield $1/T_1$. We worked with the long-lived exponential both because it is generally determined with considerably greater accuracy, and because it is insensitive to electronic averaging ($\tau_1 \gg \Delta t$). Sample measurements of T_1 are shown in Fig. IV-2 and in Sec. V.

4. Measurement of the Amplitude Ratio A_2/A_1

Pumping transients were observed for different values of buffer-gas pressure and the digital output of the mcs fed to an IBM 7094 computer programmed to fit the data to two exponentials by the least squares method; the program is an adaptation of the Los Alamos Least-Squares Program.[19] Initial values were obtained from a graphical separation of the exponentials.

5. Determination of the Total Absorption of D_1 Light in the Resonance Cell

Prior to making any measurements, it was necessary for us to estimate both the total absorption in the vapor cell and the alkali density. A high alkali density will complicate the pumping process by introducing a new relaxation mechanism, namely self-spin exchange.[20] We can estimate the density that can be tolerated from the measured cross section for Rb^{87}-Rb^{87} spin exchange measured by Moos and Sands.[21] From this cross section of $\sigma_{ex} \approx (1\times10^{-14})$ cm^2 we get a spin-exchange time of $T_2 = \frac{1}{\sigma_{ex} n\bar{v}} \approx \frac{2\times10^9}{n}$, where n is the alkali density and $\bar{v}$ the mean relative speed of the alkali atoms ($\approx 5\times10^4$ cm/sec). If the spin-exchange process is to be unimportant then we must have $T_2 \gg T_1$, which leads to $n << \frac{2\times10^9}{T_1}/\text{cm}^3$. Typically $T_1 \approx 40$ msec so that $n << (4\times10^{10})/\text{cm}^3$. The amount of absorption in the cell is important not only because the pumping rate will vary along the cell but also because the distribution of the hyperfine components of the D_1 line will change due to unequal absorption rates, the ratio being 5:3 in favor of the F = 2 state absorbing

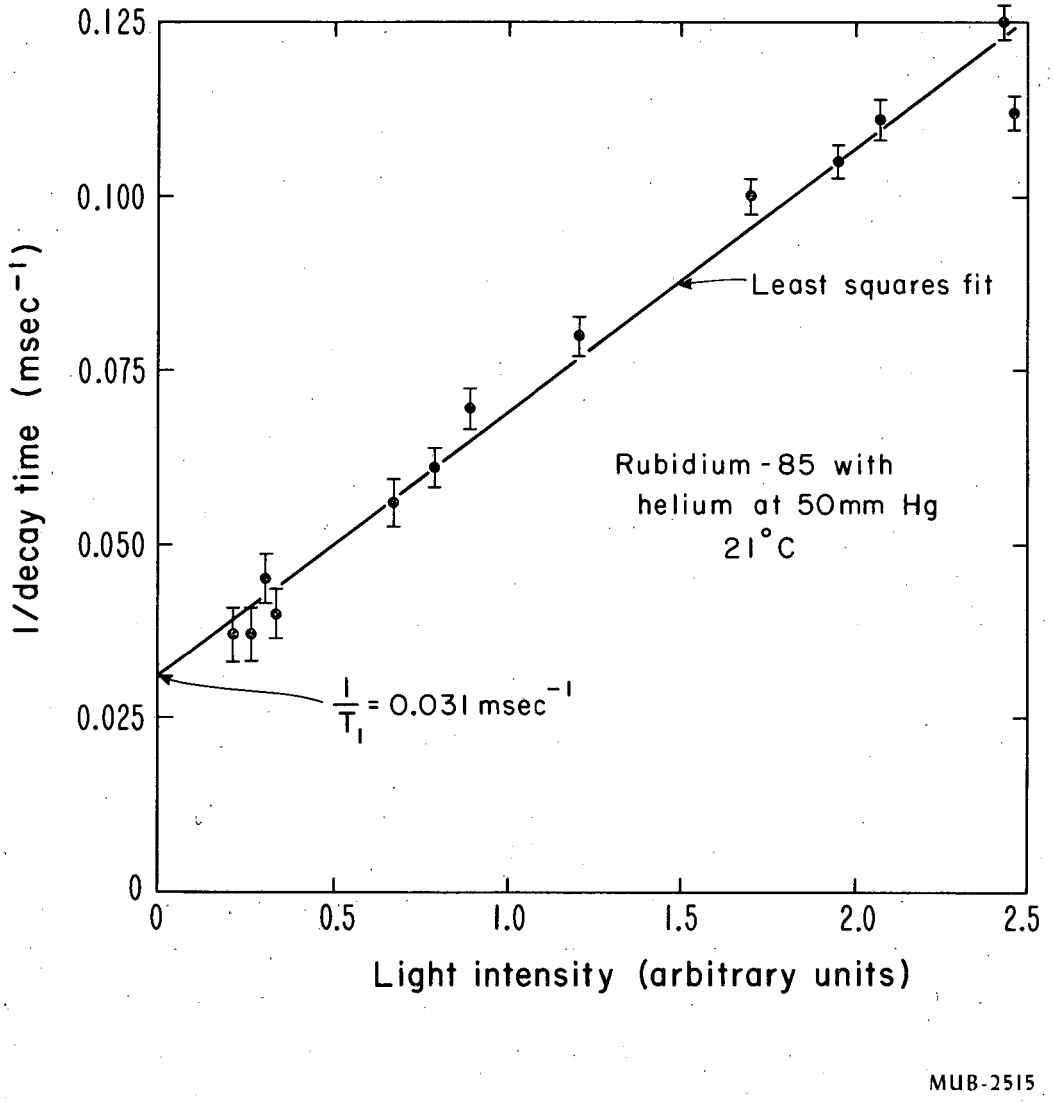

Fig. IV-2. Sample relaxation-time measurement for Rb^{85} in 5 cm Hg of He.

over the $F = 1$ state. The absorption can be determined from the light transmitted through the cell when the vapor is pumped and when it is not pumped, as for example when the rf is on. From the absorption, A, the density can be estimated from the expression for the absorption coefficient at the center of a Doppler-broadened line[10]

$$k_0 = \frac{2}{\Delta\nu_D}\sqrt{\frac{\ell n\, 2}{\pi}}\ \frac{\lambda_0^2}{8\pi}\ \frac{N}{\tau}$$

and the length of the cell L, provided the absorption is low enough that $e^{-k_\nu L} \approx 1 - k_\nu L$. In that case

$$A \approx \frac{(\Delta\nu)_{\text{emission}}}{\Delta\nu_D}\, Lk_0$$

or

$$N \approx \frac{(\Delta\nu_D)^2}{(\Delta\nu)_{\text{emission}}}\ \frac{4\pi\tau}{\lambda_0^2 L}\sqrt{\frac{\pi}{\ell n\, 2}}\ A.$$

The method is described below.

If an alkali absorption cell having an infinitely long ground-state relaxation time is pumped with circularly polarized $P_{1/2}$ resonance radiation, the entire population is placed in the $m_F = \pm F_{max}$ level according to whether right circularly polarized light, σ^+, or left circularly polarized light, σ^-, is used. In either case a state of 100% polarization is achieved and the vapor ceases to absorb light so that the cell transmits the incident radiation, I_0, unattenuated except for absorption in the cell windows. The transmitted light intensity is then

$$I(100\%\,\text{polarization}) = I_0\,(1 - A_g),$$

where A_g is the attenuation due to the windows. If the polarization is somehow destroyed, the vapor becomes absorbing and the transmitted light intensity is

$$I(0\%\,\text{polarization}) = (1 - A_g)(1 - A_v)\, I_0,$$

where A_v is the attenuation of the vapor. Thus,

$$\frac{I(0\%\,\text{polarization})}{I(100\%\,\text{polarization})} = 1 - A_v. \tag{16}$$

This result can be corrected for differences in the emission- and absorption-line widths by multiplying A_v by $(\Delta\nu)_{\text{emission}}/(\Delta\nu)_{\text{absorption}}$.

In practical situations the relaxation time is always finite and only partial polarization is attained. The above result must be corrected for the absorption which takes place even when the vapor is pumped. The parameter describing the absorption is β, the equilibrium relative-absorption probability; it is related to the ground-state level populations p_i by

$$\beta = \sum_{i=1}^{n} r_i p_i(\infty), \tag{17}$$

where r_i is the relative absorption rate of level i. For an unpolarized ensemble p_i equals $1/n$, where n is the number of levels; hence $\beta(\infty)$ equals $\frac{1}{n}\sum_{i=1}^{n} r_i = 1$ as $\sum r_i = n$. For a completely polarized ensemble, p_i equals 0, with i = all m except $m = F_{max}$ but $r_{F_{max}} = 0$; hence β equals 0. The populations are governed by the rate equations

$$\dot{p}_i = \sum_j B_{ij} p_j + \frac{1}{nT\beta_0}, \tag{18}$$

where b_{ij} are relative transition rates. At equilibrium p_i equals 0; hence

$$\sum_j B_{ij} p_j(\infty) = -\frac{\rho}{n}. \tag{19}$$

This system of equations has been solved by computer and the quantity β computed as a function of ρ. The results for an alkali of nuclear spin I = 3/2, for both no reorientation and complete mixing in the P state, as well as electron randomization, are shown in Fig. II-7.

We now derive the correct expression for A_v. The light transmitted by the cell when the polarization is zero is again

$$I(0) = I_0 (1 - A_g)(1 - A_v);$$

when the polarization is finite, we replace A_v by βA_v. Then $I(P) = I_0 (1 - A_g)(1 - \beta A_v)$. Thus

$$\frac{I(0)}{I(P)} = r = \frac{1 - A_v}{1 - \beta A_v}$$

or

$$A_v = \frac{1 - r}{1 - \beta r} \quad . \tag{20}$$

If the emission-line width is not the same as the absorption-line width, A_v is replaced by $[(\Delta\nu)_{\text{emission}}/(\Delta\nu)_{\text{absorption}}]\ A_v$.

Prior to making absorption measurements it is necessary for one to determine the appropriate values of ρ, which may be done as follows: Pumping times, τ, are measured as a function of light intensity and their reciprocal is plotted against the light intensity. It has been shown that if the absorption cell contains no buffer gas the pumping process may be described by a single exponential with a decay rate for $I = 3/2$ of $\lambda = 0.35\ \beta_0 + \frac{1}{T} = \frac{1}{\tau}$. As β_0 is proportional to the light intensity, extrapolation of the measured $(1/\tau)$ to zero light intensity yields T^{-1}. Moreover, the slope of the line determines β_0. Thus $\rho = 1/T\beta_0$ is determined. If some other means were available for measuring T_1 as for example a Franzen type experiment, then a single pumping time would be all that were needed to determine β_0. In case the absorption cell contained enough buffer gas to completely mix the excited state, then the pumping transient consisted of two exponentials, the longest of which has a decay rate of $\lambda = 0.108\ \beta_0 + 1/T$. If the P state were only partially mixed, then the two extreme values of ρ could be used to fix limits on the absorption.

A typical absorption measurement is shown in Fig. IV-1. The purpose of the rf is to destroy the polarization by resonating the Zeeman sublevels. Sufficient rf power must be used to equalize the populations. The amount of power required depends on the intensity of the pumping radiation; the more intense is the light source the more rf power is required. In practice one should determine the rf power needed for the most intense light anticipated on the basis of a plot such as Fig. IV-3. Here the transmitted light is measured as a function of rf current, showing saturation of the resonance. A quicker way to determine the rf level needed is to observe the rf-induced decay of the transient. The power should then be adjusted so that the decay time is much shorter than the pumping time.

Table IV-1 and Fig. IV-4 show the results for a Rb^{87} spherical 200-ml absorption cell having no buffer gas but a wall coating. A typical pumping transient from which Fig. IV-4 was obtained is shown in Fig. IV-5.

From the slope of the line in Fig. IV-4 we can calculate the absolute light intensity. We have $0.35\,\beta_0 = (3.65\times10^{-4})\,I$ or $\beta_0 = (0.001\,I)$ $msec^{-1}$, but $\beta_0 = I_0 \frac{\pi e^2}{mc} f$ with $f = 1/6$, the oscillator strength. Thus $\beta_0 = 8.8\times10^{-3}\, I_0 = I/sec$ or $I_0 = 2.28\times10^{2}\, I$ photons/cm^2-sec-cycle at the center of the line. For the maximum light intensity used, I is about 400 and I_0 is about 9.2×10^{4} photons/cm^2-sec-unit frequency interval.

The value of equilibrium absorption deduced here is based on a theory for which no absorption is assumed. However, to the extent that "some" absorption does not seriously alter the phenomenological rate equations, β is correct. What we mean by "some" can be inferred from the distortions observed in the pumping transients as the density of absorbing atoms is increased. Figure IV-6 exhibits pumping transients in the same spherical 200-ml wall-coated absorption cell as a function of temperature. Up to about 40°C the transients are exponentials with decay times corresponding to the average light intensity across the cell, as can be inferred from Fig. IV-4. At 40°C the absorption is about 20%. It is likely that spin exchange plays a prominent role in the distortion observed above 40°C.

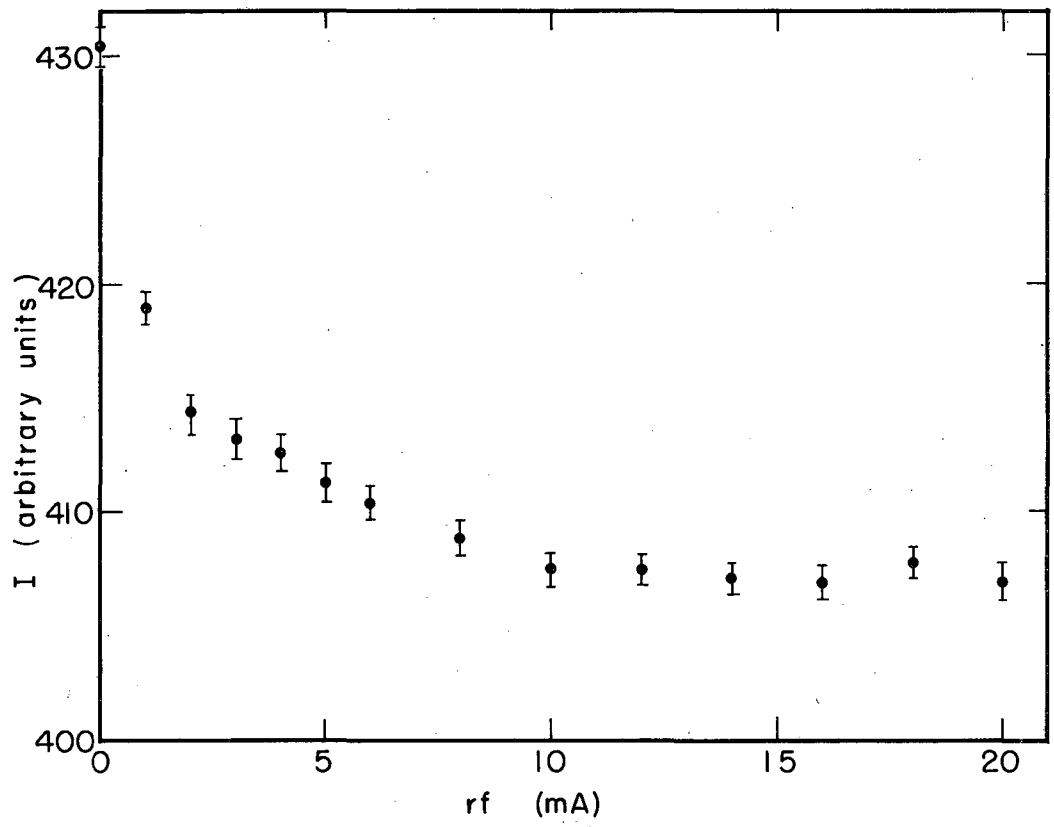

Fig. IV-3. Determination of rf level needed to equalize the populations of the ground state of Rb^{87}.

Table IV-1. Determination of absorption by optical pumping. The absorption of $\approx 6\%$ corresponds to a Rb^{87} density of $\approx 10^9$ cm^3.

I						
rf on	rf off	r[a]	β_0 ($msec^{-1}$)	ρ	β	$A = \frac{1-r}{1-\beta r}$
355.7(1)	374.1(1)	0.951	0.356	0.066	0.190	0.060
299.9	314.6	0.953	0.300	0.079	0.216	0.059
243.1	255.0	0.953	0.243	0.097	0.252	0.062
204.0	213.7	0.954	0.204	0.115	0.282	0.064
172.0	180.3	0.954	0.172	0.137	0.320	0.066
171.2	179.5	0.954	0.171	0.138	0.321	0.066
147.0	153.3	0.959	0.147	0.160	0.355	0.062
86.2	894.0	0.964	0.086	0.274	0.483	0.067

[a] Here r is the ratio $\frac{I\,(rf\ on)}{I\,(rf\ off)}$.

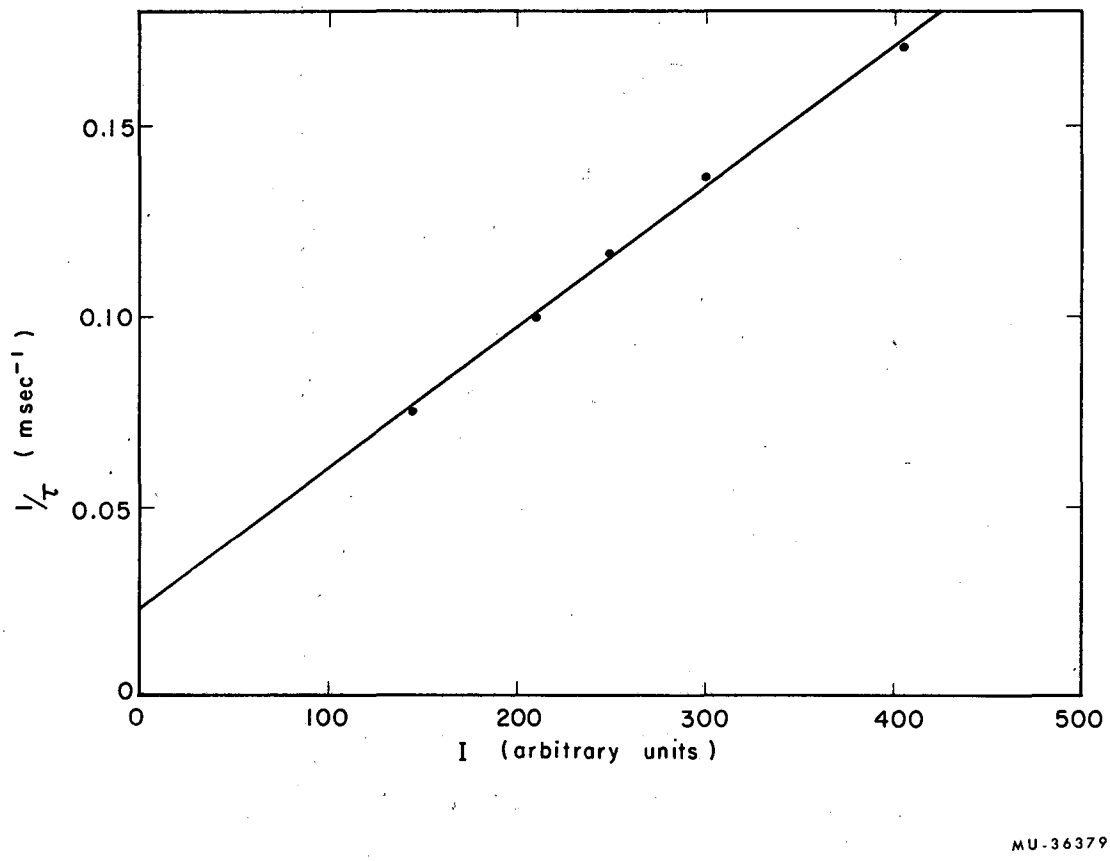

Fig. IV-4. Measurement of β_0 and ρ in a 200-ml spherical wall-coated absorption cell with Rb^{87} at 25 °C. $\beta_0 = 0.001\ I$, $\rho = 24/I$.

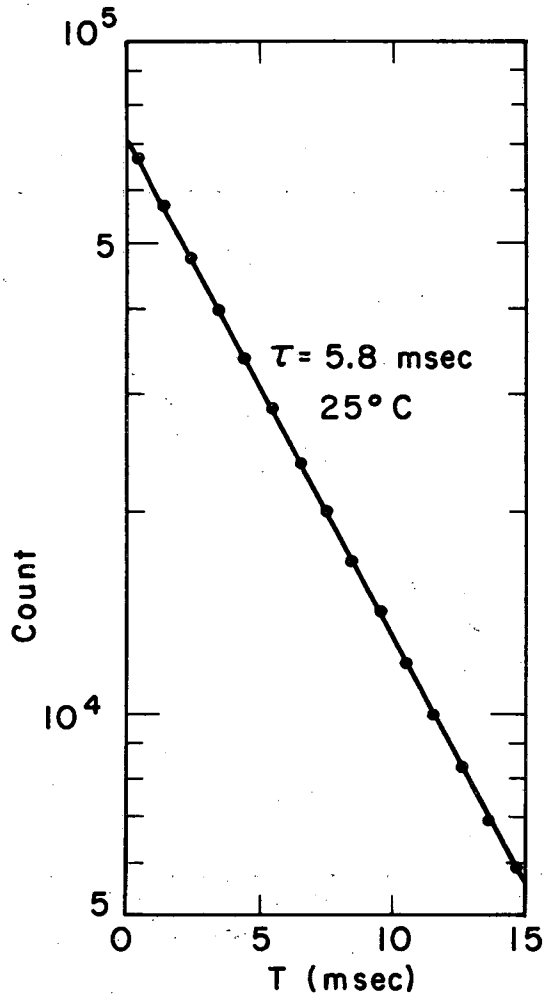

Fig. IV-5. A typical optical pumping transient from which Fig. IV-4 was obtained.

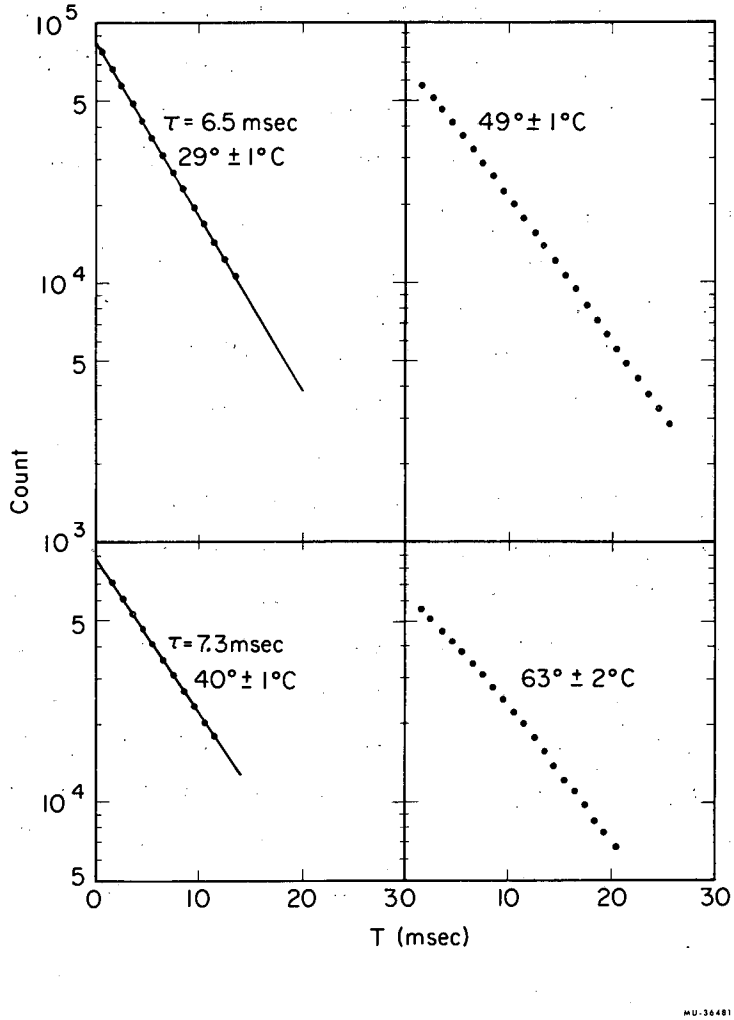

Fig. IV-6. Distortion of a Rb^{87} pumping transient by excessive absorption and/or spin exchange.

6. Summary of Experimental Procedure

The first step of our experiment was the determination of β_0. A Dehmelt type of experiment was performed in the evacuated cell and from the slope of the line of $1/\tau$ vs I, β_0 was obtained. If m is the slope and I the light intensity (arbitrary units), then $\beta_0 = mI/0.35$ for Rb^{87}. In the second stage of the experiment buffer gas was introduced into the cell and the cell isolated from the diffusion pump. For each value of buffer-gas pressure, pumping transients were observed for several values of the light intensity I. The light intensity was varied by insertion of glass plates between the resonance lamp and the circular polarizer. At the beginning and end of each observation the light intensity was measured by integrating the output of the lamp for 10 sec and repeating 5 to 10 times. The light intensity ascribed to each transient was the average of the average light intensity at the beginning and end of each observation; if the light intensity changed by more than $\approx 3\%$ over the run, the transient was rejected. The digital output of the mcs was fitted to two exponentials by the least-squares method to determine the best values of the decay constants and corresponding amplitudes. The smallest decay rate $(1/\tau_1)$ was extrapolated to zero light intensity to yield $1/T_1$ for each value of buffer-gas pressure. Amplitude ratios were tabulated along with the corresponding values of ρ, β_0, and gas density, and these data then interpreted in terms of cross sections.

B. Apparatus

In this subsection we describe the experimental apparatus, which we conveniently divide into three parts: (a) the vacuum and gas-delivery system, (b) the optical pump, and (c) the detection system.

1. Vacuum and Gas-Delivery System

In order to obtain enough statistics to resolve the transient pumping signal into its exponential components, it is necessary to isolate the absorption cell, at some particular value of foreign gas pressure, from the diffusion pump for periods ranging from a few minutes to many hours, depending on the initial signal-to-noise ratio.

For this reason it was deemed necessary to use a bakeable vacuum system with all metal values. A schematic diagram of the vacuum assembly is shown in Fig. IV-7. That portion of the assembly above the diffusion pump (beginning with the liquid nitrogen trap) was baked by an oven suspended above the assembly by means of a counterweight. To permit high temperatures $\geq 250°C$, the Vitron O-rings of the valves were removed and replaced with copper gaskets and the Teflon valve seats were replaced by ones of indium metal. As indium has a low melting temperature, 156.4°C, it would reseat the valve during bake-out; furthermore, by closing of the valve while it was hot, a hermetic seal could be formed as the indium solidified, although this was not found necessary in practice. Baking the vacuum system at 250°C for about 24 hours was usually sufficient to outgas the metal parts, principally the Veeco valves, but not the glass. If valve A were closed after baking, the pressure would quickly rise to $\approx 2\times10^{-4}$ mm Hg. This rise was traced to outgassing from the glass, in particular from the ion gauge (Veeco RG75P). For this reason, heating tape was wrapped around the glass portions of the vacuum system, exclusive of the resonance cell, between valves A and B and outgassing continued at $\approx 360°C$ until a pressure of $\approx(4\times10^{-6})$ mm of Hg could be sustained for a few hours with valve A closed. The gas-delivery system was outgassed by a torch. It was not possible to outgas several portions of the gas-delivery system because of the proximity of graded Pyrex valves. In addition to through-outgassing, one other precaustion was taken to ensure a good clean vacuum. Two barium gettering tubes, a schematic of which is shown in Fig. IV-8, were fired up from time to time and were found helpful when working with Rb and to remove impurities from the gas. When we were working with Cs the Ba getters were not needed as Cs itself is an extremely good gettering agent. Rubidium is also a good getter but as only a few mg of the enriched isotope, Rb^{87}, were available per cell, it was essential to have a clean vacuum before the Rb^{87} was introduced to the absorption cell. Enough Ba was removed from the absorption cell so that there was no noticeable effect on the Rb vapor pressure; i.e., there was no indication

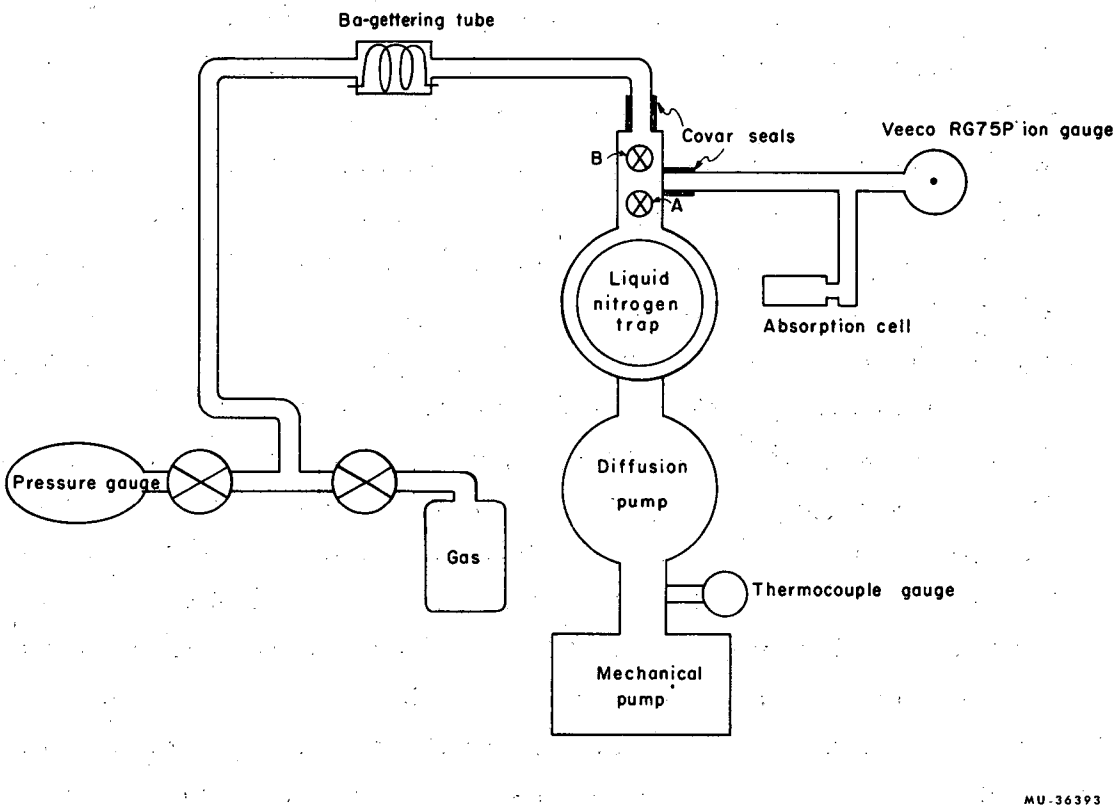

Fig. IV-7(a). Block diagram of vacuum and gas-delivery system.

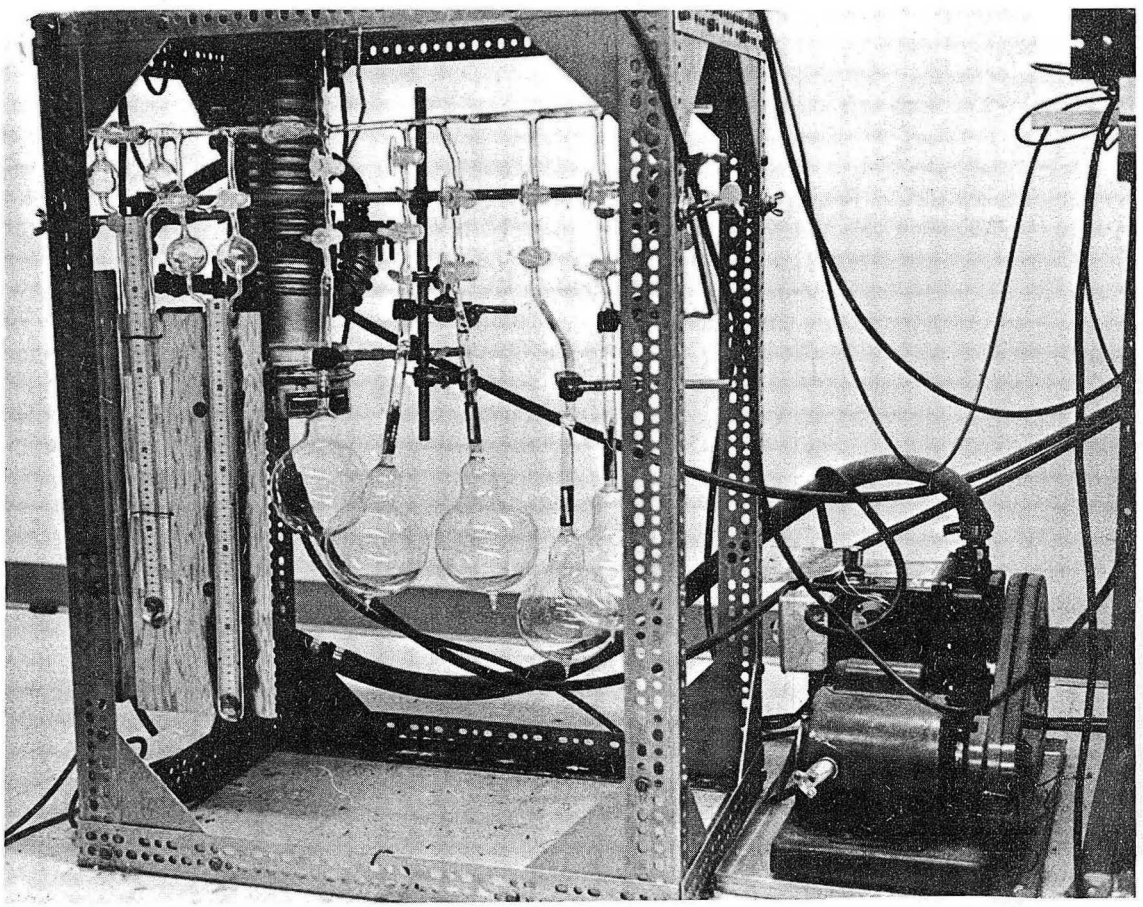

ZN-5083

Fig. IV-7(b). Photograph of vacuum and gas delivery system.

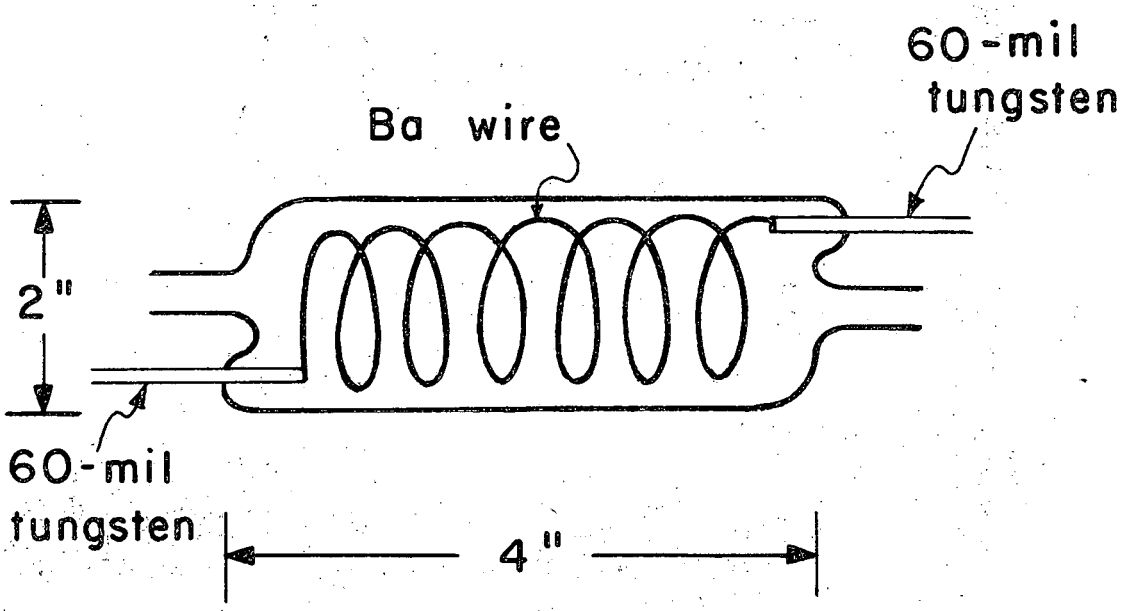

Fig. IV-8. Ba-gettering tube (not to scale).

that Ba was diffusing into the absorption cell.[22]

The gas-delivery system consisted of an oil manometer, a mercury manometer and up to five 1-liter atmosphere flasks of noble gases obtained from Linde and having a purity of $\approx 1:10^5$. We used the oil manometer principally when making measurements on the heavier noble gases, Kr and Xe, since low pressures are involved (up to about 3 cm (Hg) whereas in most other instances involving pressures in excess of 4.5 cm we used the mercury manometer. To permit fine control over the pressure, each flask was followed by two graded 2-mm valves separated by a length of tubing 7 cm long and 2 mm inside diameter. In this way, a slug of gas could be introduced into the space between the valves and the flask then isolated prior to opening of the top valve. The ratio of the volume filled by the gas to the volume between the valves was about 500:1 so that the pressure changed by no more than $\approx$1.5 mm per slug. A schematic of the gas-delivery system is shown in Fig. IV-7 (a) and a photograph of the whole vacuum system in Fig. IV-7(b).

2. Optical Pump

a. Resonance lamp

The essential consideration in selecting a resonance lamp is stability against long-term drifts, long with respect to the integration time for one transient (this varies from a few minutes to several hours). Short-term fluctuations (short with respect to the integration time) average out in the integration and in principle may be ignored. However, since excessive noise may jam the detection system when operated with maximum gain (see below), a highly stable low-noise lamp is desirable (if maximum gain is to be utilized). For these reasons a Varian lamp was used.[22] The lamp oscillator was purchased from Varian, but the resonance lamps were made roughly according to the procedure outlined by Bell et al.[23] Several enriched Rb^{87}, Rb^{85}, and Cs lamps were made and filled with Kr at a pressure of 2 mm of Hg; this pressure was obtained simply by immersing the Kr flask in liquid nitrogen. The Rb isotopes were obtained from Oak Ridge National Laboratory in their chlorides, the Rb^{87} isotope having a purity of 99.16%. Figure IV-9 is a densitometer curve of a typical Rb^{87} lamp.[24]

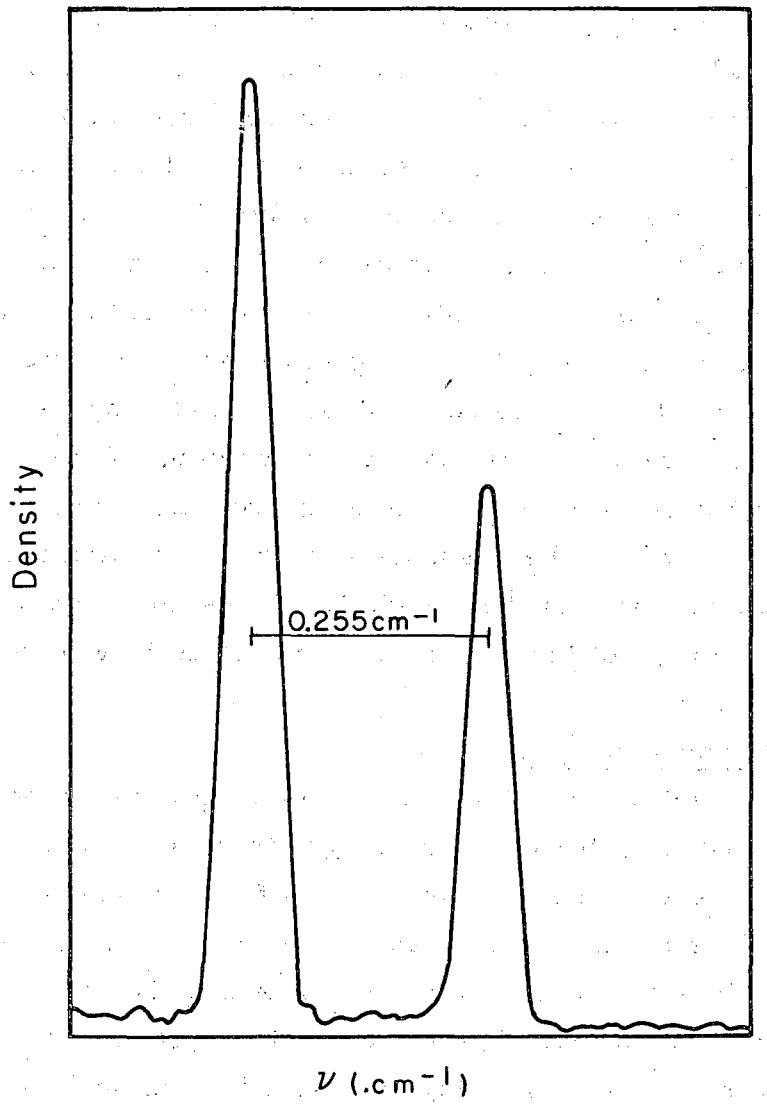

Fig. IV-9. Densitometer curve of Rb^{87} lamp (7947 Å).

We measured the stability of the lamps by integrating the light output for a specified length of time over periods of time much longer than the integration time; for example, the light output was integrated over 1-second intervals every second for 400 seconds. Such measurements were repeated for 5- and 10-second integration times, with typical results shown in Figs. IV-10 and IV-11. Figure IV-12 is the result of an unstable lamp, the instability being due to an excessive amount of Cs in the lamp. A schematic of the experimental arrangement is given in Fig. IV-1.

b. Absorption cell

Two considerations must be taken into account in the preparation of absorption cells: (a) The evacuated cell must have a reasonably long relaxation time ($\tau \geq 5$ msec), and (b) the cell must be optically thin. The former requirement means that a wall coating must be used, and the latter limits the size and temperature of the absorption cell. It has been pointed out that once the mean free path of an alkali atom becomes very small compared with the dimension of the cell ($\approx$ 1 mm Hg of foreign gas) the wall coating is ineffective, as an atom having once collided with the wall is likely to make many more collisions before entering the pumping region again.[1]

Spherical Pyrex cells ranging from 25 to 500 ml were tried with both Rb and Cs; for Rb, satisfactory results were obtained with a 200-ml cell at the operating temperature of $\approx$24°C. The length of the optical path, $\approx$ 6 cm, made possible enough absorption to produce a good signal, yet not so much absorption that the cell could not be regarded optically thin. For Cs the results were less satisfactory and smaller cells ranging from 50 to 100 ml were used. Because an appreciable amount of light is reflected and conducted by the surface of the spherical cells, we used cylindrical cells for the disorientation cross-section measurements since it is important to have high light intensity. The flat ended cylindrical cells were Pyrex, about 4 cm long and 6 cm in diameter for Rb, and about 1 cm long and 6 cm in diameter for Cs. The alkali or alkali chloride plus reducing agent, was contained in a side arm, and the wall-coating material (Paraflint) was in a side arm followed by a distillation chamber.

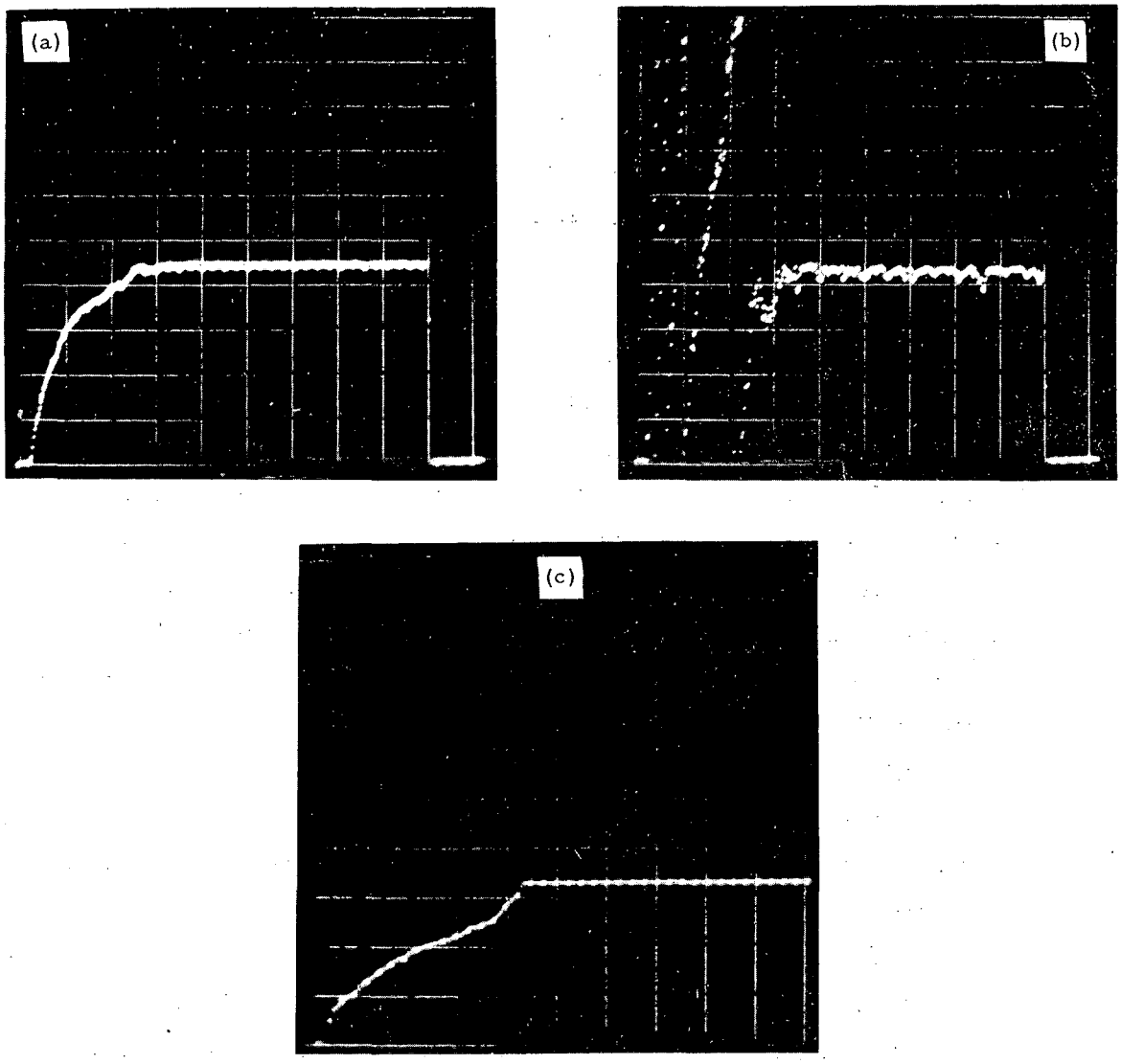

ZN-5086

Fig. IV-10. Stability of Varian lamp. (a) Rb^{87} lamp warming up and equilibrating. Horizontal scale is 400 sec/div, vertical scale 100 000 counts/div. (b) Amplification of (a) with vertical scale 10 000 counts/div showing scatter of about 0.7%. An integration time of 10 sec/chn was used. (c) Same as (a) except lamp has enriched Rb^{85}. Scale is 200 sec/div.

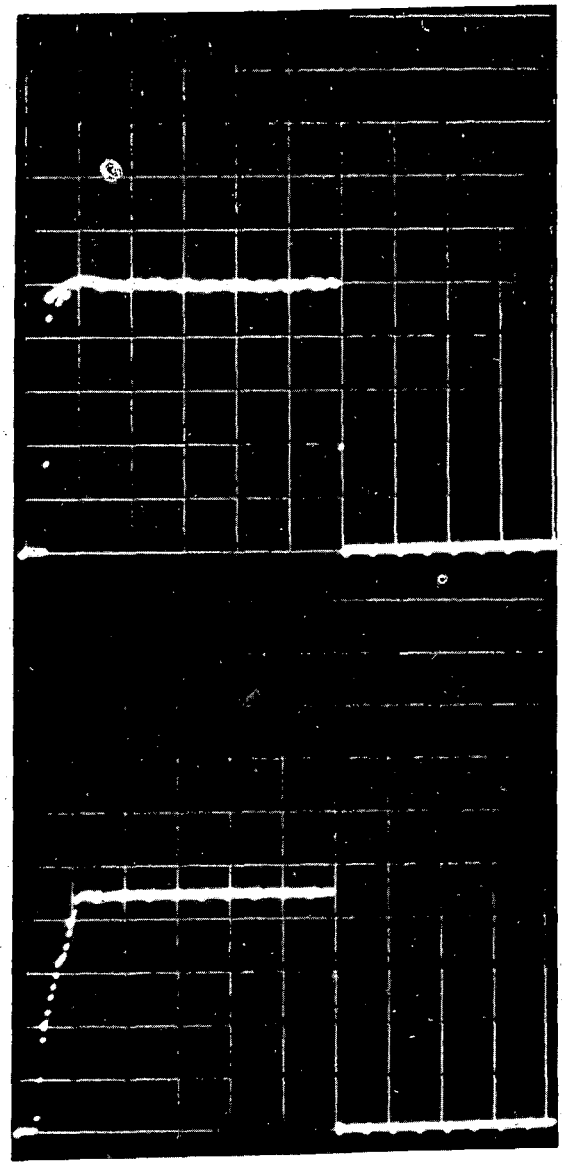

ZN-5081

Fig. IV-11. (Upper) A Cs lamp warming up and equilibrating. (Lower) A Rb^{87} lamp warming up and equilibrating. Lamp shell in both upper and lower was warm prior to turning-on.

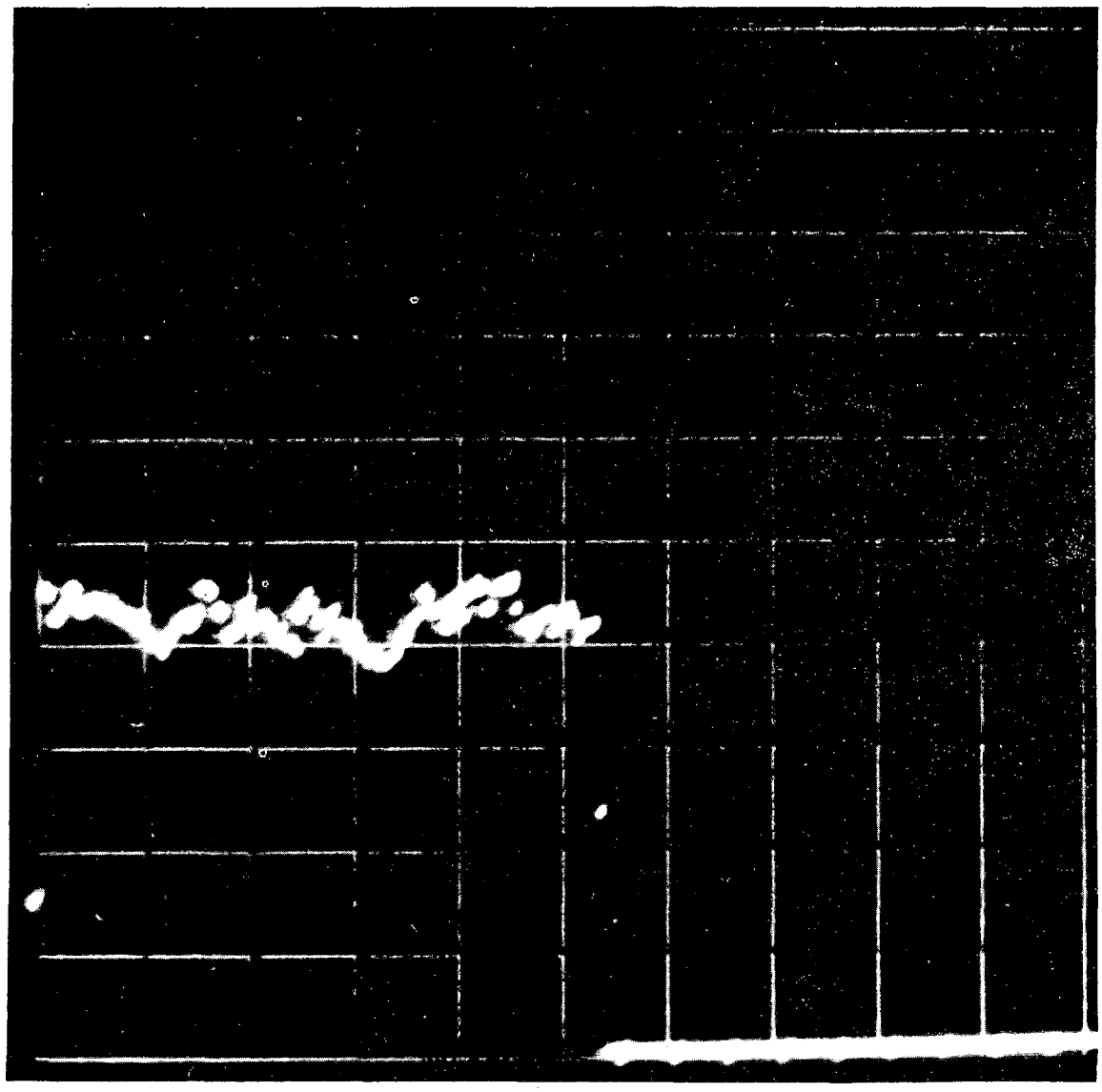

ZN-5082

Fig. IV-12. An unstable Cs lamp. Instability is due to an excessive amount of Cs.

Although the cells were usually clean when they left the glass-shop annealing oven, if they were not, they were cleaned with acetone. Once the cells were mounted on the vacuum system, the Paraflint was gently heated to drive out trapped air; at the same time the alkali chloride was also heated to drive out its water of hydration. Following this the Paraflint was distilled from the side arm into the distillation chamber and the side arm was then sealed off. At this point the pressure was about 10^{-4} mm of Hg. After reaching a pressure of 10^{-5} to 10^{-6} mm of Hg, the cell was outgassed by a torch at as high a temperature as possible without cracking the glass.[25] Outgassing continued at intervals until the pressure remained at about 10^{-6} mm with the cell at maximum temperature. Prior to this high-temperature outgassing, the vacuum system (from trap on up) was baked out at about 250°C by an over that was lowered over the vacuum apparatus and served to outgas the vacuum system and to further purify the Paraflint. However, it is possible that the effectiveness of the wall coating was altered during the long bake-out through fracture of the molecules.

c. Magnetic field H_0

A Helmholtz coil 25 inches in diameter provided the field H_0. Its current supply was regulated to better than a part in 10^4. No attempt was made to cancel local field gradients except to place the apparatus in the best place available. A Cs line-width measurement, shown in Fig. IV-13, was obtained by feeding the dc output of a phase detector into the Vidar and sweeping the field synchronously with the mcs.

d. Isotopes

The Rb^{87} isotope was obtained from Oak Ridge National Laboratory in its chloride form with a purity of 99.16%, the chief impurity being the other isotope, Rb^{85}. In preparing the absorption cell, about 4 mg of a particular isotope chloride were placed in a 10-mm quartz tube about 3 in. long along with the reducinb agent, calcium. The quartz tube was then joined to the Pyrex side arm of the absorption cell by means of a Pyrex-quartz graded seal. The quartz is necessary

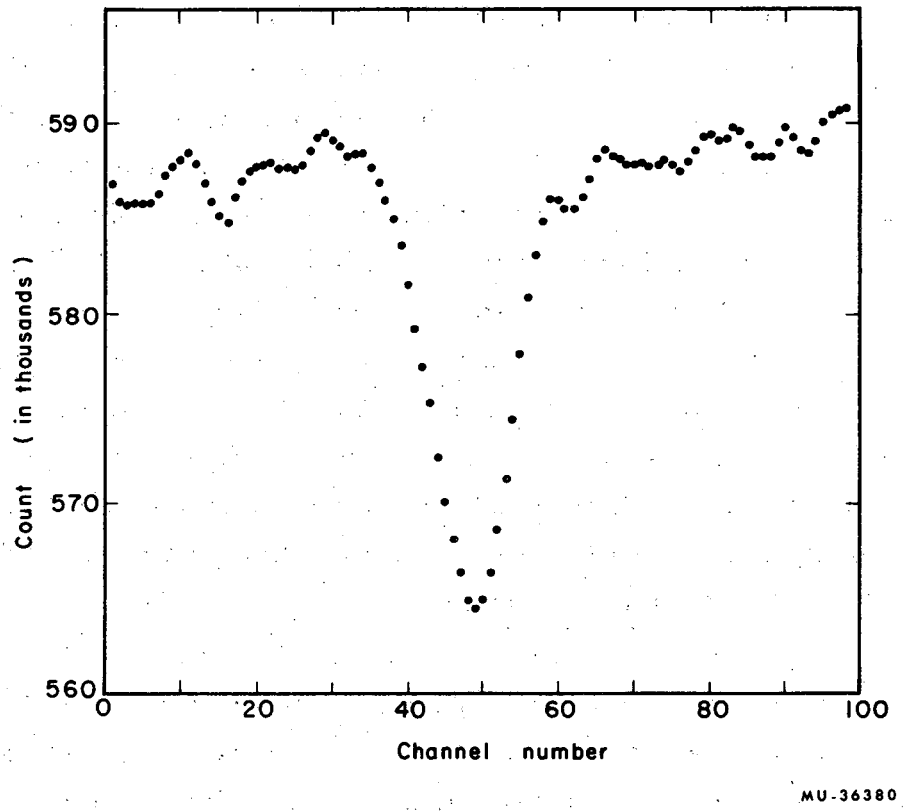

Fig. IV-13. Cs line width measurement in optical pumping apparatus. 0.56 kc/chn.

since Pyrex would soften at the temperature needed to reduce the chloride.

3. Detection System

A schematic of the detection system is shown in Fig. III-2. As the operation of the data-accumulation and detection apparatus was described in Sec. III, we discuss here the critical characteristics of the gadgetry. It was important that every piece of equipment associated with the detector have a response time that was fast (compared with the optical pumping transients) and was stable against drift, the criterion for stability depending on the integration time. We discuss below the various pieces of apparatus.

a. Detector

A Hoffman type 2A silicon detector was employed for picking up the pumping signals. The detector was placed behind a slit in a metal enclosure which was necessary to shield the Si diode from the rf. This detector has a 20-μsec recovery time, and the spectral response of the detector made it almost ideal for the Rb and Cs resonance lines, as it peaked at about 8200 Å. The noise output was very low. While in general the output of a semiconductor is not proportional to the incident light intensity, the response was linear for the small light-intensity changes encountered at resonance (absorption in resonance cell ≈ 2%). Infact, for the light intensities reaching the detector, the response was linear over the whole range of light intensities used. This made it possible for us to measure the incident light (in arbitrary units) with the same detector as was used for the transients. The linearity was determined by measuring the attenuation of several plates of glass together and comparing with the product of the attenuation of the individual plates measured separately (≈12% attenuation per plate). These two results differed by ≈1%, which was about the experimental error. Further tests were made by placing the lamp (with reflector removed) and detector on an optical bench and measuring the detector output as a function of the separation between the two. The response was inversely proportional to the square of the separation to < 1%. Noise in the output of the silicon cell was limited by the light source although the cell

was sensitive to temperature and could vary by as much as 2.2 mV/°C. Temperature drift was slow enough that it was of no consequence as far as transient response was concerned; but as the total light intensity was also measured with the cell, care was taken to operate at constant temperature.

b. Amplifier

The output of the silicon detector was fed into a Keithley 103 amplifier with the low-frequency cutoff (3 db point) set at 0.1 cps and the high-frequency cutoff at 100 000 cps (3 db point). This frequency response was ample for the transients encountered, as a Fourier analysis shows:

$$\text{Signal} = e^{-\lambda t} = \sum_{n=-\infty}^{\infty} c_n e^{in\pi\lambda t},$$

with $$c_n = \frac{\lambda}{2} \int_{-1/\lambda}^{+1/\lambda} e^{-\lambda t} e^{-in\pi\lambda t}\, dt = (-1)^n \frac{\sinh 1}{1 + n\pi i}.$$

Thus the ratio of the amplitude of the $n/2\tau$ frequency component to the $1/2\tau$ frequency component, where $\frac{1}{\tau} = \lambda$, is

$$\frac{A_n}{A_1} = \frac{1 + \pi^2}{1 + n^2\pi^2} \approx \frac{1}{n^2}$$

for large n. Suppose, for example, that we have a transient with $\tau = 15$ msec and we want to find the largest value of n that we have to worry about if we require that the amplitude of this nth harmonic decrease a thousandfold. Then $(1+\pi^2)/(1+n^2\pi^2) = 10^{-3}$ and $n \approx 32$. This means that $32/(2\times15\times10^{-3}) \approx 1100$ cps, so that the required bandwidth is 30 to 1100 cps. The noise level at the input with terminals shorted is about 3-μV rms. A warm-up time of a few hours was necessary to stop the dc level from drifting. Stability of the dc output was important for reasons clarified below.

c. Voltage-to-frequency converter (v-to-f)

In order to store the signals in a multichannel scaler for the purpose of improving statistics, it was necessary to convert the voltage signals into a proportional pulse rate; the analyzer, in other words, does not "understand" voltages; it can only count. The instrument that converts voltages into a proportional pulse rate is a voltage-to-frequency converter (called a digital voltmeter when combined with a counter). Three important considerations in selecting such a unit are linearity, response time, and sensitivity. Stability is not an important consideration so long as the output frequency (for a given voltage) does not change appreciably in the time characteristic of a pumping transient sporadically, for such noise will not average out. Random fluctuations in the output average out.

At the time these experiments were undertaken, a Dymac with a 100 000 maximum pulse rate and a 0.1-V range (among others) was tried and found satisfactory; however, most of the data were taken with a Vidar 240A. The specifications of the Vidar are not quite as good as the Dymac, but the difference is not significant for our purposes; the Vidar is simpler to operate. We quote here the specifications of the Vidar: output frequency range 0- to 100 kcps; signal range 0-to 0.1 volt (among others), therefore 1-μvolt sensitivity;[26] linearity better than 0.025% of full scale from best zero-based straight line; long-term drift less than ± 0.1% per week; drift with temperature less than ± 0.01% per °C, 0°C to 50°C.

So far nothing has been said about the response time of the converter. According to the maker, the V-to-f responds to a change in voltage within one cycle of the final frequency output. For example, if the Vidar is set on the 0.1-V scale and the input voltage is changed instantaneously from 0.05 to 0.10 V the frequency output will change from 50 000 cps to 100 000 cps in 10 μsec. For this reason, it is important to ride the signals on a dc level that is a large portion of the V-to-f full-scale setting, care being taken to keep the signal level small enough so that the input to the Vidar does not exceed the full-scale rating. In this way, the response time can be kept small and approximately

constant over the whole signal. In practice, the dc level of the Keithley amplifier was adjusted so it was about 70% of the full-scale setting of the V-to-f, and the gain was adjusted so the signal comprised no more than 30% of full scale. Thus the response time of the V-to-f was kept under 20 μsec. It is this characteristic of the V-to-f that necessitates a steady dc output from the amplifier. A drift in the dc level could on the one hand jam the Vidar by exceeding the maximum rating of the scale, and on the other hand could distort the transient by increasing the response time. In Appendix A we estimate the count loss resulting from time delay.

No attempts were made to check these specifications except that the response of the Vidar was checked by comparing signals reproduced by the analyzer with their sources. The results of such measurements and the experimental arrangement are described in Fig. IV-14, and testify to the capability of the Vidar.

d. Multichannel scaler

The multichannel scaler is the heart of the data-accumulation system. It receives the V-to-f output, a counting rate which changes in direct proportion to the signal, and performs a gross count. This count is interrupted in fixed intervals (a millisec, for example), and the total count accumulated in each interval is stored in a different channel of the analyzer, the register being cleared at the end of each interval. For example, the count between $t = 0$ and $t = 1$ msec is stored in channel 1; the count between $t = 1$ msec and $t = 2$ msec is stored in channel 2; and so on. In this way the signals are digitized. By piling many signals on top of one another in such a way that each point in the evolution of the signal always falls into the same channel of the analyzer, a large signal-to-noise ratio can be built up since the signals are then in phase, whereas the noise is not. The signal appears superposed on top of a large background that is due to the dc input to the V-to-f. This background is flat as can be seen in Fig. IV-15 which was obtained by connecting a battery to the input terminal of the Vidar.

A pulse-height analyzer (pha) with a 10^6-memory capacity RIDL34-12B operating in time mode served as the multichannel scalar.

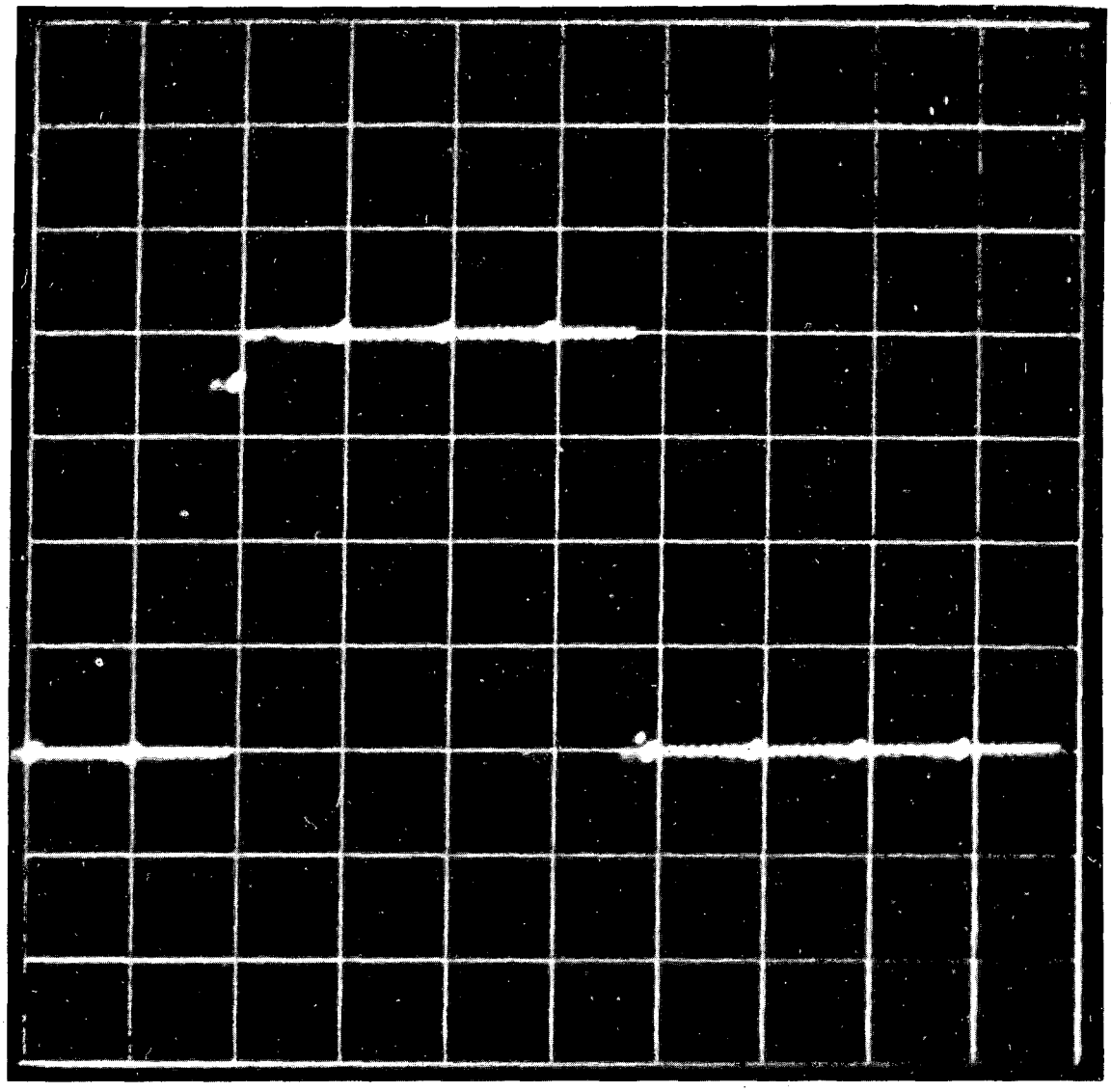

ZN-5078

Fig. IV-14. Recovery of a square wave by the mcs. The square wave was fed directly into the Vidar atop a dc level. Scale 1.0 msec per major division.

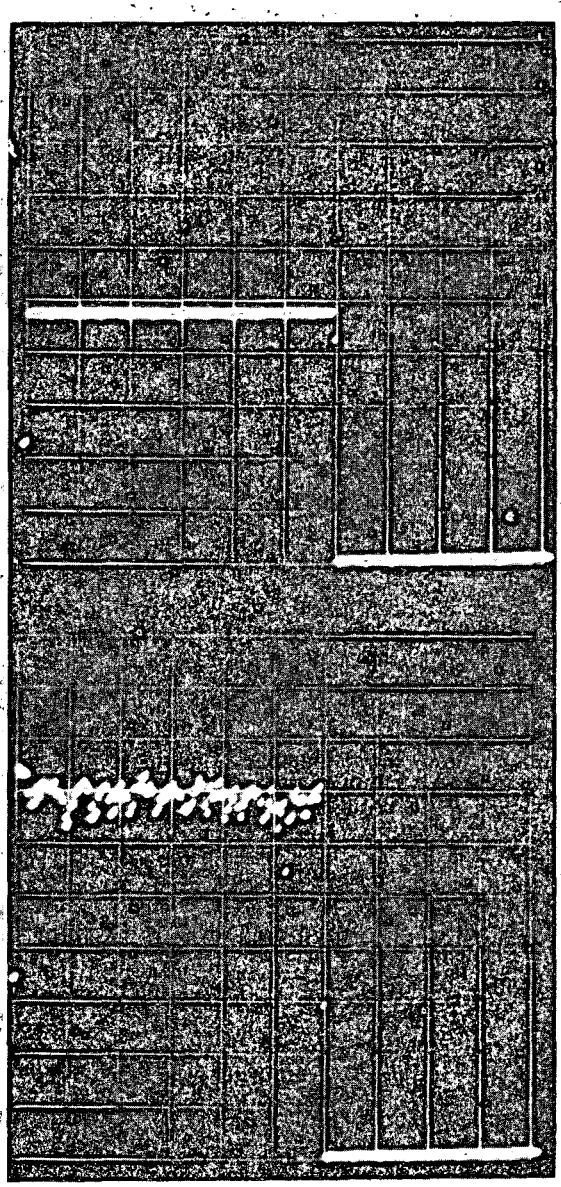

ZN-5080

Fig. IV-15. Noise output of Vidar. (Upper) Vidar output integrated for 10 sec/chn with battery at input. (Lower) Amplification of upper, showing scatter due to fluctuations of Vidar output (≈0.02%). Vertical scale 50 000 counts/div for upper and 100 counts/div for lower.

This pha had a 1 mc/sec scalar and a 10-μsec cycle time, which means that a maximum of one count per channel was lost in scaling (since the output of the Vidar is 100 kcps). Associated with the RIDL was much external circuitry used to synchronize the scalar with the signal, control the data-sampling interval--i.e., the channel advance rate--and shape the pulses going into the analyzer. The signal was phased by taking the pha-produced overflow signal after it reached the last channel and using it to gate the rf off so that a new pumping signal commenced synchronously with the sweep of the analyzer. About halfway through the sweep the rf was turned on, equalizing the Zeeman populations of the pumped sample in preparation for the next pumping transient. The external circuitry associated with the analyzer is shown in Fig. III-2 and is self explanatory. A photograph of the electronics is shown in Fig. IV-16.

e. rf Supply and rf gate

The pumping transients were generated in rapid succession by pulsing an rf source tuned to the Larmor precession of the alkali atoms. Since the magnetic field H_0 was not particularly homogeneous and sufficient power was used to broaden the resonance, the Zeeman resonances overlapped and the rf pulse equalized the Zeeman populations. For an rf supply a Tektronix 190B rf generator was used. This source was followed by a linear gate having a rejection ratio of >200:1 and a gating time of < 10 μsec (Fig. IV-17). The gate was actuated by the pha in a manner described above and shown in Fig. III-2. Following the gate were two IfI amplifiers, a 510 and a 500, which delivered the power to the rf coil placed about the resonance cell. Schematic diagrams for these two gates are shown in Figs. IV-18 and IV-19. The one in Fig. IV-18 was designed to operate in the frequency range of about 0.5 to 4 mc/sec and worked best when actuated by a symmetrical square wave. Application of a nonsymmetric square wave resulted in distortion of the rf wave form and hence loss of power (at the fundamental frequency). For frequencies below 0.5 mc/sec and above 4 mc/sec, the gate shown in Fig. IV-19 was used. Although this gate had a bandwidth of 0 to about 50 mc/sec, it could not handle much power,

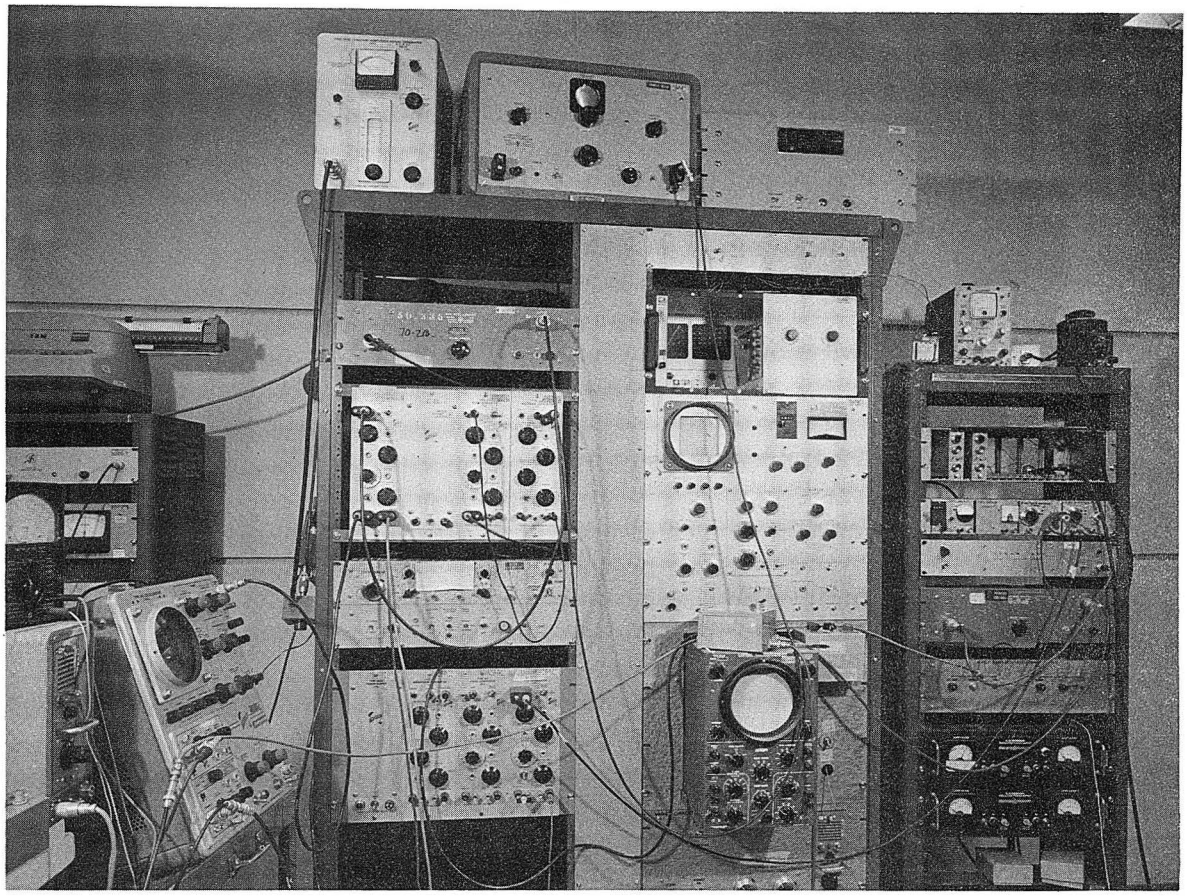

ZN-5075

Fig. IV-16. View of electronics (If I and Keithley amplifiers not shown).

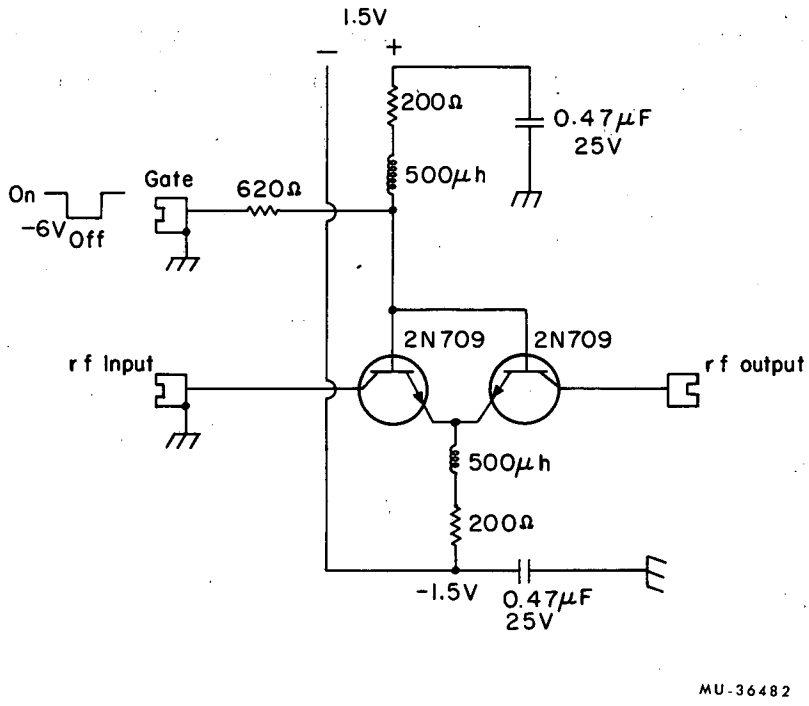

Fig. IV-19. rf gate, ≈ 0 to 50 Mc/sec; designed by M. Nakamura.

so that more amplification had to follow it.

The rf power required can be estimated from the condition $\gamma H_{rg} T_1 \approx 1$ (from first-order perturbation theory for a spin-1/2 system). Neglecting the nuclear spin γ = 1 Bohr magneton and taking $T_1 = 10^{-3}$ sec, we find the shortest relaxation time anticipated, $H_{rf} \approx 0.4 \times 10^{-3}$ gauss. The power density that must be delivered to the spin system is then $\frac{\omega}{8\pi} H_{rf}^2 \approx 4 \times 10^{-9}$ watts/cm^3-unit frequency interval. Dissipation in the circuit is $\approx$ 1 watt.

V. EXPERIMENTAL DATA AND RESULTS

A. Results for Rb^{87}

1. Rubidium-87—Argon

Rubidium-87 optical pumping transients were studied in a cylindrical Pyrex absorption cell 6.0 cm in diameter and 3.0 cm long. Argon pressures ranging from 1.8-cm Hg to 17-cm Hg were covered and for each value of Ar pressure transients were observed for three or more values of the light intensity, I, to determine the ground-state relaxation times. Experience has shown that when the absorption cell is stable, three points are sufficient. The digital output of the mcs was analyzed by computer to determine the best values of the lifetimes and amplitudes. From the variation of the long lifetime with light intensity T_1 was determined, and from the variation of the amplitude ratio A_2/A_1 with buffer-gas density the excited state relaxation was determined. The total absorption in the cell, determined to be $\approx 2\%$ by the rf technique, corresponded to a Rb^{87} density of $\approx 10^9/cm^3$.

Figures V-1 to V-7 and Table V-1 summarize the data for Ar. Halfway through this run the pressure failed and it was necessary to drive more Rb^{87} into the cell. Because of a slightly heavier layer of Rb on the cell walls, or possibly through a shifting of the wall coating while the cell was warmed by the flame driving the Rb from the side arm into the cell, the intensity of pumping radiation inside the cell was changed. Moreover, as the intensity of light was monitored through the cell the reading for a given incident light intensity may have changed due to a change in the absorption occurring at the cell walls. We decided to redetermine β_0 before continuing the run after the pressure failure. Thus for data taken at 1.8-, 5.1-, 10.3-, and 17-cm Ar, $\beta_0 = 0.00065\ I$, and for data taken at 2.6-, 3.5-, and 16.5-cm Ar, $\beta_0 = 0.00057\ I$.

In doing a least-squares analysis of the data we have adopted the criteria that a minimum of two lifetimes of the slowly decaying exponential be given the computer and that this lifetime as determined by the computer agrees closely with the graphical value obtained from the

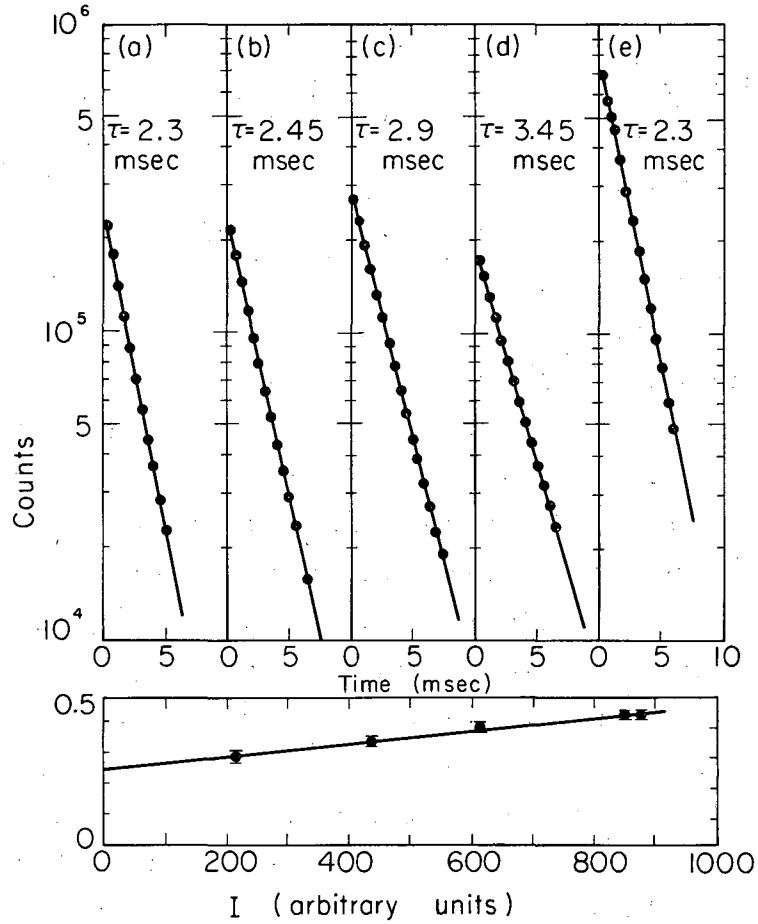

Fig. V-1. Determination of β_0. Note that in (e) the light intensity is measured with rf on and rf off. The difference of 0.7% when corrected for finite relaxation time is the absorption in the cell. (a) I = 848.7, (b) I = 610.6, (c) I = 438.0, (d) I = 210.9, (e) I(rf on) = 858.6, I(rf off) = 864.7, (f) β_0 = 0.000652 I, 24°C. Note the exponential nature of the transients.

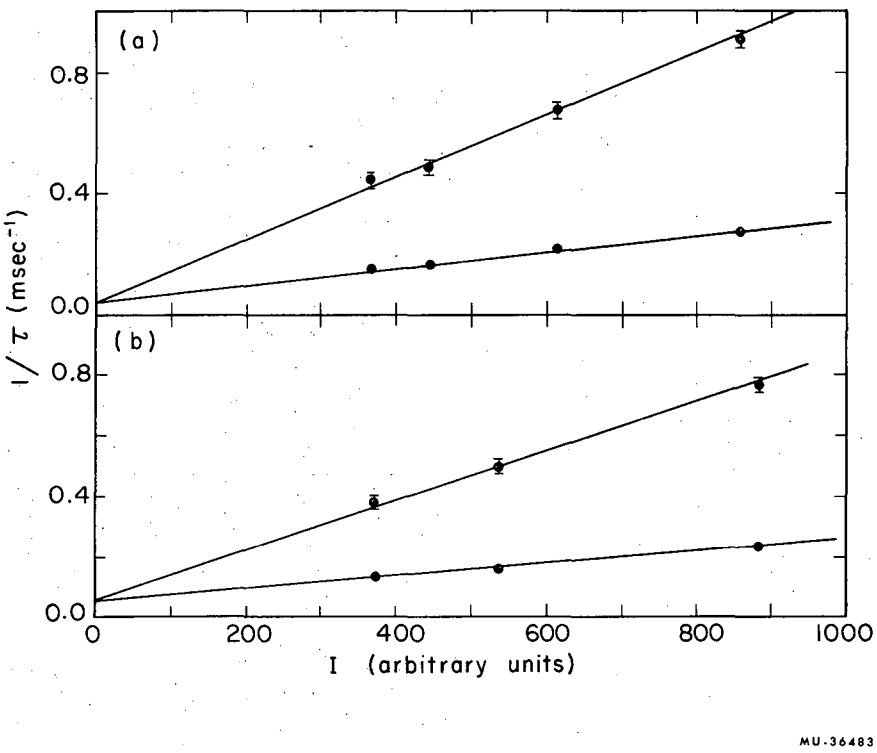

Fig. V-2. Relaxation-time measurements for Rb^{87} in Ar. Ar pressure (a) 1.8 cm Hg, (b) 5.1 cm Hg. Cell temperature is 24°C.

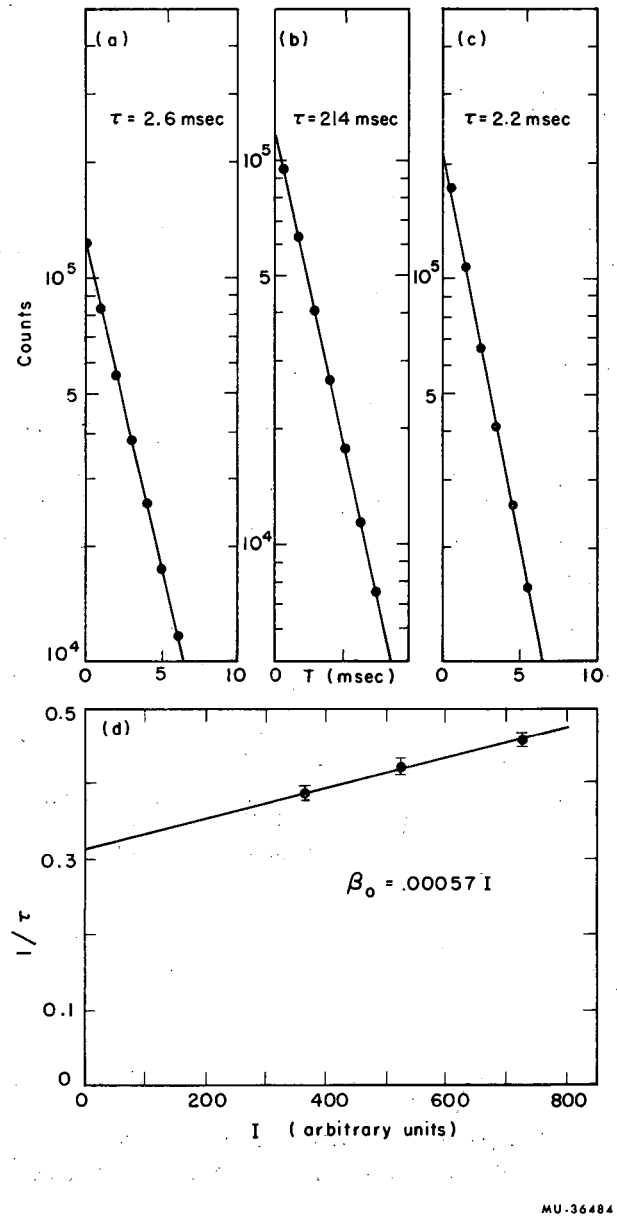

Fig. V-3. Redetermination of β_0 for measurements made at 2.6, 3.5, and 17 cm Ar. (a) I = 368, (b) I = 525, (c) I = 730.

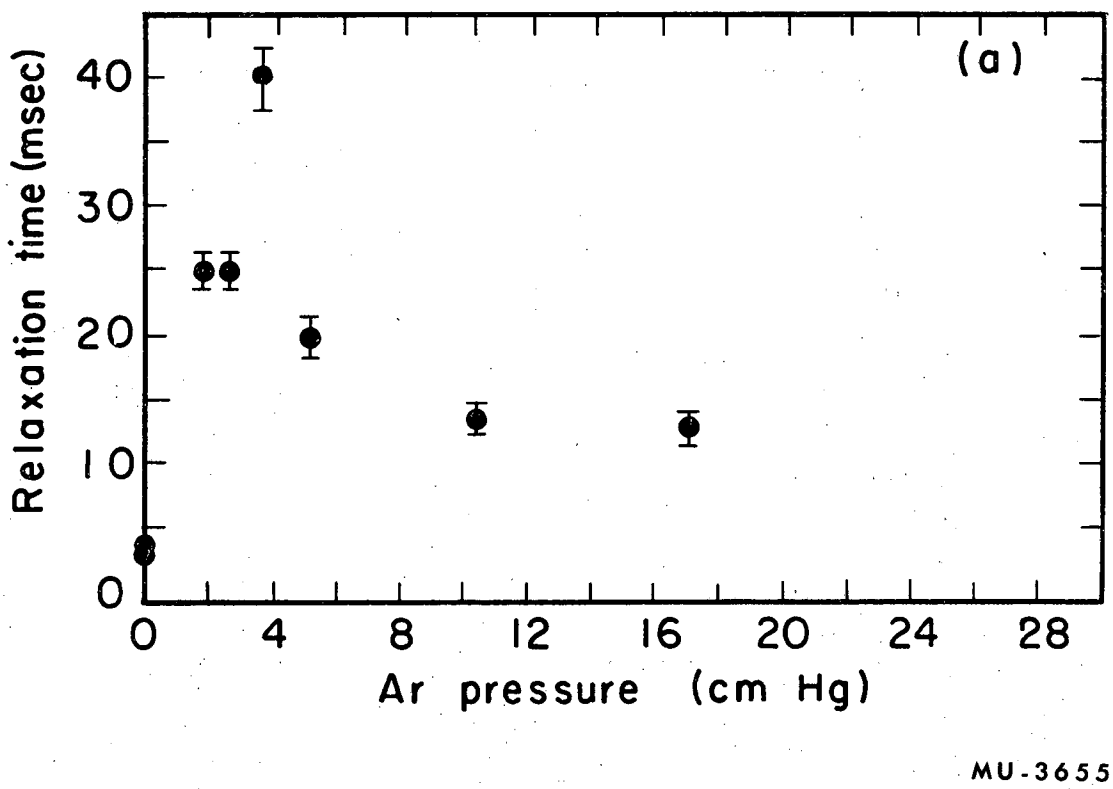

Fig. V-4. Variation of Rb^{87} relaxation time with Ar pressure at 24°C.

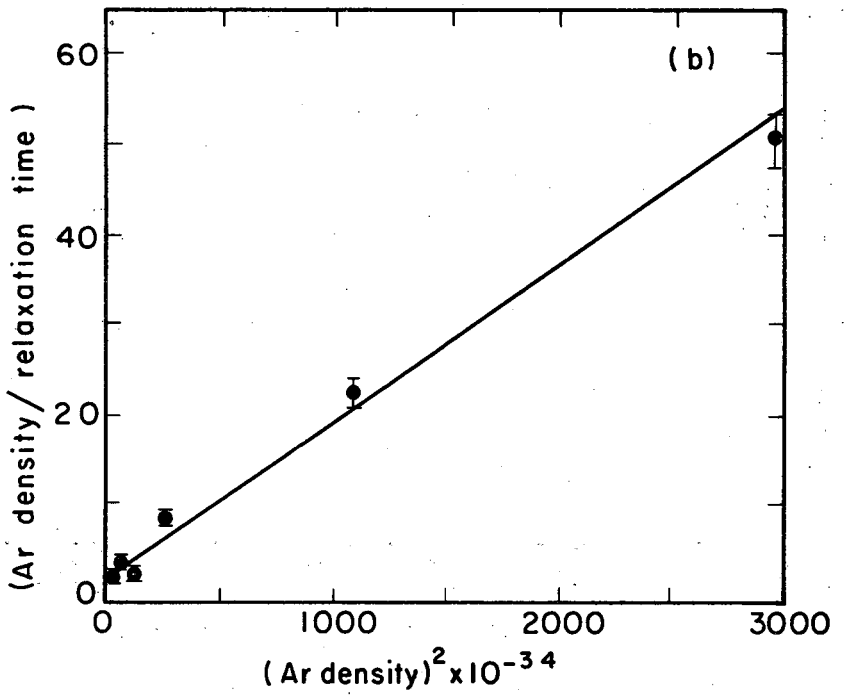

Fig. V-5. Plot of n/T_1 vs n^2.

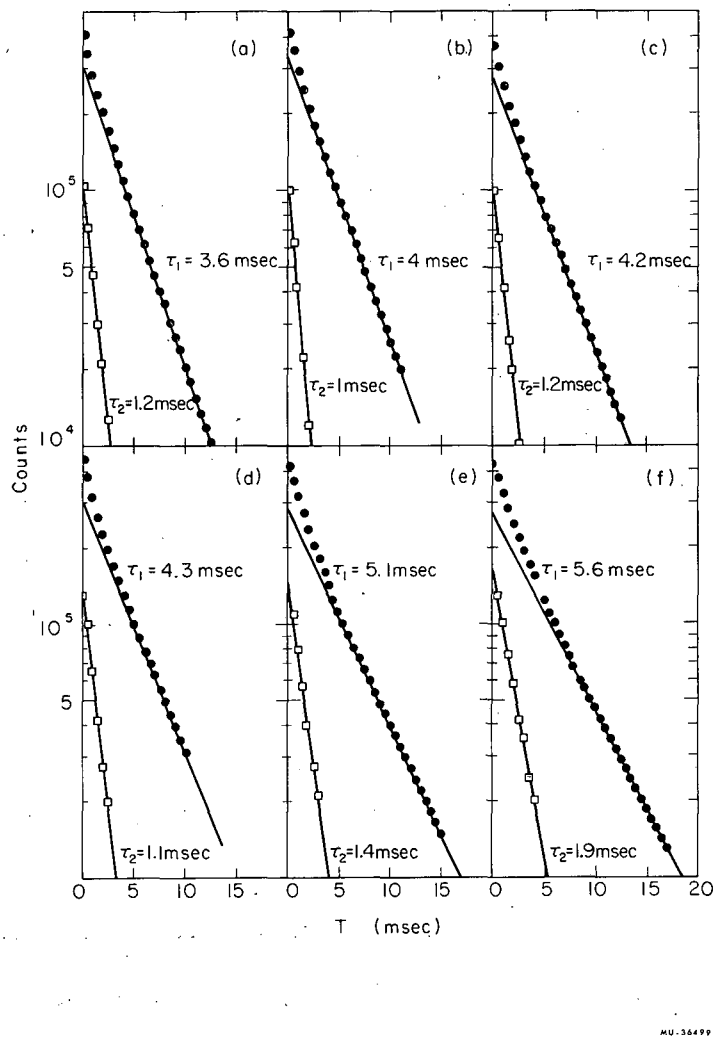

Fig. V-6. Semi-log plot of Rb^{87} pumping transients in various pressures of Ar at 24°C and at approximately equal light intensity. (a) 1.8 cm Hg, (b) 2.6 cm Hg, (c) 3.5 cm Hg, (d) 5.1 cm Hg, (e) 10.3 cm Hg, (f) 17 cm Hg. Graphical values of the lifetimes and amplitudes are used as starting values for a least-squares analysis by computer. Background due to dc level of amplifier has been subtracted.

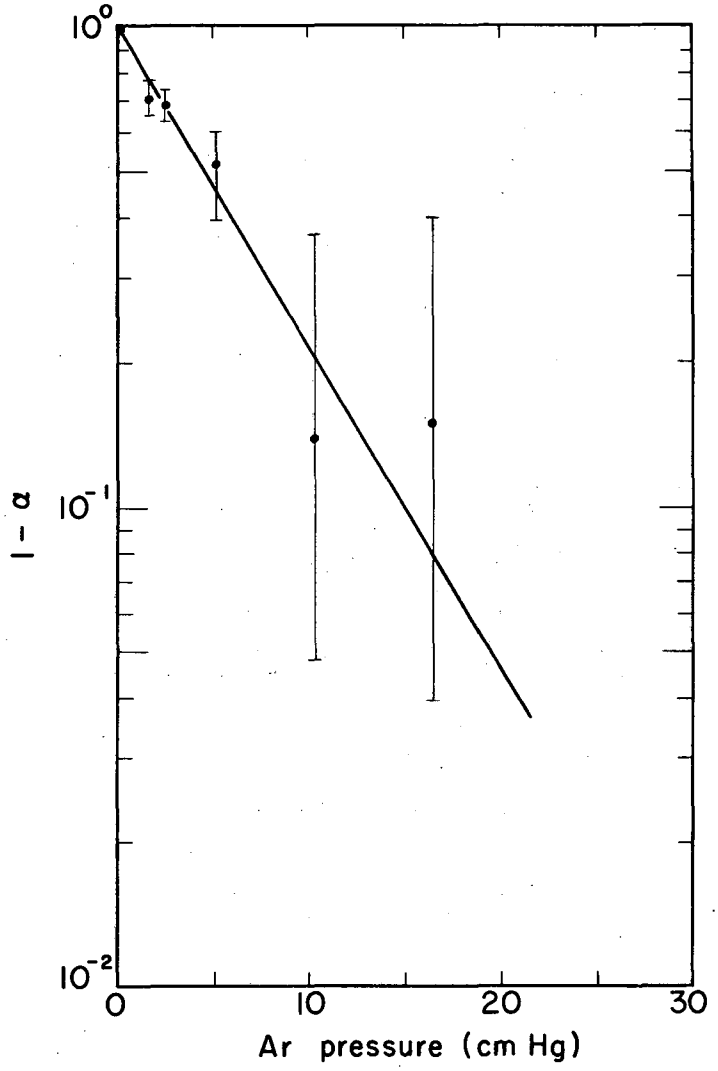

Fig. V-7. Plot of 1-α vs Ar pressure (not corrected for pressure broadening of the absorption line).

Table V-1. Summary of data needed to determine σ_{eff} for Rb^{87} - Ar collisions.

Argon pressure (cm Hg)	I (arbitrary units)	β_0 ($msec^{-1}$)	ρ	A_2/A_1	λ_2/λ_1	a	N[a]	χ^{2}[b]
			±0.005	5-10%	≈5%			
1.8	858	0.55	0.072	0.34	3.3	0.29	20	15
	614	0.40	0.100	0.36	3.3		24	26
	443	0.29	0.138	0.44	3.0		30	82
	367	0.23	0.174	0.39	3.0		30	74
2.6	809	0.46	0.087	0.37	3.4	0.31	20	24
	573	0.33	0.121	0.42	3.2		25	17
	410	0.23	0.174	0.51	3.0		30	160
3.5	821	0.47	0.053	0.44	3.3	0.60	20	40
	588	0.34	0.073	0.49	3.2		25	38
	427	0.24	0.104	0.51	3.1		27	29
5.1	882	0.57	0.088	0.47	3.2	0.48	22	58
	372	0.24	0.208	0.56	3.0		34	58
	537	0.35	0.143	0.54	3.0		30	66
10.3	814	0.53	0.132	0.69	3.0	0.86	25	18
	494	0.32	0.218	0.69	2.9		33	34
	347	0.23	0.304	0.72	2.8		40	81
17.0	784	0.51	0.176	0.70	2.9	0.67	30	44
	568	0.37	0.243	0.72	2.8		30	54
	342	0.22	0.410	0.98	3.0		40	48

[a] N is the number of data points on which the least-squares analysis is based.
[b] χ^2 is the sum of squares of the deviations.

semilog plot. The χ^2 does not appear to be a dependable guide to the reliability of the lifetimes and amplitudes of the exponentials extracted from the data. The signals, to be sure, were followed to saturation but after a few lifetimes the saturation level decreased somewhat due to the amplifier recovery cycle. Equal weights were assigned to all points after a number of reasonable weighting schemes failed to give appreciably better fits. For example, the limiting noise was usually 120 cps, which could be seen in the tail end of the semilog plot in the worst cases. The amplitude of this noise was used to estimate a weighting factor but as it generally amounted to $<1\%$, and in the majority of cases could not even be seen, it made no appreciable difference.

To determine the mixing cross section for the P state from Fig. V-7 we need the following quantities; N_0 = density of Ar atoms per cm Hg pressure at 24°C = $3.2\times10^{17}/cm^3$; $\bar{v}$ = mean relative Ar-Rb^{87} speed = 4.8×10^4 cm/sec; and τ = lifetime of the $P_{1/2}$ state of Rb^{87} = 2.85×10^{-8} sec.[27] From the slope of the line in Fig. V-7 and the relation $1 - a = \exp[-(\sigma_{eff} N_0 \bar{v} \tau)p]$, where p is the Ar pressure in cm of Hg, we obtain $\sigma_{eff}(P) = 3.5\times10^{-16}$ cm^2. We consider the error when we obtain the results for Ne and He. The ground-state disorientation cross section is obtained from Fig. V-5(b) where we have plotted N/T_1 vs N^2, where N is the Ar density and T_1 the corresponding Rb^{87} relaxation time. The slope of the resulting line is $\sigma(S_{1/2})\bar{v}$ and yields $\sigma(S_{1/2}) = (3.5\times10^{-22})$ cm$^2 \pm (1\times10^{-22})$ cm^2. This value was obtained from a least-squares analysis[28] according to which the slope

$$m = \frac{n \sum N^3/T_1 - (\sum N^2)(\sum N/T_1)}{n \sum N^4 - (\sum N^2)^2}$$

where n is the number of points. We could also obtain the diffusion coefficient from the intercept $k = gD_0(76\ N_0)$, where g is a geometrical factor (see Appendix E) and the $76\ N_0$ is the density at atmospheric pressure and 24°C, were it not for the great uncertainty in the effective value of g. The difficulty is due to the fact that in our

experiment there may not be time for atoms to diffuse out of the pumping region so that the proper geometry is not that of the cell but rather of the pumping volume. This is certain to be the case at the high pressure points, but at low pressures some diffusion will occur and the boundaries of the pumped region will not be well defined; and moreover, the polarization will not be uniform in the boundary region. If we calculate the diffusion coefficient (D_0) using the cell geometry, $g = 1.72$, we find from least squares

$$k = \frac{(\sum N/T_1)(\sum N^4) - (\sum N^3/T_1)(\sum N^2)}{n\sum N^4 - (\sum N^2)^2} = 2.46 \times 10^{19}$$

or $D_0 = 0.58\ cm^2/sec$. However, if we calculate g from the geometry of the light beam whose diameter is somewhat smaller ($\approx 2/3$) than the cell, we get a smaller and more reasonable D_0 since g is inversely proportional to the square of the dimension of the polarized region. For example, if we take $2a/3$ as the effective radius of the cell, then $g_{eff} \approx 2.5$ and $D_0 \approx 0.4\ cm^2/sec$.

2. Rubidium-87—Helium

Rubidium-87 pumping transients were studied in a cylindrical Pyrex absorption cell of the same dimension and construction as that used for Ar. Helium pressures ranging from 1.5- to 29-cm Hg were covered and at each value of He pressure transients were observed for three or more values of the light intensity to determine the ground-state relaxation time T_1. The digital output of the mcs was analyzed by computer to determine the best values of the exponential decay times and amplitudes. Prior to making any measurements, we first determined the absorption of resonance radiation by the vapor in the evacuated cell to be $\approx 2\%$ by the rf-on—rf-off technique and then determined β_0 in the evacuated cell.

Figure V-8 summarizes the determination of β_0 and Fig. V-9 the ground-state relaxation times. Following are semilog plots of transients at about the same incident light intensity but different pressures of He (Fig. V-10). Table V-2 summarizes all the results needed to

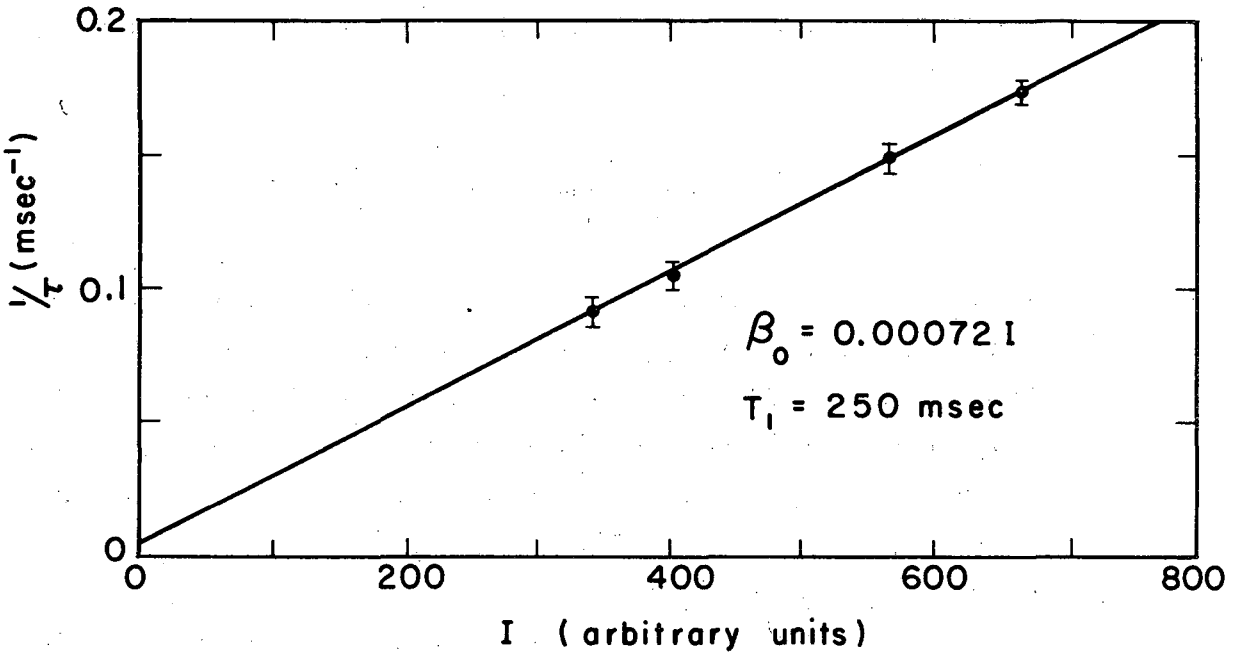

Fig. V-8. Determination of β_0 from the variation of the pumping time with light intensity I. $1/\tau = 0.0025I$ to 0.004 msec^{-1}.

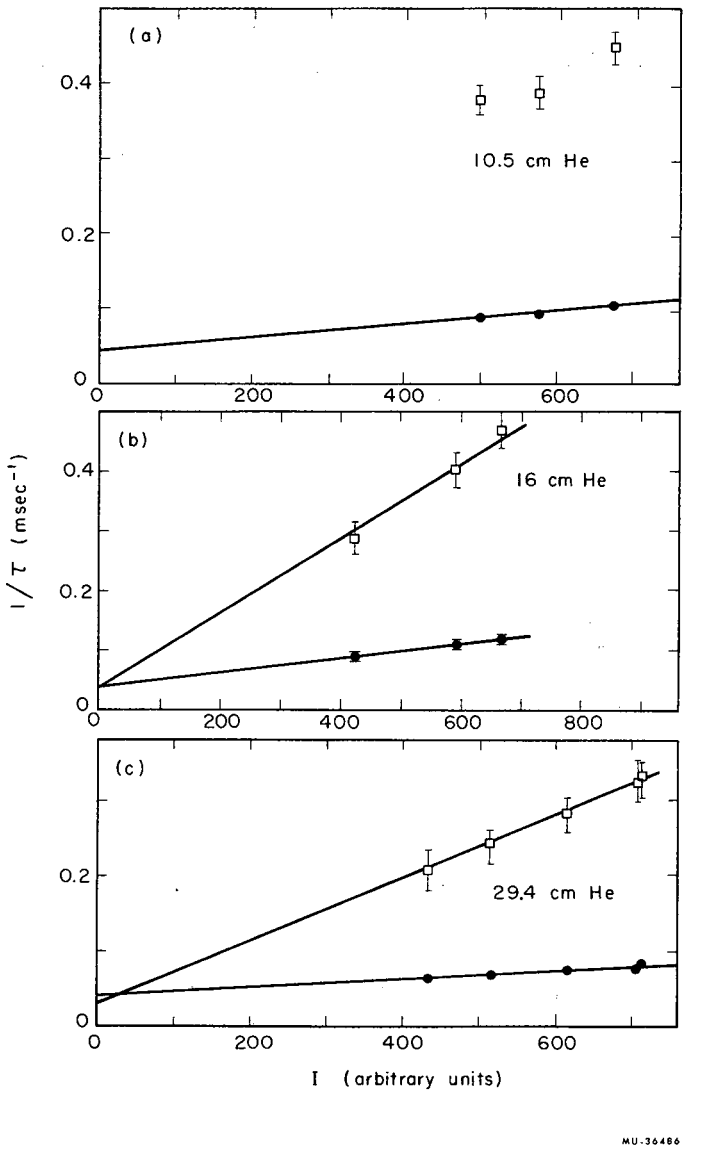

Fig. V-9. Pumping times for Rb^{87} in He at 23°C. The upper points (□) are for the fast component of the pumping transients. Relaxation times are determined from the slower ( ) component. The scatter in □ is due to the slight instabilities in the absorption cell.

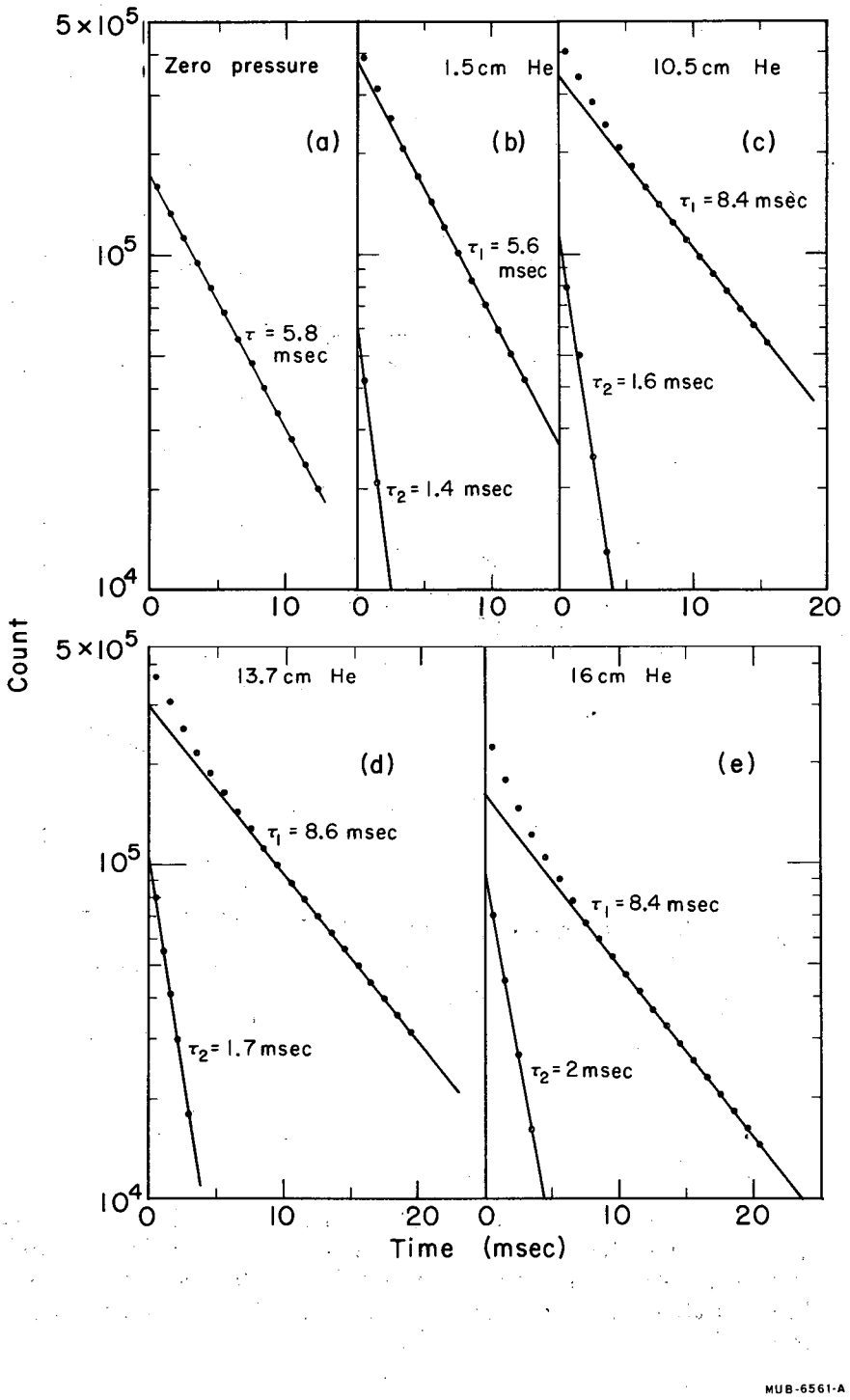

Fig. V-10. Semilog plots of Rb^{87} pumping transients in He at approximately equal light intensity.

Table V-2. Summary of data needed to determine σ_{eff} for Rb^{87}-He collisions.

Helium pressure (cm Hg)	I (arbitrary units)	β_0 ($msec^{-1}$)	ρ ±0.005	A_2/A_1 5-10%	λ_2/λ_1 ≈5%	a	N	χ^2
1.5	659	0.48	0.042	0.19	3.65	0.07	15	5
	561	0.41	0.049	0.34	3.13		20	35
	414	0.30	0.067	0.23	3.56		20	22
10.5	671	0.49	0.094	0.38	6.48	0.25	20	22
	572	0.42	0.108	0.39	6.61		23	25
	494	0.36	0.126	0.34	7.10		25	15
13.7	627	0.46	0.087	0.39	5.95	0.28	23	44
	544	0.40	0.100	0.34	6.20		25	150
	394	0.29	0.138	0.34	7.10		25	34
16	665	0.49	0.082	0.50	5.40	0.46	20	28
	588	0.43	0.093	0.49	5.35		20	24
	422	0.31	0.129	0.58	4.93		30	56
29.4	712	0.52	0.058	0.50	7.05	0.59	30	300
	709	0.52	0.058	0.53	7.29		30	64
	613	0.45	0.089	0.55	7.10		30	48
	512	0.37	0.108	0.56	6.99		35	346
	431	0.31	0.129	0.61	8.35		35	93

determine cross sections, including amplitude and lifetime ratios for all transients observed. The mixing parameter a was determined both for the case of uniform relaxation in the $P_{1/2}$ state and for electron randomization only. In Fig. V-11 we plot a against the He pressure.

Repeating the same analysis as in Sec. V. A.1, we get $\sigma_{eff}(P) = (2.5\times10^{-17})cm^2$ where we have used $\bar{v}(Rb^{87}\text{-He}) = (1.28\times10^5)$ cm/sec. The ground-state relaxation data yields a cross section that is much too large ($\approx10^{-23}$), judging by the results of others. Because of the extremely small cross section for He $< 10^{-24}$ cm^2, the measurements are very sensitive to the presence of impurities and the relaxation times observed were probably due in part to Rb^{87}-impurity-atom collisions. This has no effect on the excited-state cross section so long as no collisions occur within the lifetime of the $P_{1/2}$ state, (2.85×10^{-8}) sec. If the cross section for $Rb^{87}(P_{1/2})$-impurity-atom disorienting collisions were as high as 10^{-13}cm^2, a partial pressure of ≈ 0.1 mm Hg would be required to disorient the P state, but such a high impurity concentration is absurd. The pressure in the vacuum system prior to introduction of the He was $\approx10^{-6}$-mm Hg and in leak checks would rise to $\approx10^{-4}$-mm Hg a few hours after the diffusion pump was isolated from the cell and gas-flow system. The He itself had a purity of $1:10^5$. Such minute impurities can account for discrepancies in the ground-state relaxation time but can have no effect on the excited-state measurements (chemical reaction, however, could lead to a distortion of the signals).

3. Rubidium-87—Neon

The Ne data were measured in the same cell used for He and the same light calibration applies. The results are summarized below similarly to the He data in Figs. V-12 to V-15 and Table V-3. The excited-state cross section deduced from Fig. V-15 is $\sigma_{eff}(P) = (4.4\times10^{-17})cm^2$ and the ground-state cross section $\sigma(S_{1/2}) = (1.0\times10^{-22})cm^2 \pm 0.3\times10^{-22}$ cm^2. In Table V-4 our results are compared with those of other workers.

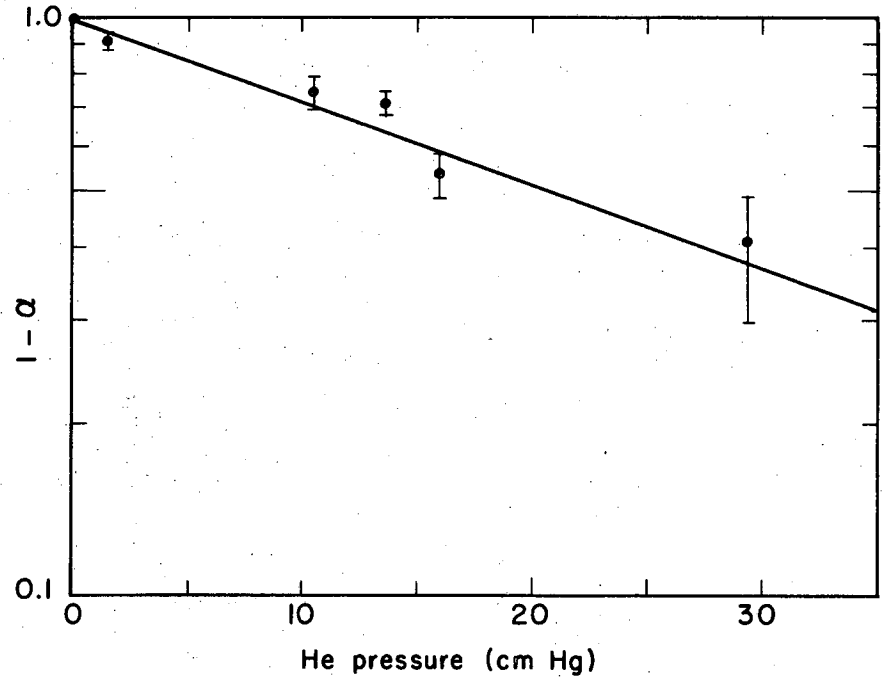

Fig. V-11. Semilog plot of 1 - α against He pressure.

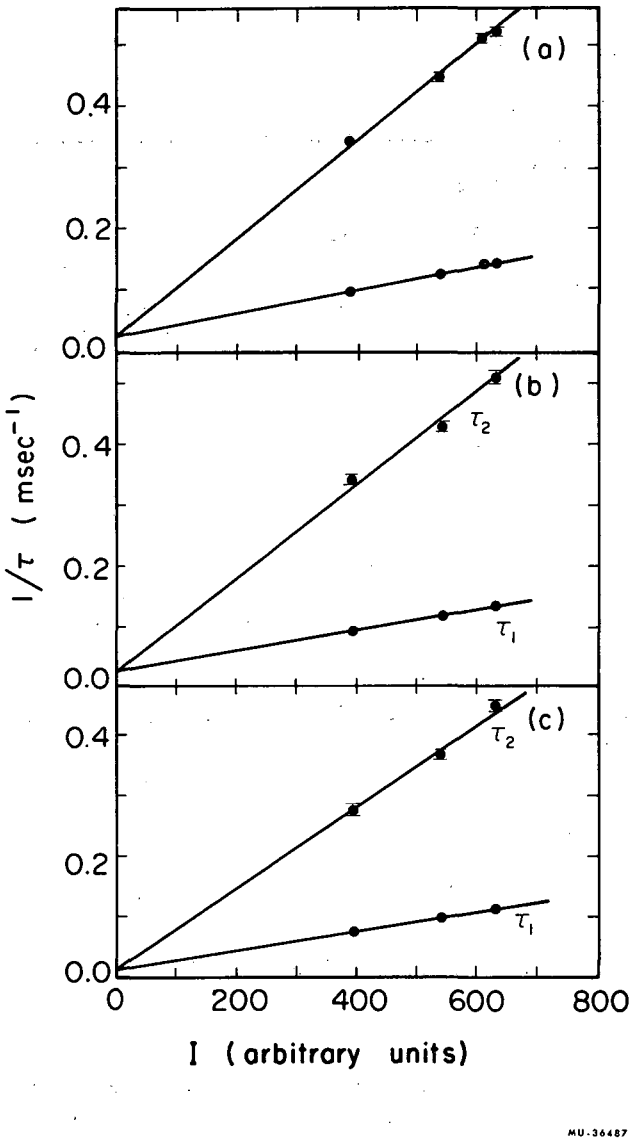

Fig. V-12. Sample pumping times for Rb^{87} in Ne at 23°C. (a) 7.4 cm Hg, (b) 10.1 cm Hg, (c) 19.7 cm Hg.

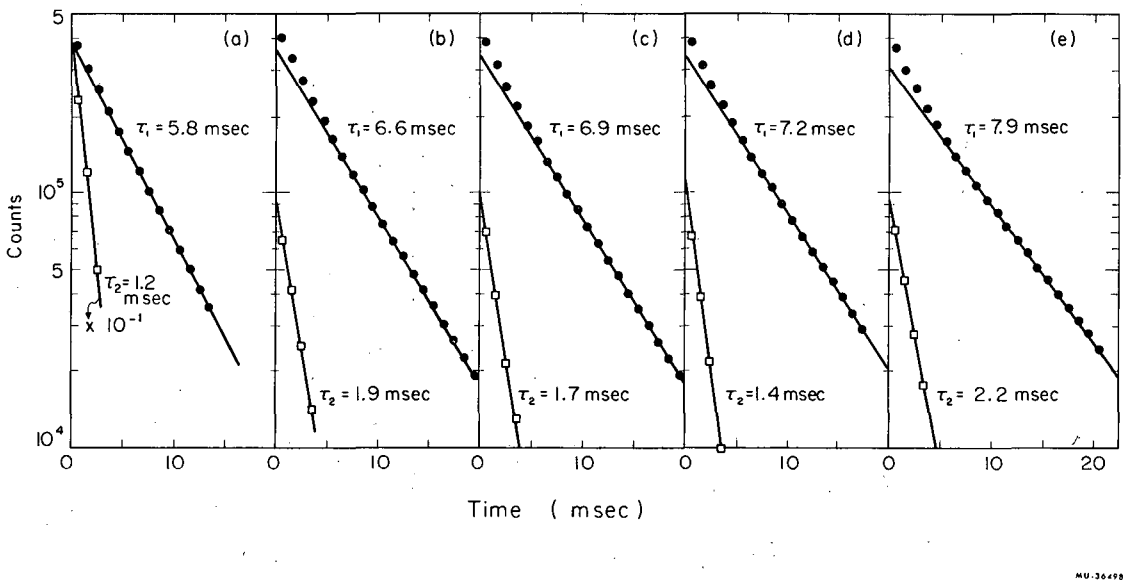

Fig. V-13. Semilog plots of Rb^{87} pumping transients in Ne. (a) 1.4 cm Hg, (b) 5.1 cm Hg, (c) 7.4 cm Hg, (d) 10.1 cm Hg, (e) 19.7 cm Hg.

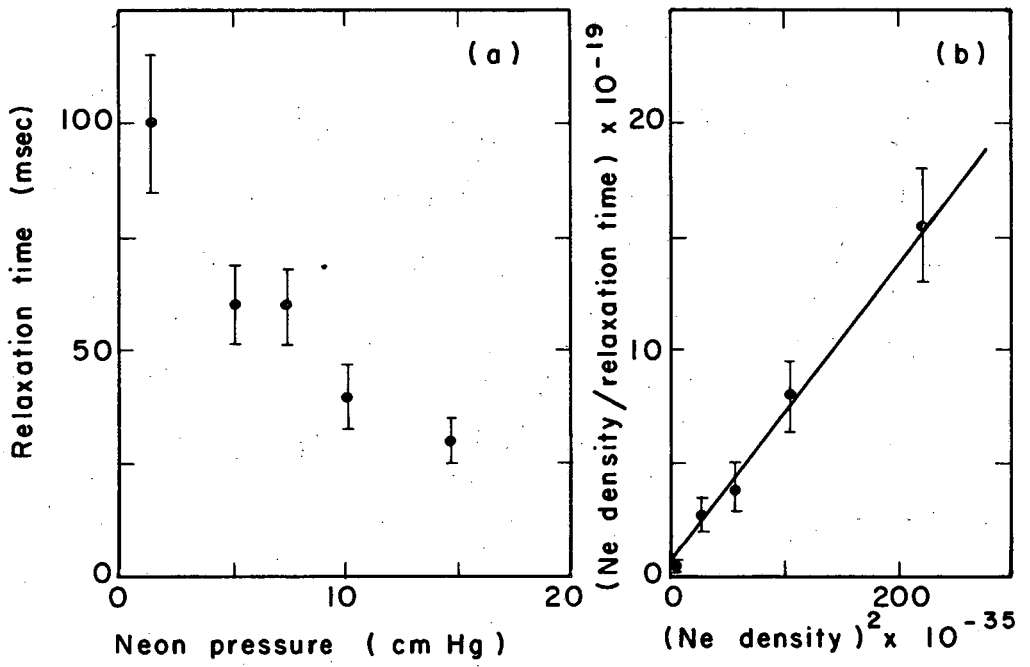

Fig. V-14. (a) Variation of Rb^{87} relaxation times T_1 with Ne pressure (cm of Hg). (b) Plot of n/T_1 vs n^2.

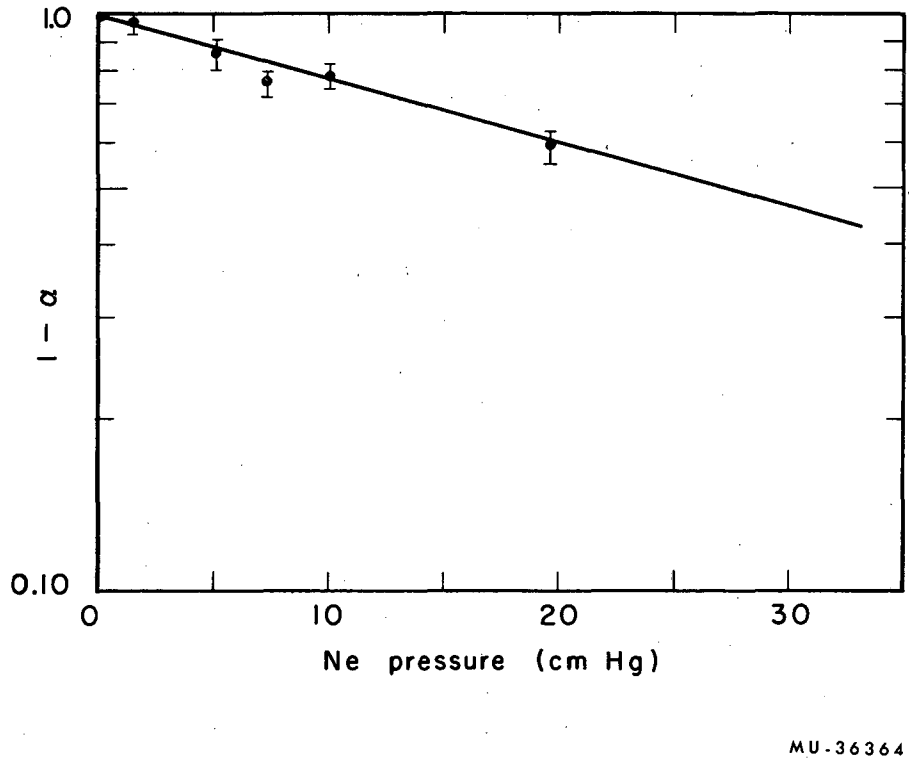

Fig. V-15. Semilog plot of 1 - α against Ne pressure.

Table V-3. Summary of data needed to determine σ_{eff} for Rb^{87}-Ne collisions.

Neon pressure (cm Hg)	I (arbitrary units)	β_0 ($msec^{-1}$)	ρ	A_2/A_1	λ_2/λ_1	a	N	χ^2
			±0.005	5-10%	≈5%			
1.4	634	0.464	0.022	0.11	3.8	0.03	15	40
	532	0.389	0.026	0.13	3.6		18	23
	390	0.285	0.035	0.16	3.4		20	13
5.1	653	0.477	0.036	0.26	4.1	0.14	17	10
	566	0.413	0.040	0.36	3.8		18	12
	400	0.292	0.057	0.25	4.2		24	18
7.4	631	0.461	0.036	0.30	4.1	0.23	18	6
	609	0.445	0.037	0.31	4.1		18	4
	538	0.393	0.042	0.32	4.0		20	13
	388	0.284	0.059	0.32	3.5		23	9
10.1	630	0.460	0.055	0.30	4.6	0.20	17	8
	541	0.395	0.063	0.32	4.5		20	5
	391	0.286	0.087	0.29	4.7		23	7
19.7	632	0.462	0.027	0.38	4.2	0.40	20	17
	539	0.394	0.032	0.39	4.0		25	11
	393	0.287	0.044	0.40	4.1		25	22

Table V-4. Ground-state disorientation cross sections for Rb-noble-gas collisions.

Buffer gas	Rb^{87} (25° C)	Rb^{87} (44° C)	Rb (50° C)	Rb (67° C)
He			6.2×10^{-25} cm^2 [a]	3.3×10^{-25} cm^2 [b]
Ne	1.0×10^{-22} cm^2	1.6×10^{-22} cm^2 [c]	5.2×10^{-23} cm^2 [d]	3.3×10^{-24} cm^2 [b, c]
Ar	3.3×10^{-22} cm^2	9×10^{-22} cm^2 [c]	3.7×10^{-22} cm^2 [d]	1.1×10^{-22} cm^2 [b, c]
Kr	2.0×10^{-20} cm^2		5.9×10^{-21} cm^2 [d]	7.3×10^{-21} cm^2 [e]
Xe	1.8×10^{-19} cm^2		1.3×10^{-20} cm^2 [d]	1.3×10^{-19} cm^2 [e]

a. See R. A. Bernheim, J. Chem. Phys. 36, 135 (1962).

b. See F. A. Franz, Phys. Rev. (to be published).

c. See M. Arditi and T. R. Carver, Phys. Rev. 136, A643 (1964).

d. See Ref. 6.

e. See F. A. Franz, Phys. Letters 13, 123 (1964).

4. Discussion

a. Effect of pressure broadening of the absorption line

We have interpreted our data so far without considering Lorentz broadening of the absorption line. Pressure broadening of the Rb resonance line $5S_{1/2} \leftrightarrow 5P_{1/2}$ was measured by Ch'en,[29] from whose data we get $(\Delta\nu)_L = 0.0075$ cm^{-1}/cm Hg of Ar at 25°C and $(\Delta\nu)_L = 0.0072$ cm^{-1}/cm Hg of He at 25°C. We assume a similar number for Ne as this appears not to have been measured. It has been assumed (Sec. II) that the emission line is infinitely broad so that $\beta_0 \propto I_0$, but actually the width of the emission line $(\Delta\nu)_e$ is approximately $6(\Delta\nu)_D$, where $(\Delta\nu)_D \approx 0.017$ cm^{-1} is the Doppler width of the absorption line. This means that for pressures ≥ 3-cm Hg, $\beta_0 = \int I_\nu \sigma_\nu d\nu$ will decrease noticeably so that $\rho = 1/T_1\beta_0$ will increase, and this in turn will affect the value of α. To estimate the corrections to be applied at the high-pressure points we assume a Lorentzian shape for I_ν and σ_ν. The assumption of a Lorentzian emission line is justified by the measurements of Jarrett[30] and a Lorentzian σ_ν is justified for high pressures where $(\Delta\nu_{Lorentz} \gg (\Delta\nu)_D$.[10] Taking $I_\nu \propto b/[b^2+(\nu-\nu_0)^2]$ and $\sigma_\nu \propto a/[a^2+(\nu-\nu_0)^2]$, with $b = \frac{1}{2}(\Delta\nu_e)$ and $a = \frac{1}{2}\Delta\nu_L$, we get $\beta_0 \propto 1/[\Delta\nu_L + \Delta\nu_e]$.

In Fig. V-16 we have plotted β_0, normalized to unity at zero pressure, and using this figure we corrected ρ and redetermined α. This is an extreme correction representing the worst that can be expected from pressure broadening in the range covered. The new values of ρ for the most part do not fall in the linear range shown in Fig. II-10, and consequently α was determined only approximately from a limited number of calculations done for values of $\rho > 0.1$. Results of these crude corrections for He and Ne are shown in Fig. V-17 and indicate a $\sigma_{eff}(P) \approx 25\%$ smaller. For Ar the new values of ρ were even larger and no reliable values of α could be obtained without considerable computation. However, it is clear that the corrected $\sigma_{eff}(P)$ are smaller.

Other chief sources of error in α are the measured amplitude ratio (A_2/A_1) and relaxation time T_1. These errors are indicated by the bars in Figs. V-7, V-11, and V-15. As the error introduced by

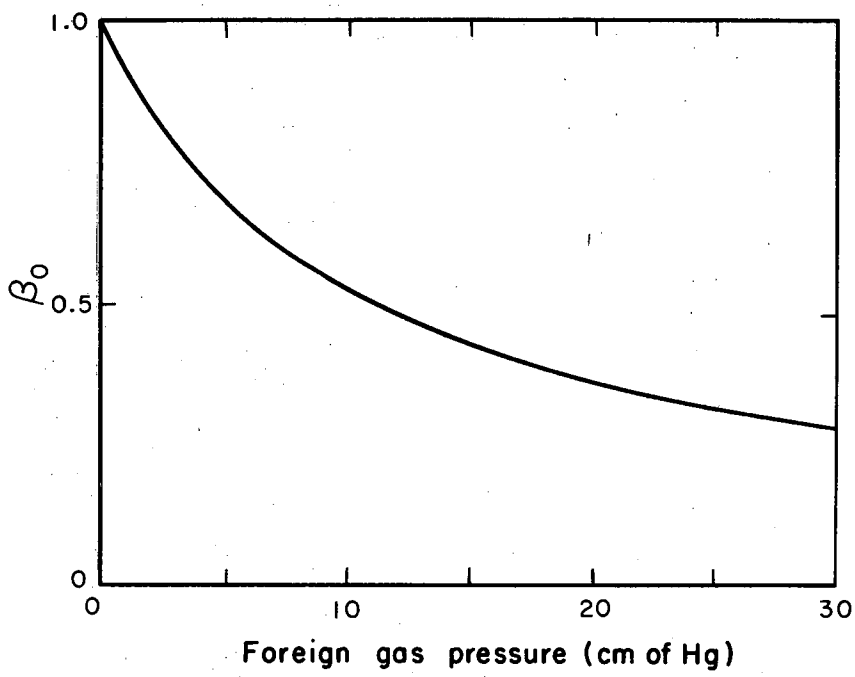

Fig. V-16. β_0 corrected for pressure broadening of the absorption line (normalized to one at zero pressure).

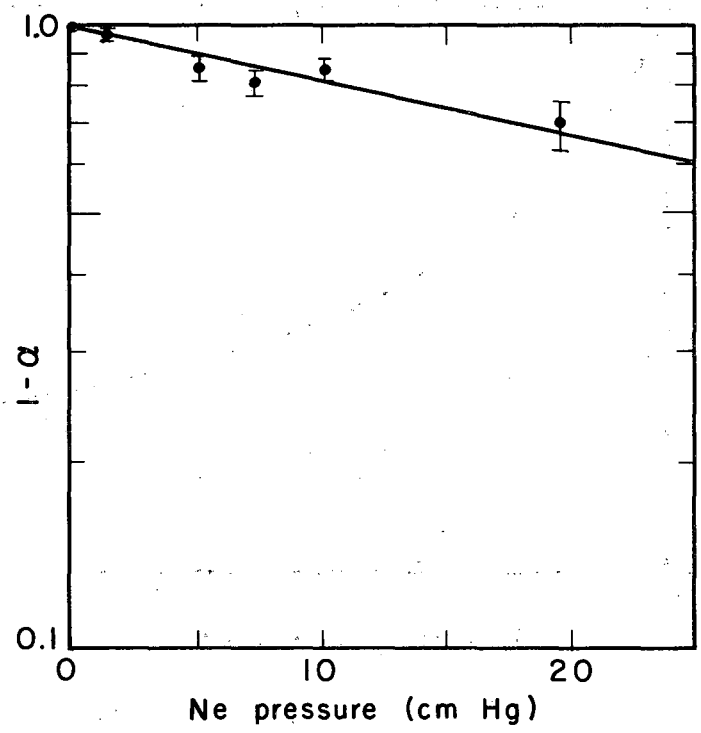

Fig. V-17. Values of α approximately corrected for pressure broadening for Ne data.

pressure broadening is systematic and not known accurately it is difficult for us to assign a net error, but the values of $\sigma_{eff}(P)$ should be reliable to 50% or better from the crude estimates made. From our effective cross sections and the measurements of Beahm et al.[14] we can deduce a $\sigma_{1/2,\,1/2}(Rb^{87}\text{-He}) \approx (1.5\times10^{-17}\ cm^2$. For Ar and Ne Beahm reports cross sections considerably smaller than for He $(1\times10^{-17}\ cm^2)$ so that $\sigma_{eff}(P) \approx \sigma_{1/2,\,1/2}(P)$.

b. Electron randomization or uniform relaxation in the $5^2P_{1/2}$?

Values of α used to determine $\sigma_{eff}(P_{1/2})$ above are based on the assumption that the collisional relaxation of the $P_{1/2}$ state is uniform. Although the evidence in support of this mode of relaxation is not clear-cut, it is difficult to interpret the data in terms of a cross section for randomizing the electron spin in the $P_{1/2}$ state. The reason for this difficulty is shown in Figs. II-7(a and b) and II-8. Transient signals expected with electron randomization are very similar to those expected in the limit of no reorientation of the $P_{1/2}$ state, and although they are doubly exponential, the amplitude ratio A_2/A_1 of the two-exponential components are smaller than for the case of uniform relaxation, and in fact a number of the experimental ratios cannot be fitted to Fig. II-1 whereas all can be fitted to Fig. II-10. An exception occurs in Ne, where all the experimental ratios are permissible by electron randomization, but if we plot $1-\alpha$ against the pressure we do not get a smooth line. Further evidence in support of uniform relaxation is found in the lifetimes (exclusive of the relaxation time) of the two exponentials.

The values of α determined from the amplitude ratio A_2/A_1 are meaningful only if they are consistent with the decay constant ratio λ_2/λ_1. This is indeed the case, as we see from Figs. V-18, V-19, and V-20 where we have plotted the experimental lifetime ratios against the theoretical ones for the value of α determined from A_2/A_1. The agreement is seen to be good for Ne and He. The experimental ratios λ_2/λ_1 are somewhat low compared with the theoretical one, which is based on α determined from A_2/A_1, but this difference may be because we have not corrected α for pressure broadening, we have

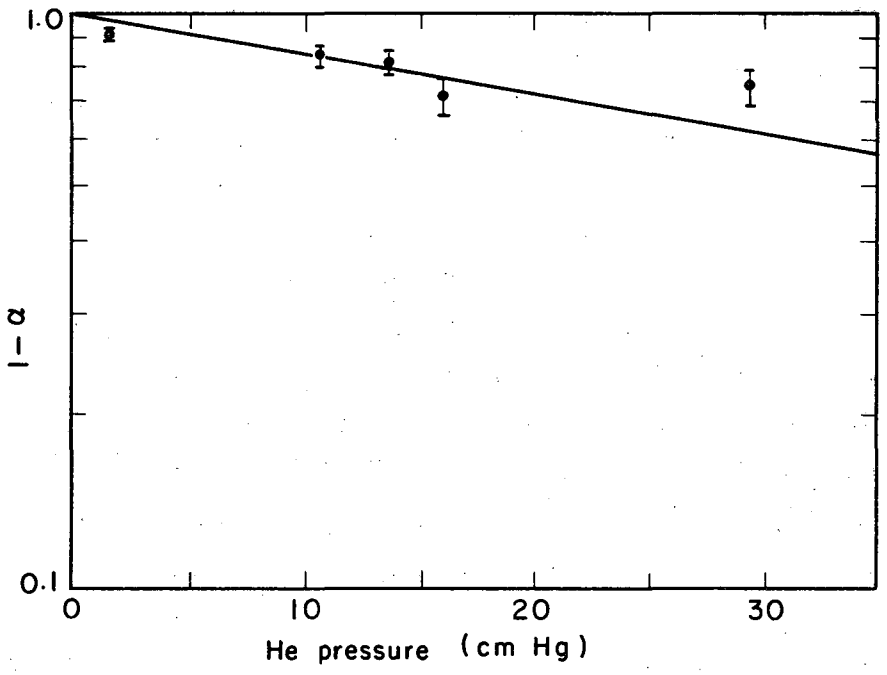

Fig. V-18. Same as V-17 for He.

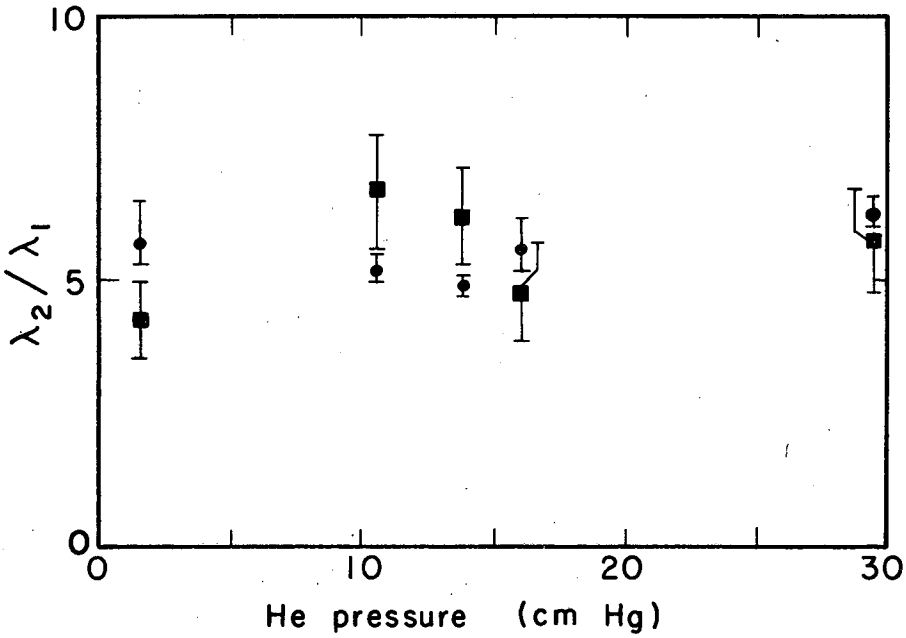

Fig. V-19. Experimental ratios λ_2/λ_1 for He compared with theory for same value of α as deduced from A_2/A_1 with uniform relaxation assumed in the P state.

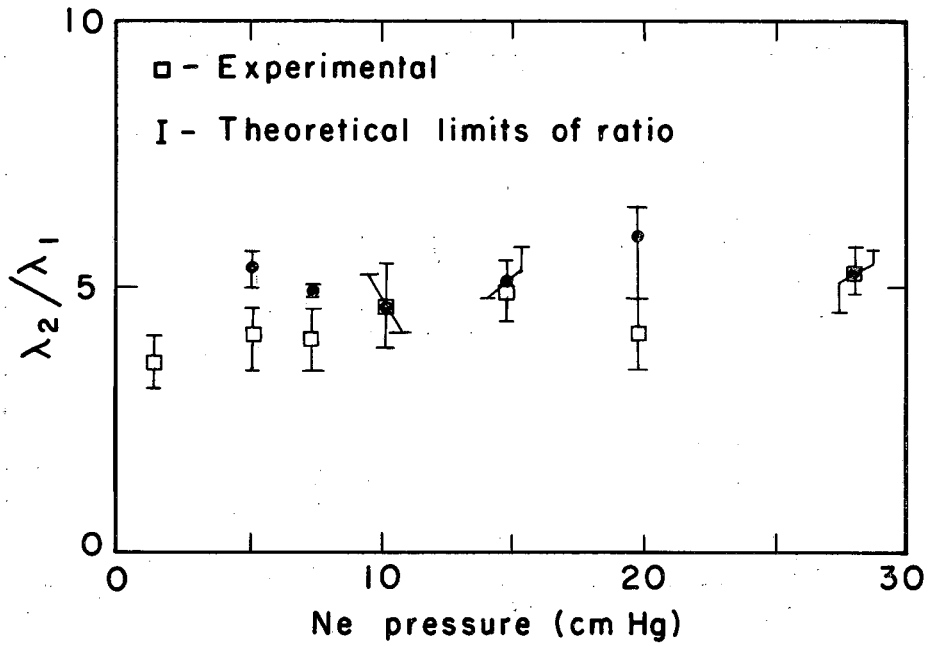

MU-36394

Fig. V-20. Same as V-19 for Ne.

shown that by not correcting α we tend to overestimate the degree of mixing. This would lead us to expect larger values of λ_2/λ_1 for $\alpha > 0.2$, as reference to Fig. II-2 reveals. For Ar the agreement is less satisfactory although a direct comparison is not made as Fig. II-2 was computed for a 1-msec averaging interval, whereas the Ar data were sampled at 0.5-msec intervals and λ_2 is more sensitive to averaging (than is A_2). We cannot rely on λ_2/λ_1 alone to fix α, as reference to Fig. II-2 reveals. First, λ_2/λ_1 is not a unique function of α, and second, it is not very sensitive to α. This insensitivity is unfortunate since λ_2/λ_1 is independent of β_0, which eliminates not only the necessity to measure β_0 (except for averaging purposes where an estimate would suffice) but also the complication of pressure broadening of the absorption line. The above evidence suggests that in the pressure range covered, uniform relaxation is a more likely mode of relaxation.[31]

5. Rubidium-87—Krypton and Xenon

The ground-state relaxation time (T_1) for Rb^{87} in Kr and Xe is so short that the transient signals are dominated by T_1. Since every decay rate in the signal contains $\rho \doteq 1/T_1$ additively, the signal would be singly exponential if T_1 were only small enough. For example, $T_1 \approx 1$ msec and $\beta_0 \approx 0.5$ msec^{-1}; thus $\rho \approx 2$. This is larger than any of the eigenvalues of B_{ij} (exclusive of ρ) so that $\beta \approx e^{-\rho t}$. Because of the short relaxation time structure cannot be observed in the transients, and thus the excited-state disorientation cross section cannot be measured by the transient technique. Better luck might be had by observing the steady-state signals, but even this may not be a simple matter because of the very low signal levels at high buffer-gas pressures (> 1 cm). However, we can measure the ground-state disorientation cross sections and diffusion coefficients.

The first attempt to measure the Rb ground-state disorientation cross section associated with Kr and Xe was made by Franzen;[6] however, because of mechanical limitation he was not able to use his own method but used instead Dehmelt's to measure relaxation times in Kr and Xe. Correcting the Ne diffusion coefficient for the Ne-Kr and

Ne-Xe mass difference, Franzen was able to estimate the Rb-Kr and Rb-Xe ground-state disorientation cross sections. Since then Anderson and Ramsey and Franz and Lüescher adapted Franzen's method to the indirect measurement of short relaxation times by diluting highly relaxing buffer gases with less relaxing gases such as Ne. The net relaxation time is then long enough to permit use of mechanical shutters (limited to ≈ 10 msec opening time for 1-in. apertures). To separate the contribution to the relaxation time due to the dilute gas, the diffusion equation is resolved with two source terms [e.g., $-\sigma(\text{Rb-Ne})N(\text{Ne})\bar{v}(\text{Rb-Ne}) - \sigma(\text{Rb-Kr})N(\text{Kr})\bar{v}(\text{Rb-Kr})$] with the reasonable assumption that, provided the dilute gas density is low enough, it does not contribute to diffusion but only to collisional relaxation. The measurements of Anderson and Ramsey pertained to Na and those of Franz and Luescher to Cs. More recently, Gibbs[32] eliminated some of the mechanical limitations of the Franzen method by employing a Kerr cell in conjunction with a mechanical shutter.

Measurements reported here were obtained by the Dehmelt method, which is here applicable directly because of the single-exponential nature of the signal. The Kr transients were observed in a cell of 6 cm in diameter and 4.2-cm long (inside dimensions), and the Xe data obtained in a cell 6 cm in diameter and 2.7-cm long (inside dimensions). Results for Kr are shown in Figs. V-21 to V-23, and for Xe in Figs. V-24 to V-26. The cell temperature was 24°C for Kr and 25°C for Xe ±1°C.

The relaxation times shown in Fig. V-27 were obtained in a cell with dimensions similar to those shown in Fig. V-26 and are consistent with the cross section determined from Fig. V-26. Data for the points at 1.5 and 3 mm were taken one day apart. The Xe data were also checked by measuring pumping times at a few pressure points and correcting for the pumping-time characteristic of the resonance lamp as determined from earlier experiments. The relaxation times thus determined were in agreement with the data shown but the uncertainty was larger than that in Fig. V-26(a). Special precaution was taken to ensure that the transients were not distorted by too large

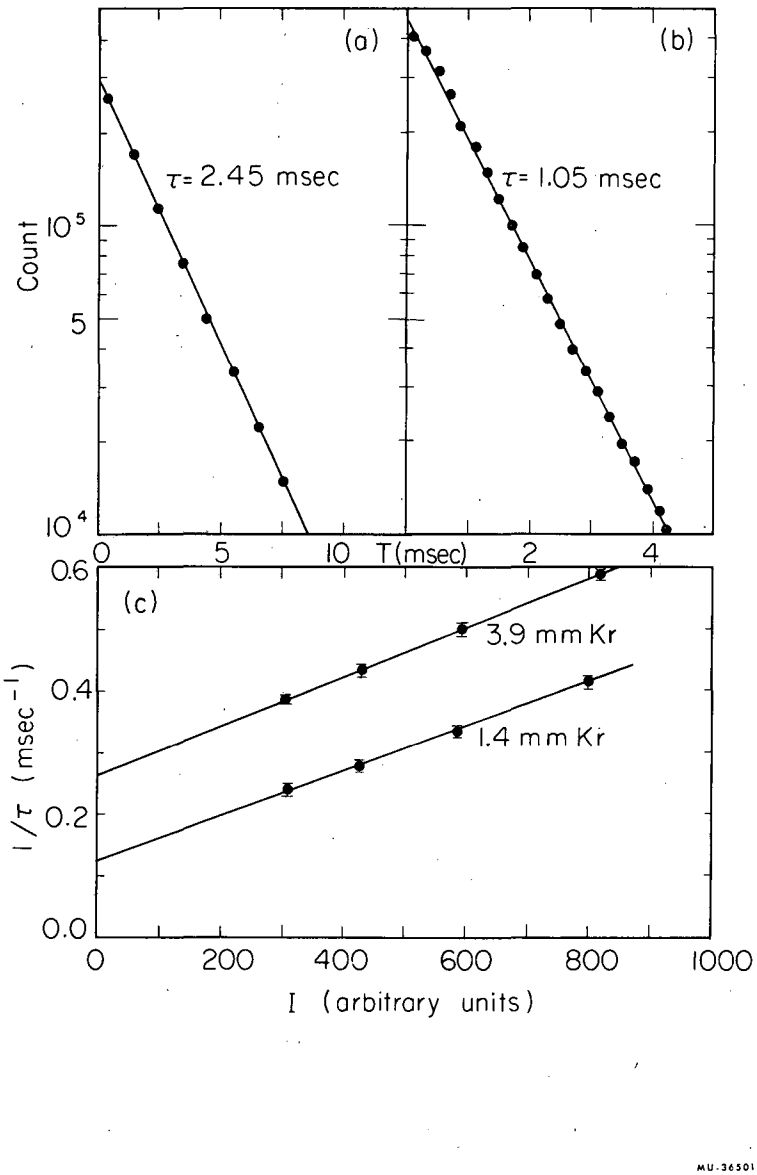

Fig. V-21. Typical Rb^{87} relaxation times in Kr. Curve a, 1.4 mm Kr. Curve b, 3.9 mm Kr.

Fig. V-22. Rb^{87} pumping transient (Kr buffer).

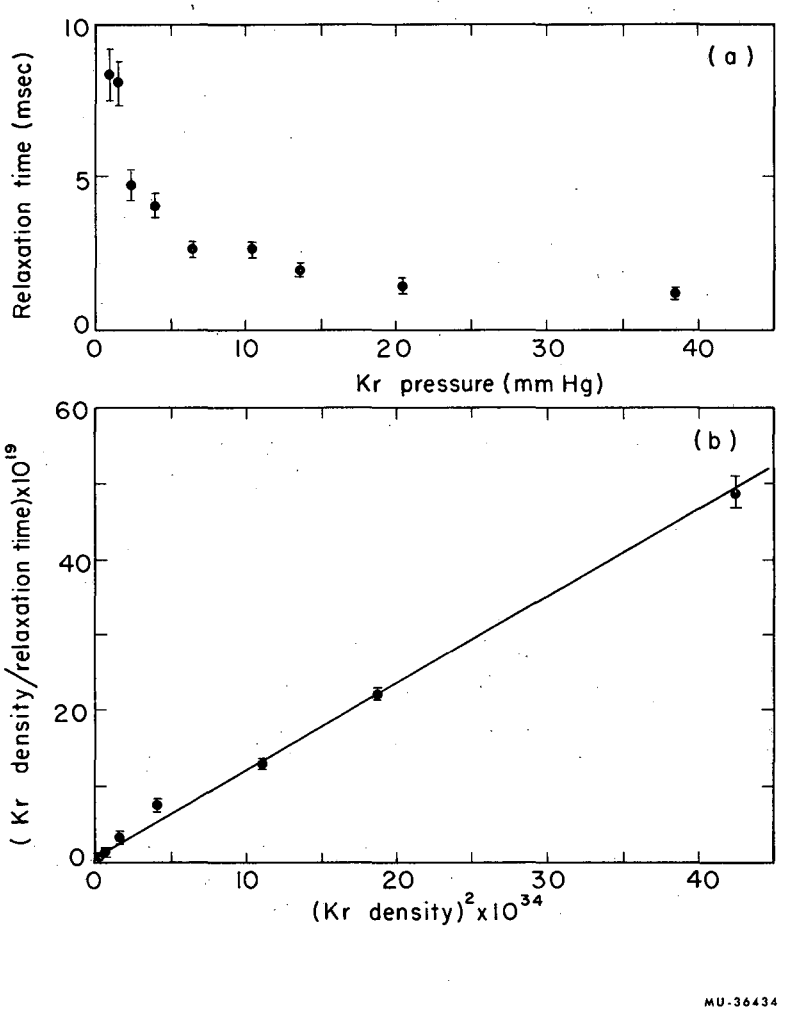

Fig. V-23. (a) Variation of Rb^{87} relaxation times T_1 with Kr pressure 24°C±1°C. (b) Plot of n/T_1 vs n^2.

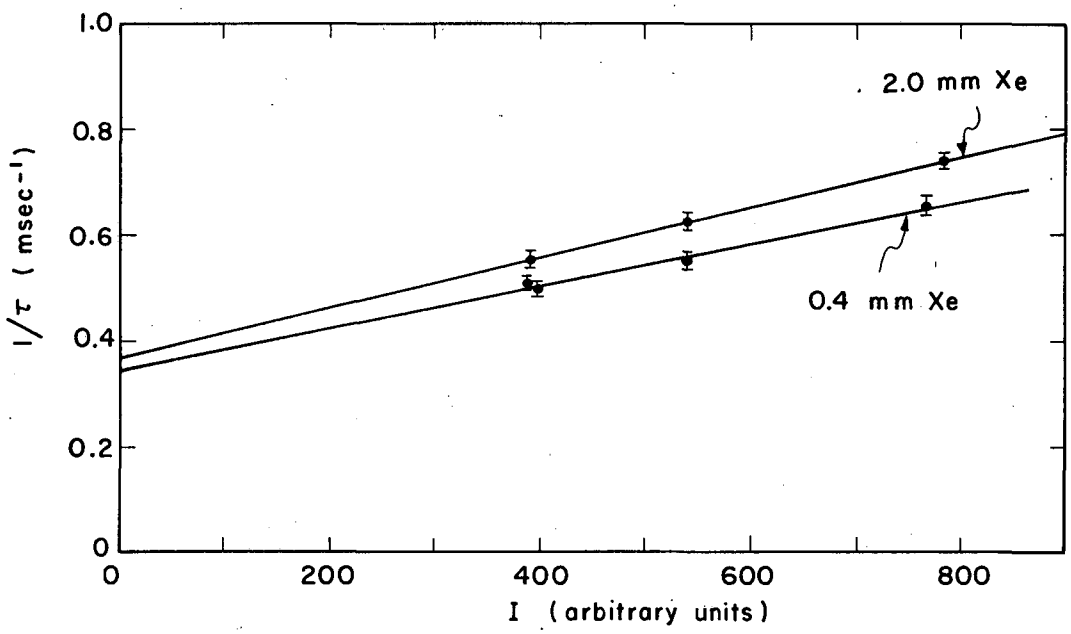

MU-36435

Fig. V-24. Typical Rb^{87} relaxation times in Xe at 25± 1°C.

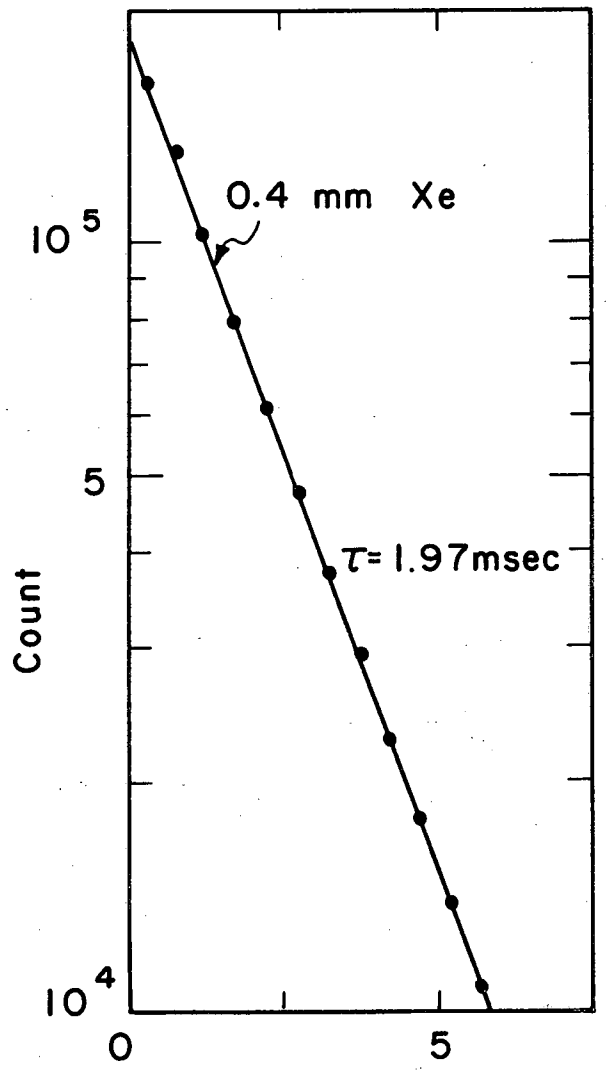

Fig. V-25. Rb^{87} pumping transients (Xe buffer), 0.4 mm Xe.

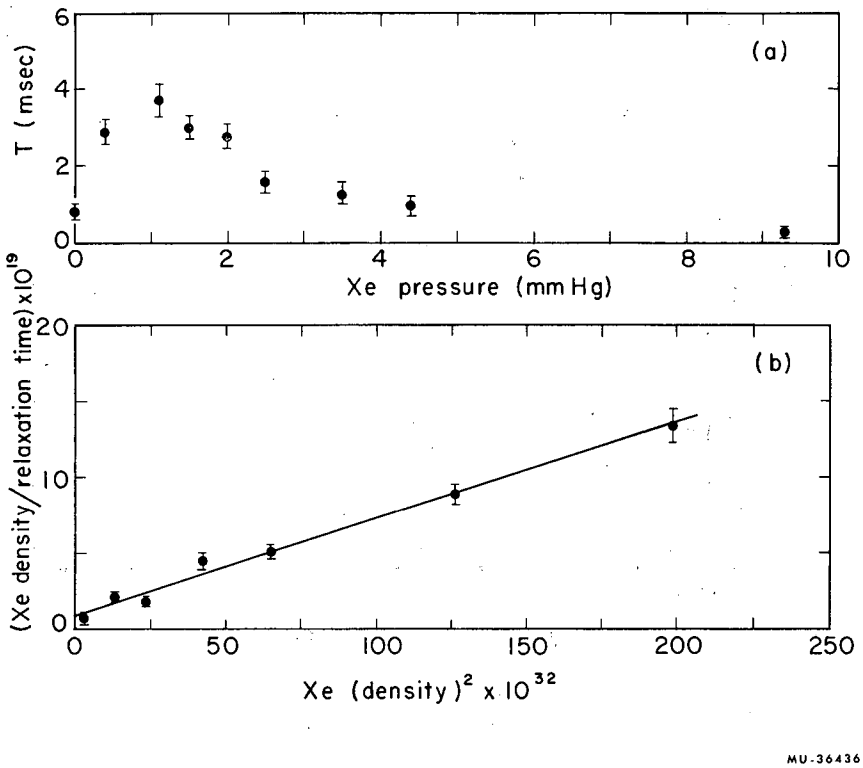

Fig. V-26. (a) Variation of Rb^{87} relaxation time with Xe pressure at 25± 1°C. (b) Plot of n/T_1 vs n^2.

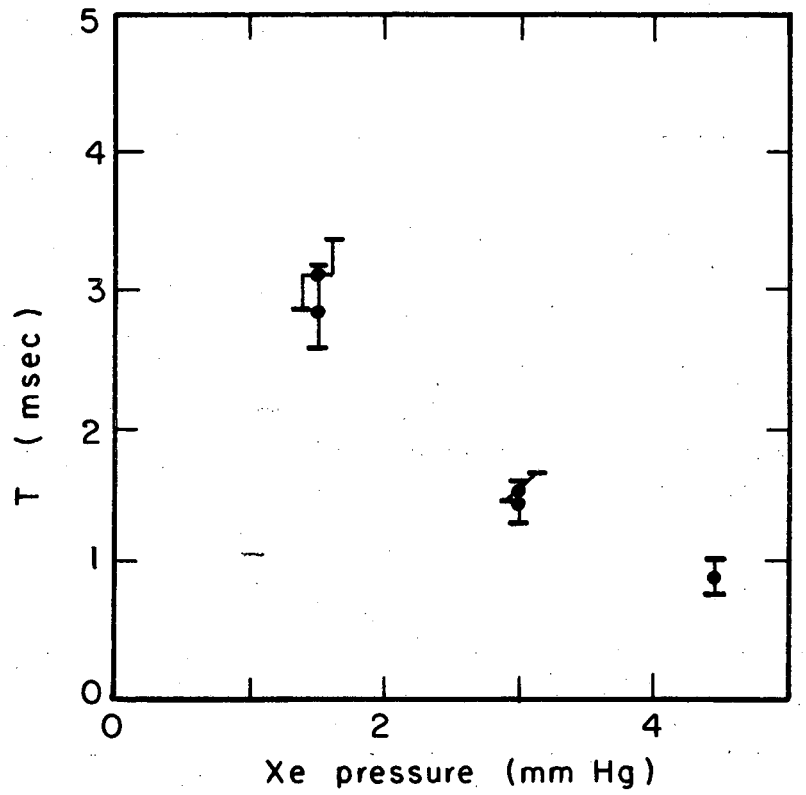

Fig. V-27. Same as V-26(a) but for a different cell of similar dimensions (6 cm in diameter, 2.7 cm long, i.d.).

a sampling interval. The 0.5 msec/chn interval used is an appreciable fraction of the transient lifetime but does not lead to appreciable distortion so long as we are dealing with a single exponential. Although this can be demonstrated easily, to play it safe we checked several transients by stepping down the sampling interval to 0.1 msec/chn but saw no significant difference. Cross sections established by the above data are summarized in Table V-4 below along with the results (estimated) of Franzen and Franz.[6,33] Diffusion coefficients for Kr and Xe are respectively 0.17 cm^2/sec and 0.14 cm^2/sec.

B. Results for Cesium-133

1. Cesium-Argon

Cesium relaxation times in Argon were measured in a cylindrical Pyrex cell 6 cm in diameter and 2 cm long (inside dimensions) at 25°C ± 1°. The transients were singly exponential except at the highest pressures where some deviations were observed. This probably means that the cross section for mixing the Cesium ^2P state is small (compared to the same cross section for Rb), as indeed one would expect from the fact that the fine structure splitting of the Cesium 6^2P state is more than twice the mean kinetic energy available in collisions. No attempt was made to pursue the excited-state disorientation cross section, but the ground-state disorientation cross section was determined and is in fair agreement with the results of Franz and Luescher but in disagreement with the results of Legowski.[34] In figures V-28 and V-29 the results are summarized and in Table V-5 our results are compared with those of Franz and Luescher and Legowski.

2. Cesium-Krypton

Ground-state relaxation times for Cs and Kr were measured in a cell 4 cm diameter and 1 cm long (inside dimension) at 25°C ± 1°. The cell tipoffs (one from the side arm that contained the Cs and the second from an unused side arm) represented 10 to 15% of the cell volume; but this figure should not have a significant effect on the applicability of the diffusion equation in which cylindrical boundaries are assumed, since the total area represented by the tipoffs plus cell pump

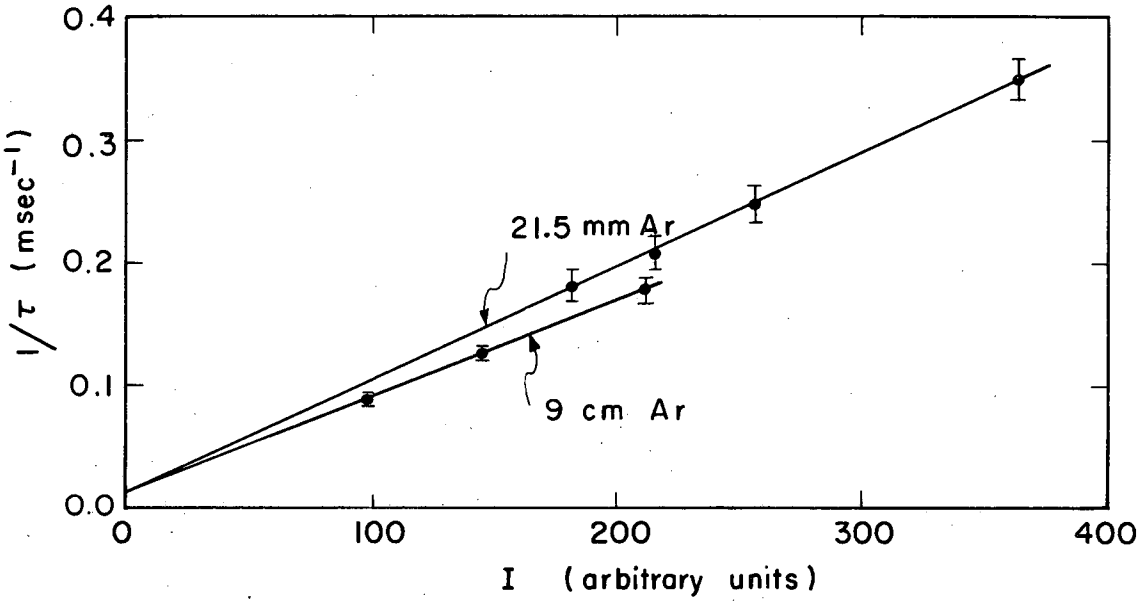

Fig. V-28. Cs^{133} relaxation times in Ar at 25±1°C.

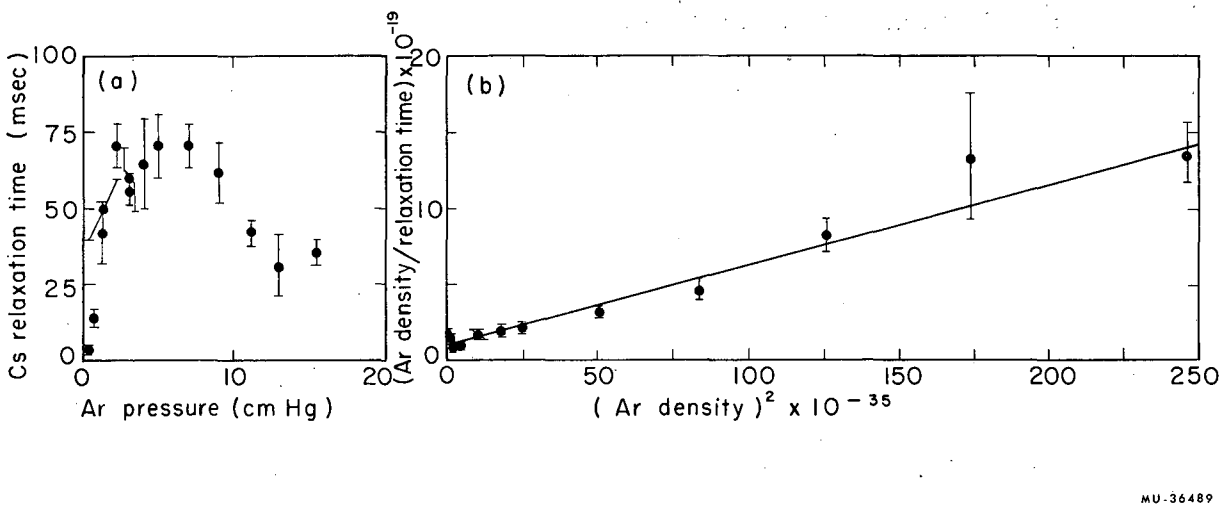

Fig. V-29. (a) Variation of Cs^{133} relaxation times with Ar pressure at 25 ± 1°C. (b) Plot of n/T_1 vs n^2.

out amounted to only ≈5% of the wall area. Relaxation times and their interpretation are summarized in Figs. V-30 to V-31 and Table V-5. Data for some points were successively gathered two and four days apart. The disagreement between our cross section for Cs-Kr and that of Franz and Luescher is striking. During this run a number of relaxation times were measured in Ar to check for contamination of the vacuum system. The results were consistent with those of Franz and Luescher and our own results above.

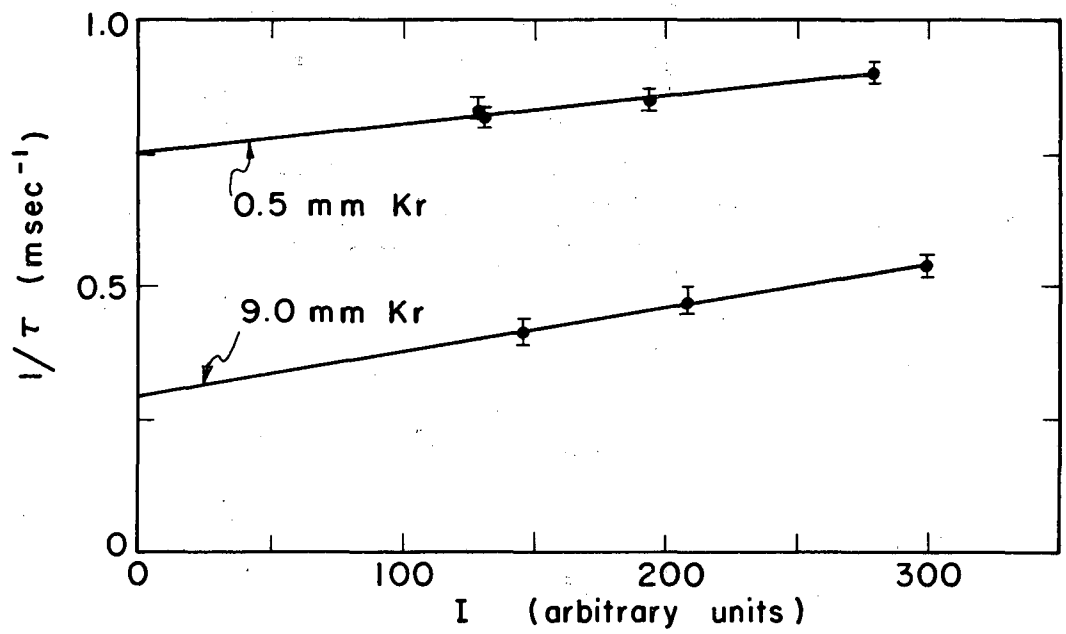

Fig. V-30. Cs^{133} relaxation times in Kr at 25± 1°C.

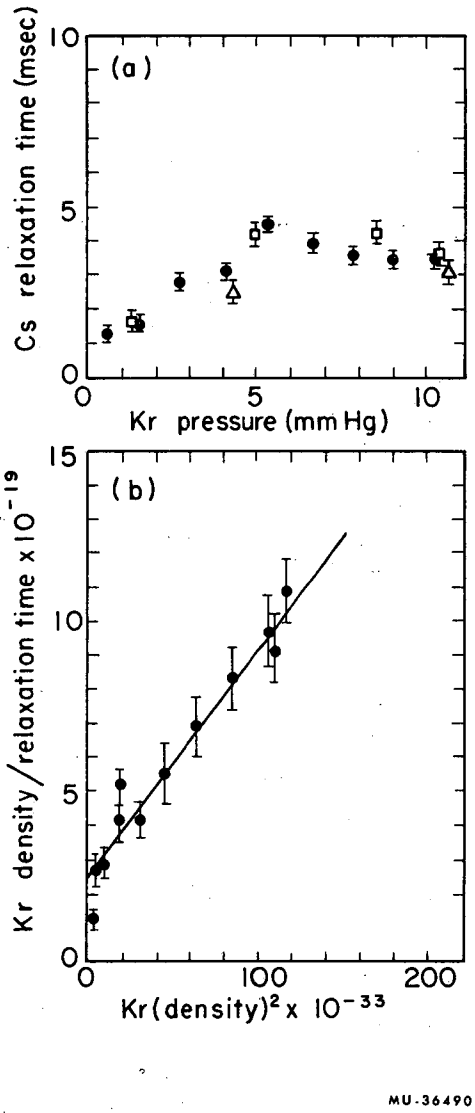

Fig. V-31. (a) Variation of Cs^{133} relaxation times with Kr pressure at 25± 1°C. (b) Plot of n/T_1 vs n^2.

Table V-5. Ground-state disorientation cross section for Cs.

Buffer gas	This work 25°C	Franz and Franz[a] 44°C	Legowski[b]
He	---		2.5×10^{-24} cm^2
Ne	---	5.2×10^{-24} cm^2	8.4×10^{-24}
Ar	$1.2(0.2)\times10^{-22}$ cm^2	8.0×10^{-23}	2.6×10^{-24}
Kr	$1.9(0.2)\times10^{-20}$	2.1×10^{-21}	
Xe		4.6×10^{-20}	

[a] See Ref. 33.

[b] See Ref. 34.

VI. FURTHER STUDIES

A. Observation of D_2 Light in Forward Scattering

The phase-sensitive detection system used in our experiments raised an interesting possibility for measuring $\sigma_{1/2,\,3/2}$ by an optical pumping adaptation of the classical experiment of Lochte and Holtgraven.[35-39] Since the Rb vapor is most absorbing when it is not pumped and least absorbing when it is we would expect the scattered D_2 light to be maximum when the rf is on and minimum when it is off; i.e., the scattered D_2 light is 180° out of phase with the direct D_1 signal (but not the scattered D_1 signal), and moreover it is modulated 100% (the roles of D_1 and D_2 can be reversed to measure $\sigma_{3/2,\,1/2}$). Thus if we place a D_2 filter in front of the detector we should observe an inverted signal. Such a signal was observed in a sealed-off Rb^{87} cell with 23-cm He and is shown in Fig. VI-1. Although a search for forward-scattered D_2 light was made at a few lower He pressures (also in sealed cells), it was unsuccessful. This lends support to the small mixing cross section measured.

B. Optical Pumping in a Cell Containing neither a Buffer Gas nor Wall Coating

The extreme sensitivity of the detection scheme makes possible observation of optical pumping under extreme conditions. For example, one could study relaxation of oriented alkali atoms by foreign gases and wall coatings without the limitations imposed by conventional techniques (≈10 msec). Relaxation by substances present as impurities in optical pumping systems (e.g., O_2 adsorbed in glass or wall coating) in either wall coatings or buffer gases is of interest. A step in that direction is the observation of pumping in a Pyrex cell with no buffer gas,[40] shown in Fig. VI-2. Because τ_{pumping} is very much greater than T_1, the transient lifetime is essentially T_1. From the measured relaxation time of 0.6 msec and the cell geometry we can calculate the number of wall collisions N required to disorient a Rb (Cs) atom. If r is the distance traveled between collisions and v the velocity, then

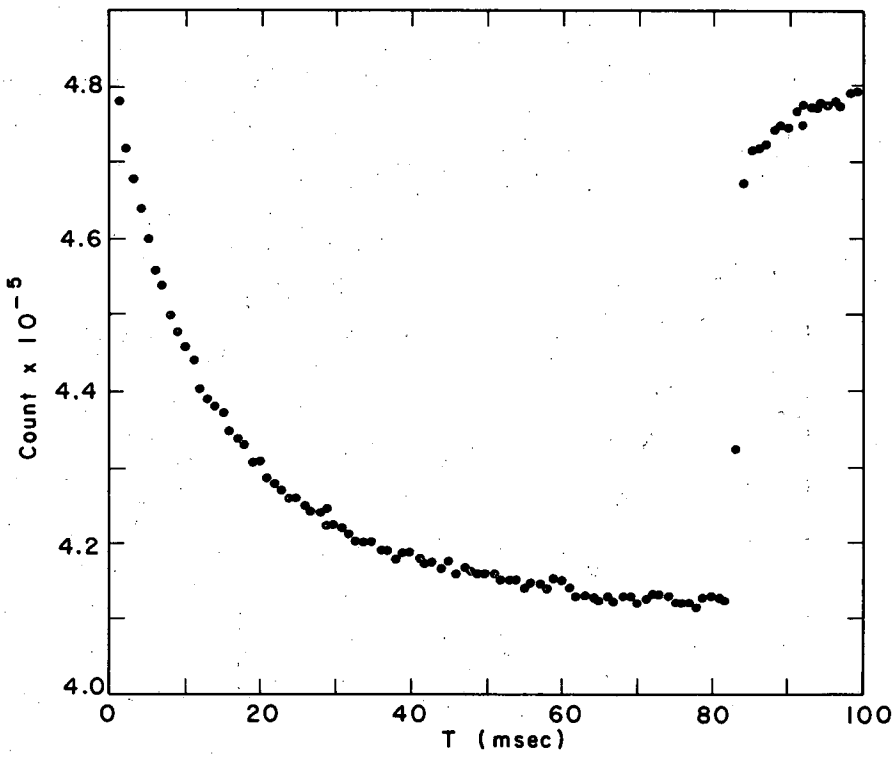

Fig. VI-1. D_2 signal observed in a Rb^{87} cell containing He at 23 cm of Hg and pumped with D_1 light.

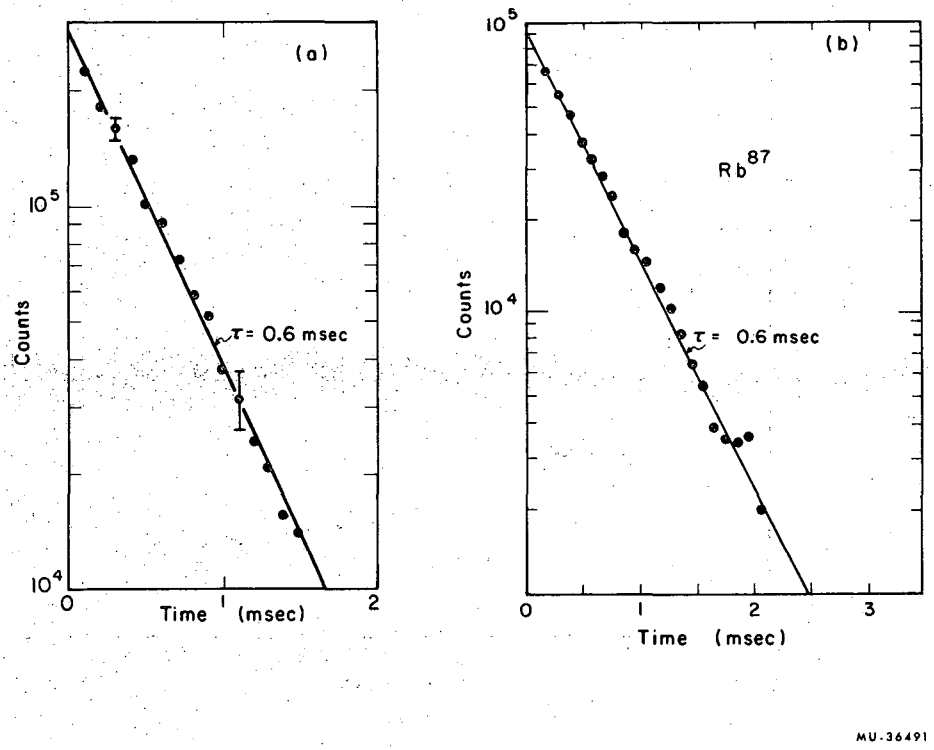

Fig. VI-2. Optical pumping signals in a Pyrex cell having no buffer. (a) Cs. (b) Rb.

T_1 equals $N\left\langle\frac{r}{v}\right\rangle$, where r is averaged over the spherical cell and v is averaged over all velocities. Hence T_1 equals $N\langle r\rangle\left\langle\frac{1}{v}\right\rangle = \left(\frac{4}{3}a\right)\sqrt{\frac{2m}{\pi kT}}\,N$, where a is the radius of the cell, from whcih we get N = 2 for Cs and N = 2.5 for Rb, taking a = 3.7 cm, $\left\langle\frac{1}{v}\right\rangle_{Cs}=(5.8\times10^{-5})$ sec/cm, and $\left\langle\frac{1}{v}\right\rangle_{Rb}= (4.7\times10^{-5})$ sec/cm. For the longest relaxation times observed in a wall-coated cell, T_1 is approximately 1 sec and N is approximately 10^4 collisions.

C. Hyperfine Relaxation by a Double-Transient Technique

Hyperfine relaxation has been observed previously by Bouchiat and Brossel,[40] who selectively pumped one of the hyperfine components of Rb^{87} with unpolarized light from a Rb^{85} lamp and conducted a Franzen-type experiment to determine the relaxation time. More recently Arditi and Carver[41] observed hyperfine relaxation in Rb^{87} also by selective pumping with unpolarized light to produce a hyperfine population difference and then looking at stimulated microwave emission. It is also possible for one to determine the hyperfine relaxation time by looking at the above pumping transients and extrapolating the reciprocal of the pumping times to zero light intensity. However, to obtain enough statistics, the pumping transients would have to be regenerated many times and this would call for a microwave cavity with associated electronics that would greatly complicate the experiment. There is, however, a way to observe hyperfine relaxation by inducing only Zeeman transitions. It works as follows: Instead of using unpolarized hyperfine light, we use circularly polarized hyperfine light, say σ^+. We then have four nonabsorbing levels, using Rb^{87} as a model (see Fig. VI-3). The $m_F= 2$ level has zero absorption probability ($5\,P_{1/2} \leftrightarrow 5\,S_{1/2}$) and the three sublevels of the F = 1 state are also nonabsorbing (because there is no light to absorb, in this case). The pumping process will then distribute the atoms principally among these four "metastable" levels. If we now resonate the Zeeman levels, the atoms which were in the F=2 state become absorbing once again as the $m_F=2$ level is shorted out, but the F=1 state is still nonabsorbing. Thus the pumping process now favors the F=1 levels, which may be treated as a

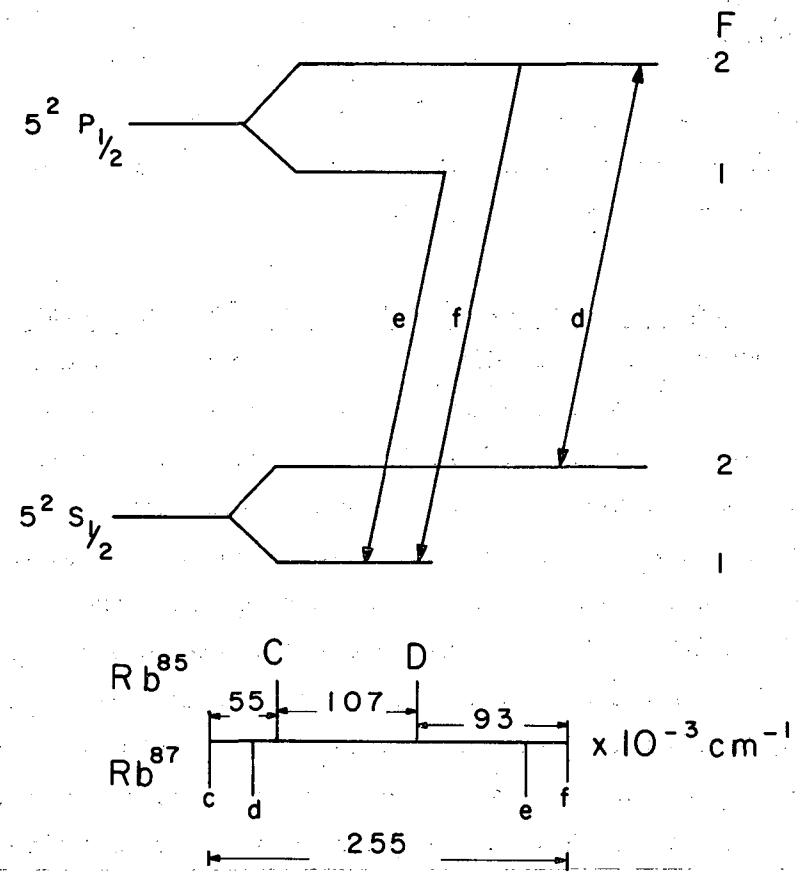

Fig. VI-3. Level diagram illustrating hyperfine pumping of Rb^{87} by a Rb^{85} D_1 light source.

single level since the rf equalizes the three levels, and one observes a new pumping transient simultaneously with the appearance of the rf-induced decay of the primary transient. This secondary transient due to a net transfer of atoms from the F = 2 to the F = 1 state is of a simpler nature than the primary transient, as we are dealing effectively with a two-level system (the rf maintains the populations of each state equal). The secondary transient is dependent on the hyperfine relaxation that can be obtained by extrapolation of the pumping times to zero light intensity.

Preliminary observations of the hyperfine transient discussed above have been made and the results shown in Fig. VI-4. These measurements were made with Rb^{87}(99.16%) in a cylindrical cell 4-in. long and 2 in. in diameter and containing 4.6-cm Ne. The Ne pressure was sufficient to broaden the absorption line so as to increase the pumping efficiency, yet not sufficient to appreciably disorient the P state, so that the primary transient is practically a single exponential. The pumping source was an enriched Rb^{85}(99.54%) Varian-type lamp with 2 mm Kr. Extrapolation of the two transients to zero light intensity indicated a longer relaxation time for hyperfine transient, i.e., $T_1(\Delta F = \pm 1) > T_1(\Delta F = \pm 1, 0)$. The relaxation rate appearing in the first transient (rf off) is the sum for $\Delta F = 0$ and $\Delta F = \pm 1$. One would expect that as the Rb density is increased and spin exchange becomes a dominant relaxation factor, the hyperfine population difference would diminish and with it the amplitude of the secondary transient (rf on). This was in fact observed and the results shown in Fig. VI-5.

We note in concluding that the temperature at which the hyperfine transient vanishes is about the same as that at which distortions become prominant in the primary transient.

D. Spin Exchange

A pumping transient in an evacuated cell containing a single species of alkali atoms has been shown to be singly exponential. One might inquire about the nature of the signal if a second species were present and spin exchanging with the pumped specie. The circumstance

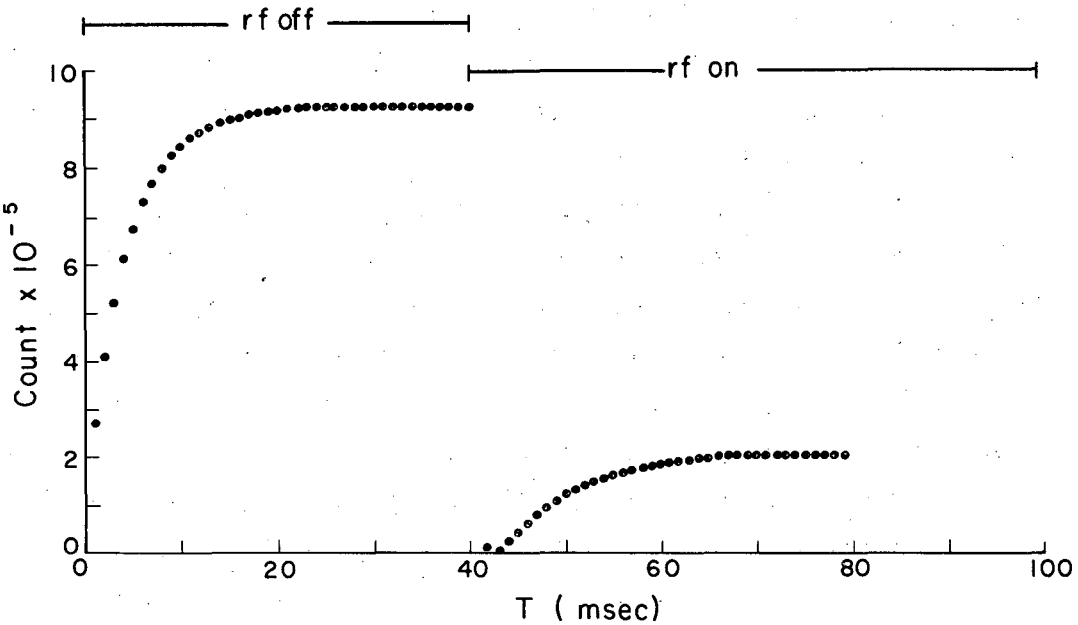

Fig. VI-4. Pumping transient due to Rb^{85} light source pumping Rb^{87}.

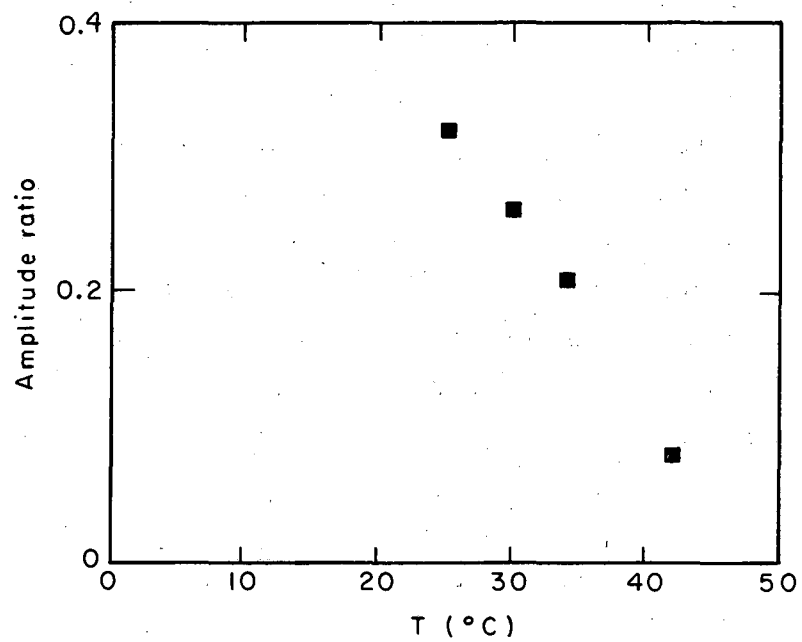

Fig. VI-5. Ratio of hyperfine pumping transient amplitude to Zeeman pumping transient amplitude as function of temperature.

that a single exponential adequately describes a single species indicates that the pumping can be defined by a single rate equation as in the absence of nuclear spin. Two species may then be expressible by a system of two rate equations coupled by spin exchange. If this is the case, then the pumping transient will show a structure that can be simply related to the spin-exchange cross section.

Observations were made on a Cs-Rb system in a wall-coated cell showing structure in the signal. The shape of the Cs signal at 25°C appeared to be a sum of two exponentials with amplitudes of 10:1. No attempt was made to get quantitative data but it is clear that the structure was due to spin exchange as no exception to the rule that a single species (Rb^{85}, Rb^{87}, Cs^{33}) gives a singly exponential signal in an evacuated cell has been observed at low alkali densities. Incidentally, distortions observed in single-species signals at high densities cannot be expressed as a sum of exponentials.

E. Radio-Frequency-Induced Decay of Polarization

All of our information so far has come to us from the transitory pumping signal (rf off). It is also possible to get data from the depumping signal, i.e., from the transient that arises when the rf is turned on. The analysis is more complicated and less certain and no quantitative data were obtained, although general features were observed. The depumping transient is singly exponential in the absence of foreign gas, but in the presence of a foreign gas it is the sum of at least two exponentials. The lifetimes of the signals depend on rf power, foreign-gas pressure, and the intensity of the pumping radiation. Probably for a high rf field the signal could be treated by simply incorporating an effective rf relaxation time, τ_{rf}, into the pumping equations and taking into account the differences of the initial populations, but when $\tau_{rf} \geq \tau_{pumping}$ and $\tau_{rf} \geq T_1$, one may have to resort to the Majorana equation and calculate the rf transition rates explicitly.

VII. CONCLUSIONS

We have shown (a) that the phenomenological model of optical pumping proposed by Franzen and Emslie adequately describes the optical pumping process in alkali vapors and (b) that Dehmelt's method for measuring ground-state relaxation times is consistent with the model in the limit that the P state is not reoriented, but (c) that if mixing occurs in the P state, the Dehmelt method cannot be applied directly. We have shown too that quantitative information pertaining both to the ground state of an alkali ($S_{1/2}$) and the excited state ($P_{1/2}$) can be obtained from an analysis of the structure of transient optical pumping signals. As an application we have measured cross sections for mixing the $5^2P_{1/2}$ state of Rb^{87} through collisions with Ar, Ne, and He as well as ground-state disorientation cross sections for Ne, Ar, Kr, and Xe. We also made limited measurements on Cs^{133}. We believe that the experimental technique and the type of analysis used to interpret the results will contribute to a better understanding of relaxation encountered in optical pumping.

ACKNOWLEDGMENTS

I take pleasure in expressing my indebtedness and gratitude to the many people who have contributed to the success of this research:

Professor Richard Marrus for suggesting the experiment and for constant discussion of problems relating to the research;

Professor William A. Nierenberg for theoretical discussions of the optical pumping equations;

Professor Howard A. Shugart for assistance in the early stages of the experiment and for his generous moral support;

Dr. Douglas W. McColm from whom I have learned much experimental technique and electronics.

Dr. Tetsuo Hadeishi and Dr. Hyatt Gibbs, from whose discussions I have benefitted;

Mr. Douglas B. Macdonald for teaching me much in the way of vacuum technology and for his expert mechanical design;

Mr. Harry Powell and his staff for constructing the glass apparatus; and particular thanks to Mr. Willis Berlund for constructing and installing much of the apparatus;

Mr. G. G. Young and his staff for constructing various parts of the vacuum system;

Mr. George W. Kilian, Mr. George A. Constantian, and Mr. Mich Nakamura and their staffs for providing electronic hardware and advice.

I am especially grateful to Miss Christina Frank for typing the original draft of the thesis and making a number of helpful suggestions.

This work was supported under the auspices of the U. S. Atomic Energy Commission.

APPENDICES

A. Additional Numerical Results

In this appendix are tabulated Clebsch-Gordan coefficients (Table A-1), Racah coefficients (Table A-2), transition probabilities w_{ij}, r_i, B_{ij} (Tables A-3 to A-10), and the results of computations for an alkali of nucelar spin I = 3/2, 5/2, and 7/2 pumped with right circularly polarized D_1 resonance radiation (Tables A-11 to A-16). Figures A-1 to A-4 give the equilibrium absorption probabilities and equilibrium polarizations for Rb^{85} and Cs^{133} optically pumped with circularly polarized D_1 light.

B. Electronic and Nuclear Polarization

It is of some interest to calculate the electronic and nuclear polarizations. These calculations are readily accomplished with the aid of the density matrix whose diagonal elements are the populations. We have

$$P_{electron} = \langle J_z \rangle / (m_J)_{max} = [\text{trace}(\rho J_z)] / (m_J)_{max},$$

where ρ is the density matrix and the matrix of J_z is

$$\langle FJIm_F | J_z | F'JIm'_F \rangle = \delta_{FF'} \delta_{m_F m'_F} \sum_{m_J m_I} m_J |C(FJI; m_F m_J m_I)|^2.$$

The last relation follows from the fact that

$$|FJIm_F\rangle = \sum_{m_J m_I} C(FJI; m_F m_J m_I) |J, m_J\rangle |I, m_I\rangle$$

and

$$J_z |J, m_J\rangle = m_J |Jm_J\rangle .$$

Thus

$$P_{electron} = \sum_{m_F} p(m_F) \sum_{m_j I_I} m_J |C(FJI; m_F m_J m_I)|^2 / (m_J)_{max}$$

Table A-1. Clebsch-Gordan coefficients $C(F1F'; {}^{m_F}{}_{\mu}{}^{m'_F})$.

	m_F	F = 1			F = 2					F = 3							F = 4								
	m'_F	-1	0	1	-2	-1	0	1	2	-3	-2	-1	0	1	2	3	-4	-3	-2	-1	0	1	2	3	4
F'=1	-1	$-1/\sqrt{2}$	$1/\sqrt{2}$	0	$\sqrt{3/5}$	$-\sqrt{3/10}$	$1/\sqrt{10}$		0				-1												
	0	$-1/\sqrt{2}$	0	$1/\sqrt{2}$	0	$\sqrt{3/10}$	$-\sqrt{2/5}$	$\sqrt{3/10}$	0				0												
	1	0	$-1/\sqrt{2}$	$1/\sqrt{2}$	0	0	$1/\sqrt{10}$	$\sqrt{3/10}$	$\sqrt{3/5}$				1												
F'=2	-2	1	0	0	$-2/\sqrt{6}$	$1/\sqrt{3}$	0	0	0	$\sqrt{5/7}$	$-\sqrt{5/21}$	$1/\sqrt{21}$	0	-2	0	0	0								
	-1	$1/\sqrt{2}$	$1/\sqrt{2}$	0	$-1/\sqrt{3}$	$-1/\sqrt{6}$	$1/\sqrt{2}$	0	0	0	$\sqrt{10/21}$	$8/\sqrt{21}$	$1/\sqrt{7}$	-1	0	0	0								
	0	$1/\sqrt{6}$	$\sqrt{2/3}$	$1/\sqrt{6}$	0	$-1/\sqrt{2}$	0	$1/\sqrt{2}$	0	0	0	$\sqrt{2/7}$	$-\sqrt{3/7}$	0	$\sqrt{6/21}$	0	0								
	1	0	$1/\sqrt{2}$	$1/\sqrt{2}$	0	0	$-1/\sqrt{2}$	$1/\sqrt{6}$	$1/\sqrt{3}$	0	0	0	$1/\sqrt{7}$	1	$-\sqrt{8/21}$	$\sqrt{10/21}$	0								
	2	0	0	1	0	0	0	$-1/\sqrt{3}$	$2/\sqrt{6}$	0	0	0	0	2	$1/\sqrt{21}$	$-\sqrt{5/21}$	$\sqrt{5/7}$								
F'=3	-3				1	0	0	0	0	$-\frac{3}{2}\sqrt{3}$	$1/2$	0	0	-3	0	0	0	$\frac{1}{3}\sqrt{7}$	$-\frac{1}{6}\sqrt{7}$	1/6	0	0	0	0	0	0
	-2				$1/\sqrt{3}$	$\sqrt{2/3}$	0	0	0	$-1/2$	$-1/\sqrt{3}$	$\frac{1}{2}\sqrt{5/3}$	0	-2	0	0	0	0	$\frac{1}{2}\sqrt{7/3}$	$-1/\sqrt{3}$	$\frac{1}{2}\sqrt{3}$	0	0	0	0	0
	-1				$1/\sqrt{15}$	$\sqrt{8/15}$	$\sqrt{2/5}$	0	0	0	$-\frac{1}{2}\sqrt{5/3}$	$-\frac{1}{2}\sqrt{3}$	$1/\sqrt{2}$	-1	0	0	0	0	0	$\frac{1}{2}\sqrt{5/3}$	$-\frac{1}{2}\sqrt{5/3}$	$1/\sqrt{6}$	0	0	0	0
	0				0	$1/\sqrt{5}$	$\sqrt{3/5}$	$1/\sqrt{5}$	0	0	0	$-1/\sqrt{2}$	0	0	$1/\sqrt{2}$	0	0	0	0	0	$\frac{1}{3}\sqrt{5/2}$	$-\sqrt{2/3}$	$\frac{1}{3}\sqrt{5/2}$	0	0	0
	1				0	0	$\sqrt{2/5}$	$\sqrt{8/15}$	$1/\sqrt{15}$	0	0	0	$-1/\sqrt{2}$	1	$1/\sqrt{12}$	$\frac{1}{2}\sqrt{5/3}$	0	0	0	0	0	$1/\sqrt{6}$	$-\frac{1}{2}\sqrt{5/3}$	0	0	0
	2				0	0	0	$\sqrt{2/3}$	$1/\sqrt{3}$	0	0	0	0	2	$-\frac{1}{2}\sqrt{5/3}$	$1/\sqrt{3}$	$1/2$	0	0	0	0	0	$\frac{1}{2}\sqrt{3}$	$-1/\sqrt{3}$	$\frac{1}{2}\sqrt{7/3}$	0
	3				0	0	0	0	1	0	0	0	0	3	0	$-1/2$	$\sqrt{3/2}$	0	0	0	0	0	0	$1/6$	$-\frac{1}{6}\sqrt{7}$	$\sqrt{7/3}$
F'=4	-4									1	0	0	0	-4	0	0	0	$-2/\sqrt{5}$	0	0	0	0	0	0	0	0
	-3									$1/2$	$\frac{1}{2}\sqrt{3}$	0	0	-3	0	0	0	$-1/\sqrt{5}$	$-\frac{3}{2}\sqrt{5}$	$\frac{1}{2}\sqrt{7/5}$	0	0	0	0	0	0
	-2									$\frac{1}{2}\sqrt{7}$	$\sqrt{3/7}$	$\frac{1}{2}\sqrt{15/7}$	0	-2	0	0	0	0	$-\frac{1}{2}\sqrt{7/5}$	$-1/\sqrt{5}$	$\frac{3}{2}\sqrt{5}$	0	0	0	0	0
	-1									0	$\frac{1}{2}\sqrt{3/7}$	$\frac{1}{2}\sqrt{15/7}$	$\sqrt{5/14}$	-1	0	0	0	0	$-\frac{3}{2}\sqrt{5}$	$-\frac{1}{2}\sqrt{5}$	$+1/\sqrt{2}$	0	0	0	0
	0									0	0	$\sqrt{3/14}$	$2/\sqrt{7}$	0	$\sqrt{3/14}$	0	0	0	0	0	$-1/\sqrt{2}$	0	$1/\sqrt{2}$	0	0	0
	1									0	0	0	$\sqrt{5/14}$	1	$\frac{1}{2}\sqrt{15/7}$	$\frac{1}{2}\sqrt{3/7}$	0	0	0	0	0	$-1/\sqrt{2}$	$\frac{1}{2}\sqrt{5}$	$\frac{3}{2}\sqrt{5}$	0	0
	2									0	0	0	0	2	$\frac{1}{2}\sqrt{15/7}$	$\sqrt{3/7}$	$\frac{1}{2}\sqrt{7}$	0	0	0	0	0	$-\frac{3}{2}\sqrt{5}$	$1/\sqrt{5}$	$\frac{1}{2}\sqrt{7/5}$	0
	3									0	0	0	0	3	0	$\frac{1}{2}\sqrt{3}$	$1/2$	0	0	0	0	0	0	$-\frac{1}{2}\sqrt{7/5}$	$\frac{3}{2}\sqrt{5}$	$1/\sqrt{5}$
	4									0	0	0	0	4	0	0	1	0	0	0	0	0	0	0	$-1/\sqrt{5}$	$2/\sqrt{5}$

Table A-2. Racah coefficients.

$W(\frac{1}{2}\ F\ \frac{1}{2}\ F';\ \frac{3}{2}\ 1)$

F \ F'	1	2
1	$1/6$	$1/2\sqrt{3}$
2	$1/2\sqrt{3}$	$1/2\sqrt{5}$

$W(\frac{1}{2}\ F\ \frac{1}{2};\ \frac{5}{2}\ 1)$

F \ F'	2	3
2	$1/3\sqrt{5}$	$1/3\sqrt{2}$
3	$1/3\sqrt{2}$	$2/3\sqrt{14}$

$W(\frac{1}{2}\ F\ \frac{1}{2}\ F;\ \frac{7}{2}\ 1)$

F \ F'	3	4
3	$1/2\sqrt{14}$	$1/2\sqrt{6}$
4	$1/2\sqrt{6}$	$5/6\sqrt{30}$

Table A-3. Transition probabilities W_{ij} for Rb^{87} irradiated with D_1 resonance radiation ($5^2P_{1/2} \rightarrow 5^2S_{1/2}$).

		F' = 1			F' = 2				
		-1	0	1	-2	-1	0	1	2
F = 1	-1	1/12	1/12	0	1/2	1/4	1/12	0	0
	0	1/12	0	1/12	0	1/4	1/3	1/4	0
	1	0	1/12	1/12	0	0	1/12	1/4	1/2
F = 2	-2	1/2	0	0	1/3	1/6	0	0	0
	-1	1/4	1/4	0	1/6	1/12	1/4	0	0
	0	1/12	1/3	1/12	0	1/4	0	1/4	0
	1	0	1/4	1/4	0	0	1/4	1/12	1/6
	2	0	0	1/2	0	0	0	1/6	1/3

Table A-4. Relative transition probabilities $\sum_j b_{ij}$ $\Delta m = +1$.

	F = 1			F = 2				
	1	2	3	4	5	6	7	8
m_F	-1	0	1	-2	-1	0	1	2
r_i	1/2	1	3/2	2	3/2	1	1/2	0

Table A-5. Transition probabilities w_{ij} for Rb^{85} irradiated with D_1 resonance radiation.

		w_{ij}											
		F' = 2					F' = 3						
	m'_F	-2	-1	0	1	2	-3	-2	-1	0	1	2	3
	m_F												
F = 2	-2	4/27	2/27	0	0	0	5/9	5/27	1/27	0	0	0	0
	-1	2/27	1/27	1/9	0	0	0	10/27	8/27	1/9	0	0	0
	0	0	1/9	0	1/9	0	0	0	2/9	3/9	2/9	0	0
	1	0	0	1/9	1/27	2/27	0	0	0	1/9	8/27	10/27	0
	2	0	0	0	2/27	4/27	0	0	0	0	1/27	5/27	5/9
F = 3	-3	5/9	0	0	0	0	1/3	1/9	0	0	0	0	0
	-2	5/27	10/27	0	0	0	1/9	4/27	5/27	0	0	0	0
	-1	1/27	8/27	2/9	0	0	0	5/27	1/27	2/9	0	0	0
	0	0	1/9	1/3	1/9	0	0	0	2/9	0	2/9	0	0
	1	0	0	2/9	8/27	1/27	0	0	0	2/9	1/27	5/27	0
	2	0	0	0	10/27	5/27	0	0	0	0	5/27	4/27	1/9
	3	0	0	0	0	5/9	0	0	0	0	0	1/9	1/3

Table A-6. Relative transition probabilities r_i for $\Delta m = +1$.

F = 2					m_F	F = 3						
-2	-1	0	1	2		-3	-2	-1	0	1	2	3
1/3	2/3	1	4/3	5/3		2	5/3	4/3	1	2/3	1/3	0

Table A-7. Matrix of coefficients B_{ij} for an alkali with nuclear spin I = 5/2 with no reorientation in the P state; $\rho = 1/\beta_0 T$. Primes refer to initial state.

		m'											
		F' = 2					F' = 3						
F	m	-2	-1	0	+1	+2	-3	-2	-1	0	1	2	3
2	-2	$-\frac{76}{243}-\rho$	0	0	0	0	$\frac{25}{81}$	$\frac{25}{243}$	0	0	0	0	0
	-1	$\frac{10}{243}$	$-\frac{16}{27}-\rho$	0	0	0	$\frac{20}{81}$	$\frac{50}{243}$	$\frac{4}{27}$	0	0	0	0
	0	$\frac{4}{81}$	$\frac{1}{9}$	$-\frac{22}{27}-\rho$	0	0	0	$\frac{20}{81}$	$\frac{10}{27}$	$\frac{5}{27}$	0	0	0
	+1	0	$\frac{2}{27}$	$\frac{17}{81}$	$-\frac{212}{243}-\rho$	0	0	0	$\frac{4}{27}$	$\frac{2}{9}$	$\frac{52}{243}$	0	0
	+2	0	0	$\frac{4}{81}$	$\frac{50}{243}$	$-\frac{20}{27}-\rho$	0	0	0	$\frac{4}{81}$	$\frac{29}{243}$	$\frac{5}{27}$	0
3	-3	0	0	0	0	0	$-\frac{84}{81}-\rho$	0	0	0	0	0	0
	-2	$\frac{25}{243}$	0	0	0	0	$\frac{29}{81}$	$-\frac{280}{243}-\rho$	0	0	0	0	0
	-1	$\frac{17}{243}$	$\frac{4}{27}$	0	0	0	$\frac{10}{81}$	$\frac{85}{243}$	$-\frac{32}{27}-\rho$	0	0	0	0
	0	$\frac{4}{81}$	$\frac{1}{9}$	$\frac{5}{27}$	0	0	0	$\frac{20}{81}$	$\frac{2}{9}$	$-\frac{67}{81}-\rho$	0	0	0
	+1	0	$\frac{4}{27}$	$\frac{10}{81}$	$\frac{52}{243}$	0	0	0	$\frac{8}{27}$	$\frac{10}{81}$	$-\frac{116}{243}-\rho$	0	0
	+2	0	0	$\frac{20}{81}$	$\frac{50}{243}$	$\frac{5}{27}$	0	0	0	$\frac{20}{81}$	$\frac{5}{243}$	$-\frac{8}{27}-\rho$	0
	+3	0	0	0	$\frac{20}{81}$	$\frac{5}{9}$	0	0	0	0	$\frac{10}{81}$	$\frac{1}{9}$	$-\rho$

Table A-8. Transition probabilities w_{ij} for Cs^{133} irradiated with D_1 resonance radiation ($6^2P_{1/2} \rightarrow 6^2S_{1/2}$).

		w_{ij} F' = 3							w_{ij} F' = 4									
		-3	-2	-1	0	1	2	3	-4	-3	-2	-1	0	1	2	3	4	
F = 3	-3	3/16	1/16	0	0	0	0	0	7/12	7/48	1/48	0	0	0	0	0	0	0
	-2	1/16	1/12	5/48	0	0	0	0	0	7/16	1/4	1/16	0	0	0	0	0	0
	-1	0	5/48	1/48	1/8	0	0	0	0	0	5/16	5/16	1/8	0	0	0	0	0
	0	0	0	1/8	0	1/8	0	0	0	0	0	5/24	1/3	5/24	0	0	0	0
	1	0	0	0	1/8	1/48	5/48	0	0	0	0	0	1/8	5/16	5/16	0	0	0
	2	0	0	0	0	5/48	1/12	1/16	0	0	0	0	0	1/16	1/4	7/16	0	0
	3	0	0	0	0	0	1/16	3/16	0	0	0	0	0	0	1/48	7/48	7/12	0
F = 4	-4	7/12	0	0	0	0	0	0	1/3	1/12	0	0	0	0	0	0	0	0
	-3	7/48	7/16	0	0	0	0	0	1/12	3/16	7/48	0	0	0	0	0	0	0
	-2	1/48	1/4	5/16	0	0	0	0	0	7/48	1/12	3/16	0	0	0	0	0	0
	-1	0	1/16	5/16	5/24	0	0	0	0	0	3/16	1/48	5/24	0	0	0	0	0
	0	0	0	1/8	1/3	1/8	0	0	0	0	0	5/24	0	5/24	0	0	0	0
	1	0	0	0	5/24	5/16	1/16	0	0	0	0	0	5/24	1/48	3/16	0	0	0
	2	0	0	0	0	5/16	1/4	1/48	0	0	0	0	0	3/16	1/12	7/48	0	0
	3	0	0	0	0	0	7/16	7/48	0	0	0	0	0	0	7/48	3/16	1/12	0
	4	0	0	0	0	0	0	7/12	0	0	0	0	0	0	0	1/12	1/3	0

Table A-9. Relative absorption rates r_{m_F} for Cs^{133} with $\Delta m = +1$.

	m_F															
	F = 3							F = 4								
	-3	-2	-1	0	1	2	3	-4	-3	-2	-1	0	1	2	3	4
	1/4	1/2	3/4	1	5/4	3/2	7/4	2	7/4	3/2	5/4	1	3/4	1/2	1/4	0

Table A-10. Matrix of coefficients B_{ij} for an alkali with nuclear spin I = 7/2 and no reorientation in the P state assumed.

		m'																
		F' = 3							F' = 4									
F	m	-3	-2	-1	0	+1	+2	+3	-4	-3	-2	-1	0	+1	+2	+3	+4	
3	-3	$-\frac{91}{384}-\rho$	0	0	0	0	0	0	$\frac{35}{96}$	$\frac{35}{384}$	0	0	0	0	0	0	0	
	-2	$\frac{1}{32}$	$-\frac{175}{384}-\rho$	0	0	0	0	0	$\frac{7}{32}$	$\frac{7}{32}$	$\frac{17}{128}$	0	0	0	0	0	0	
	-1	$\frac{5}{128}$	$\frac{25}{384}$	$-\frac{21}{32}-\rho$	0	0	0	0	0	$\frac{35}{128}$	$\frac{25}{128}$	$\frac{5}{32}$	0	0	0	0	0	
	0	0	$\frac{5}{64}$	$\frac{1}{8}$	$-\frac{79}{96}-\rho$	0	0	0	0	0	$\frac{15}{64}$	$\frac{5}{24}$	$\frac{17}{96}$	0	0	0	0	
	+1	0	0	$\frac{3}{32}$	$\frac{13}{64}$	$-\frac{355}{384}-\rho$	0	0	0	0	0	$\frac{5}{32}$	$\frac{13}{64}$	$\frac{25}{128}$	0	0	0	
	+2	0	0	0	$\frac{5}{64}$	$\frac{25}{96}$	$-\frac{117}{128}-\rho$	0	0	0	0	0	$\frac{5}{64}$	$\frac{5}{32}$	$\frac{25}{128}$	0	0	
	+3	0	0	0	0	$\frac{5}{128}$	$\frac{29}{128}$	$-\frac{35}{48}-\rho$	0	0	0	0	0	$\frac{3}{128}$	$\frac{29}{384}$	$\frac{7}{48}$	0	
4	-4	0	0	0	0	0	0	0	$-\frac{23}{24}-\rho$	0	0	0	0	0	0	0	0	
	-3	$\frac{35}{384}$	0	0	0	0	0	0	$\frac{29}{96}$	$-\frac{427}{384}$	0	0	0	0	0	0	0	
	-2	$\frac{5}{96}$	$\frac{17}{128}$	0	0	0	0	0	$\frac{7}{96}$	$\frac{35}{96}$	$-\frac{141}{128}-\rho$	0	0	0	0	0	0	
	-1	$\frac{3}{128}$	$\frac{13}{128}$	$\frac{5}{32}$	0	0	0	0	0	$\frac{21}{128}$	$\frac{39}{128}$	$-\frac{95}{96}-\rho$	0	0	0	0	0	
	0	0	$-\frac{5}{64}$	$\frac{1}{8}$	$\frac{17}{96}$	0	0	0	0	0	$\frac{15}{64}$	$\frac{5}{24}$	$-\frac{79}{96}-\rho$	0	0	0	0	
	+1	0	0	$\frac{5}{32}$	$\frac{25}{192}$	$\frac{25}{128}$	0	0	0	0	0	$\frac{25}{96}$	$\frac{25}{192}$	$-\frac{81}{128}-\rho$	0	0	0	
	+2	0	0	0	$\frac{15}{64}$	$\frac{5}{32}$	$\frac{25}{128}$	0	0	0	0	0	$\frac{15}{64}$	$\frac{3}{32}$	$-\frac{167}{384}-\rho$	0	0	
	+3	0	0	0	0	$\frac{35}{128}$	$\frac{35}{128}$	$\frac{7}{48}$	0	0	0	0	0	$\frac{21}{128}$	$\frac{35}{384}$	$-\frac{11}{48}-\rho$	0	
	+4	0	0	0	0	0	$\frac{7}{32}$	$\frac{7}{12}$	0	0	0	0	0	0	$\frac{7}{96}$	$\frac{1}{12}$	$-\rho$	

Table A-11. Equilibrium population for Rb^{87} pumped with $\sigma^+ D_1$ resonance radiation, assuming no reorientation in the excited state.

	$P(m_F)$							
	F = 1			F = 2				
ρ	-1	0	1	-2	-1	0	1	2
0.005	0.00190	0.00196	0.00438	0.00053	0.00096	0.00196	0.00666	0.98164
0.010	0.00374	0.00388	0.00857	0.00106	0.00190	0.00388	0.01299	0.96397
0.015	0.00555	0.00575	0.01256	0.00159	0.00283	0.00575	0.01902	0.94694
0.020	0.00731	0.00758	0.01639	0.00211	0.00375	0.00758	0.02476	0.93053
0.025	0.00902	0.00936	0.02005	0.00262	0.00465	0.00936	0.03022	0.91471
0.030	0.01070	0.01110	0.02355	0.00313	0.00554	0.01110	0.03543	0.89944
0.035	0.01234	0.01280	0.02691	0.00364	0.00641	0.01280	0.04040	0.88470
0.040	0.01394	0.01446	0.03013	0.00414	0.00727	0.01446	0.04514	0.87046
0.045	0.01550	0.01608	0.03321	0.00464	0.00812	0.01608	0.04967	0.85670
0.050	0.01702	0.01767	0.03617	0.00514	0.00895	0.01767	0.05399	0.84339
0.055	0.01851	0.01922	0.03901	0.00563	0.00977	0.01922	0.05812	0.83051
0.060	0.01997	0.02073	0.04174	0.00611	0.01059	0.02073	0.06207	0.81805
0.065	0.02140	0.02222	0.04436	0.00660	0.01138	0.02222	0.06584	0.80598
0.070	0.02279	0.02367	0.04688	0.00708	0.01217	0.02367	0.09645	0.79429
0.075	0.02415	0.02508	0.04931	0.00755	0.01295	0.02508	0.07291	0.78296
0.080	0.02549	0.02647	0.05164	0.00802	0.01372	0.02647	0.07622	0.77198
0.085	0.02679	0.02783	0.05388	0.00849	0.01447	0.02783	0.07939	0.76132
0.090	0.02807	0.02916	0.05604	0.00895	0.01522	0.02916	0.08243	0.75098
0.095	0.02932	0.03046	0.05813	0.00941	0.01595	0.03046	0.08534	0.74094
0.100	0.03054	0.03173	0.06013	0.00987	0.01668	0.03173	0.08813	0.73119

Table A-12. Equilibrium population for Rb^{87} pumped with $\sigma^+ D_1$ resonance radiation, assuming complete mixing in the excited state.

	$P(m_F)$							
	F = 1			F = 2				
ρ	-1	0	1	-2	-1	0	1	2
0.005	0.00953	0.00479	0.00320	0.00240	0.00320	0.00479	0.00953	0.96256
0.010	0.01820	0.00919	0.00615	0.00462	0.00615	0.00919	0.01820	0.92830
0.015	0.02612	0.01325	0.00888	0.00668	0.00888	0.01325	0.02612	0.89682
0.020	0.03338	0.01702	0.01142	0.00859	0.01142	0.01782	0.03338	0.86779
0.025	0.04004	0.02051	0.01379	0.01038	0.01379	0.02051	0.04004	0.84094
0.030	0.04619	0.02377	0.01600	0.01206	0.01600	0.02377	0.04619	0.81602
0.035	0.05187	0.02681	0.01808	0.01364	0.01808	0.02681	0.05187	0.79285
0.040	0.05713	0.02966	0.02003	0.01512	0.02003	0.02966	0.05713	0.77123
0.045	0.06201	0.03234	0.02187	0.01653	0.02187	0.03234	0.06201	0.75102
0.050	0.06655	0.03486	0.02362	0.01786	0.02362	0.03486	0.06655	0.73208
0.055	0.07079	0.03724	0.02526	0.01912	0.02526	0.03724	0.07079	0.71430
0.060	0.07474	0.03948	0.02683	0.02032	0.02683	0.03948	0.07474	0.69757
0.065	0.07844	0.04161	0.02832	0.02146	0.02832	0.04161	0.07844	0.68180
0.070	0.08190	0.04363	0.02974	0.02255	0.02974	0.04363	0.08190	0.66691
0.075	0.08515	0.04555	0.03109	0.02360	0.03109	0.04555	0.08515	0.65283
0.080	0.08821	0.04737	0.03238	0.02460	0.03238	0.04737	0.08821	0.63949
0.085	0.09108	0.04911	0.03362	0.02555	0.03362	0.04911	0.09108	0.62684
0.090	0.09379	0.05076	0.03480	0.03648	0.03480	0.05076	0.09379	0.61482
0.095	0.09634	0.05235	0.03594	0.02736	0.03594	0.05235	0.09634	0.60339
0.100	0.09875	0.05386	0.03703	0.02821	0.03703	0.05386	0.09875	0.59250

Table A-13. Equilibrium population for Rb^{87} pumped with $\sigma^{+}D_1$ resonance radiation, assuming electron randomization in the excited state.

	$P(m_F)$							
	F = 1			F = 2				
ρ	-1	0	1	-2	-1	0	1	2
0.01	0.00710	0.00597	0.00447	0.00139	0.00274	0.00597	0.01478	0.95758
0.02	0.01364	0.01142	0.00858	0.00271	0.00531	0.01142	0.02792	0.91900
0.03	0.01968	0.01643	0.01235	0.00398	0.00771	0.01643	0.03965	0.88376
0.04	0.02527	0.02105	0.01584	0.00521	0.00998	0.02105	0.05015	0.85146
0.05	0.03096	0.02531	0.01907	0.00638	0.01211	0.02531	0.05959	0.82175
0.06	0.03530	0.02927	0.02208	0.00752	0.01414	0.02927	0.06810	0.79433
0.07	0.03981	0.03295	0.02488	0.00862	0.01606	0.03295	0.07579	0.76895
0.08	0.04402	0.03638	0.02750	0.00968	0.01788	0.03638	0.08276	0.74539
0.09	0.04797	0.03959	0.02996	0.01071	0.01962	0.03959	0.08909	0.72346
0.10	0.05168	0.04259	0.03227	0.01172	0.02129	0.04259	0.09485	0.70301

Table A-14. Equilibrium population for Rb^{85} pumped with $\sigma^{+}D_1$ resonance radiation assuming no mixing in the excited state.

	$P(m_F)$												
	F = 2					F = 3							
ρ	-2	-1	0	1	2	-3	-2	-1	0	1	2	3
0.005	0.00191	0.00144	0.00178	0.00252	0.00427	0.00040	0.00065	0.00087	0.00163	0.00383	0.00878	0.97188
0.010	0.00376	0.00283	0.00350	0.00493	0.00827	0.00080	0.00130	0.00173	0.00321	0.00749	0.01694	0.94522
0.015	0.00554	0.00419	0.00517	0.00724	0.01202	0.00119	0.00192	0.00256	0.00474	0.01098	0.02454	0.91987
0.020	0.00726	0.00551	0.00679	0.00946	0.01554	0.00158	0.00254	0.00338	0.00622	0.01431	0.03162	0.89575
0.025	0.00892	0.00680	0.00836	0.01160	0.01884	0.00196	0.00315	0.00418	0.00767	0.01750	0.03821	0.87278
0.030	0.01053	0.00806	0.00989	0.01365	0.02194	0.00284	0.00374	0.00496	0.00907	0.02055	0.04436	0.85088
0.035	0.01208	0.00928	0.01137	0.01562	0.02486	0.00272	0.00432	0.00572	0.01043	0.02346	0.05010	0.82999
0.04	0.01359	0.01047	0.01281	0.01752	0.02761	0.00309	0.00490	0.00647	0.01175	0.02625	0.05547	0.81004
0.045	0.01504	0.01163	0.01421	0.01934	0.03020	0.00347	0.00546	0.00720	0.01303	0.02893	0.06048	0.79098
0.050	0.01645	0.01276	0.01556	0.02110	0.03264	0.00383	0.00602	0.00792	0.01428	0.03149	0.06517	0.77274
0.055	0.01782	0.01387	0.01689	0.02279	0.03494	0.00420	0.00656	0.00863	0.01549	0.03394	0.06956	0.75529
0.060	0.01915	0.01494	0.01817	0.02442	0.03711	0.00456	0.00710	0.00931	0.01667	0.03629	0.07367	0.73858
0.065	0.02043	0.01600	0.01942	0.02599	0.03917	0.00492	0.00762	0.00999	0.01782	0.03855	0.07752	0.72255
0.070	0.02168	0.01702	0.02063	0.02751	0.04111	0.00527	0.00814	0.01065	0.01844	0.04071	0.08112	0.70719
0.075	0.02289	0.01803	0.02182	0.02897	0.04294	0.00562	0.00865	0.01130	0.02003	0.04279	0.08450	0.69244
0.080	0.02406	0.01900	0.02297	0.03088	0.04408	0.00597	0.00915	0.01194	0.02109	0.04478	0.08768	0.67827
0.085	0.02520	0.01996	0.02409	0.03174	0.04633	0.00631	0.00965	0.01256	0.02212	0.04670	0.09065	0.66466
0.090	0.02631	0.02090	0.02518	0.03305	0.04789	0.00665	0.01013	0.01318	0.02313	0.04854	0.09344	0.65157
0.095	0.02739	0.02181	0.02625	0.03432	0.04937	0.00699	0.01061	0.01378	0.02411	0.05030	0.09607	0.63897
0.100	0.02843	0.02270	0.02729	0.03555	0.05077	0.00733	0.01109	0.01437	0.02507	0.05200	0.09853	0.62685

Table A-15. Equilibrium population for Rb^{85} pumped with $\sigma^{+}D_1$ resonance radiation, assuming complete mixing in the excited state.

	$P(m_F)$												
	F = 2					F = 3							
ρ	-2	-1	0	1	2	-3	-2	-1	0	1	2	3
0.005	0.01381	0.00695	0.00465	0.00349	0.00279	0.00233	0.00279	0.00349	0.00465	0.00695	0.01381	0.93428
0.010	0.02556	0.01297	0.00869	0.00653	0.00523	0.00437	0.00523	0.00653	0.00869	0.01297	0.02556	0.87765
0.015	0.03567	0.01823	0.01224	0.00922	0.00739	0.00617	0.00739	0.00922	0.01224	0.01823	0.03567	0.82835
0.020	0.04444	0.02286	0.01539	0.01160	0.00931	0.00777	0.00931	0.01160	0.01539	0.02286	0.04444	0.78502
0.025	0.05209	0.02699	0.01821	0.01374	0.01103	0.00922	0.01103	0.01374	0.01821	0.02699	0.05209	0.74665
0.030	0.05882	0.03068	0.02075	0.01568	0.01260	0.01053	0.01260	0.01568	0.02075	0.03068	0.05882	0.71242
0.035	0.06478	0.03400	0.02305	0.01744	0.01402	0.01172	0.01402	0.01744	0.02305	0.03400	0.06478	0.68170
0.040	0.07007	0.03702	0.02515	0.01905	0.01533	0.01282	0.01533	0.01905	0.02515	0.03702	0.07007	0.65396
0.045	0.07479	0.03976	0.02708	0.02053	0.01653	0.01384	0.01653	0.02053	0.02708	0.03976	0.07479	0.62879
0.050	0.07902	0.04227	0.02885	0.02190	0.01765	0.01478	0.01765	0.02190	0.02885	0.04227	0.07902	0.60585
0.055	0.08283	0.04457	0.03049	0.02317	0.01868	0.01565	0.01868	0.02317	0.03049	0.04457	0.08283	0.58485
0.060	0.08627	0.04670	0.03201	0.02435	0.01965	0.01647	0.01965	0.02435	0.03201	0.04670	0.08627	0.56555
0.065	0.08938	0.04866	0.03243	0.02546	0.02056	0.01724	0.02056	0.02546	0.03343	0.04866	0.08938	0.54776
0.070	0.09221	0.05049	0.03476	0.02650	0.02142	0.01797	0.02142	0.02650	0.03476	0.05049	0.09221	0.53130
0.075	0.09472	0.05218	0.03600	0.02748	0.02222	0.01865	0.02222	0.02748	0.03600	0.05218	0.09478	0.51602
0.080	0.09712	0.05376	0.03717	0.02840	0.02298	0.01930	0.02298	0.02840	0.03717	0.05376	0.09712	0.50181
0.085	0.09927	0.05525	0.03827	0.02928	0.02371	0.01992	0.02371	0.02928	0.03827	0.05525	0.09927	0.48854
0.090	0.10123	0.05663	0.03931	0.03011	0.02439	0.02050	0.02439	0.03011	0.03931	0.05663	0.10123	0.47614
0.095	0.10303	0.05794	0.04030	0.03090	0.02505	0.02106	0.02505	0.03090	0.04030	0.05794	0.10303	0.46452
0.100	0.10468	0.05917	0.04124	0.03165	0.02568	0.02160	0.02568	0.03165	0.04124	0.05917	0.10468	0.45360

Table A-16. Examples of transient optical pumping signals for an alkali with nuclear spin I = 5/2 and I = 7/2 and $\rho = 0.05$.

I = 7/2				I = 5/2			
No mixing in P state		Complete mixing in P state		No mixing in P state		Complete mixing in P state	
λ	a	λ	a	λ	a	λ	a
1.17137	0.95583	2.00767	0.01278	1.21469	-0.44955	1.98806	0.02027
1.00833	0.04160	1.71327	0.02516	1.08704	0.44649	1.59008	0.04023
0.27759	-0.87730	1.44601	0.03463	0.35033	-0.35580	1.22907	0.05831
1.17781	-0.73523	1.18177	0.04488	1.27016	0.19594	0.87093	0.08229
1.10137	-0.57893	0.91823	0.05776	1.05628	0.01834	0.50992	0.12544
0.69583	0.44668	0.65399	0.07657	1.01612	-0.03292	0.11194	0.35996
0.64446	-0.00286	0.38673	0.11145	0.68570	0.47288	0.00000	0.31351
0.47948	-2.21656	0.09233	0.27794	0.60762	-1.03347		
0.58490	0.50716	0.00000	0.35884	0.43367	0.08739		
1.07240	-0.02198			0.27925	1.28828		
1.03359	0.51153			0.85779	0.16508		
0.81859	-0.09916			0.00000	0.19734		
0.41537	1.11922						
0.23974	1.71166						
0.00000	0.23231						

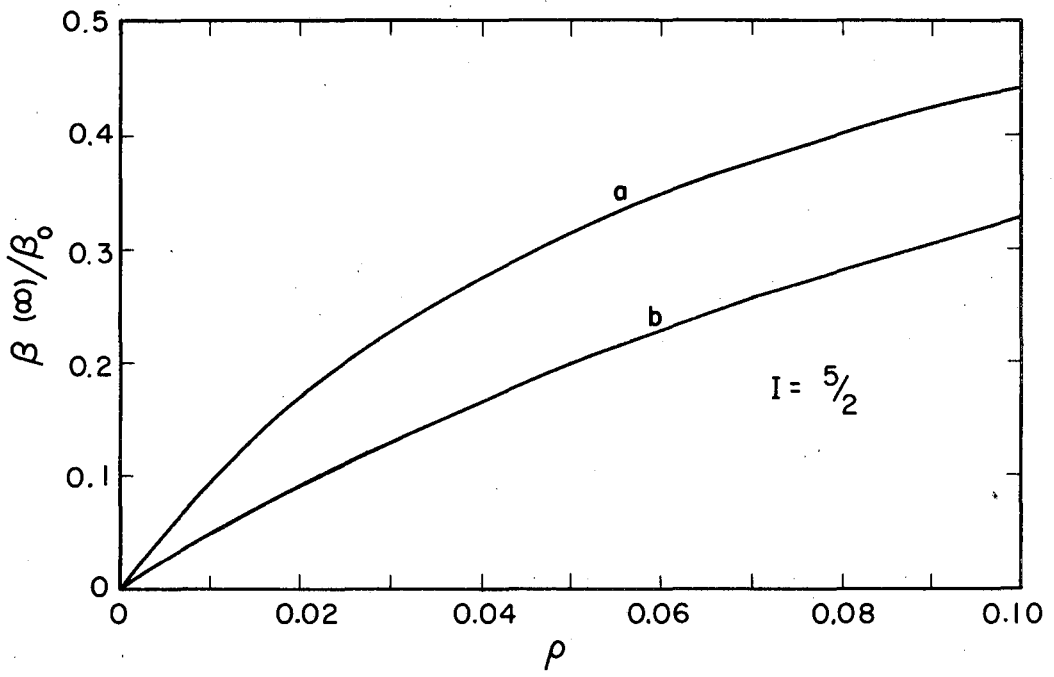

MU-36353

Fig. A-1. Equilibrium absorption probability $\beta(\infty)/\beta_0$ for Rb^{85} optically pumped with circularly polarized D_1 light. Curve a, complete mixing in the $P_{1/2}$ state. Curve b, no mixing in the $P_{1/2}$ state.

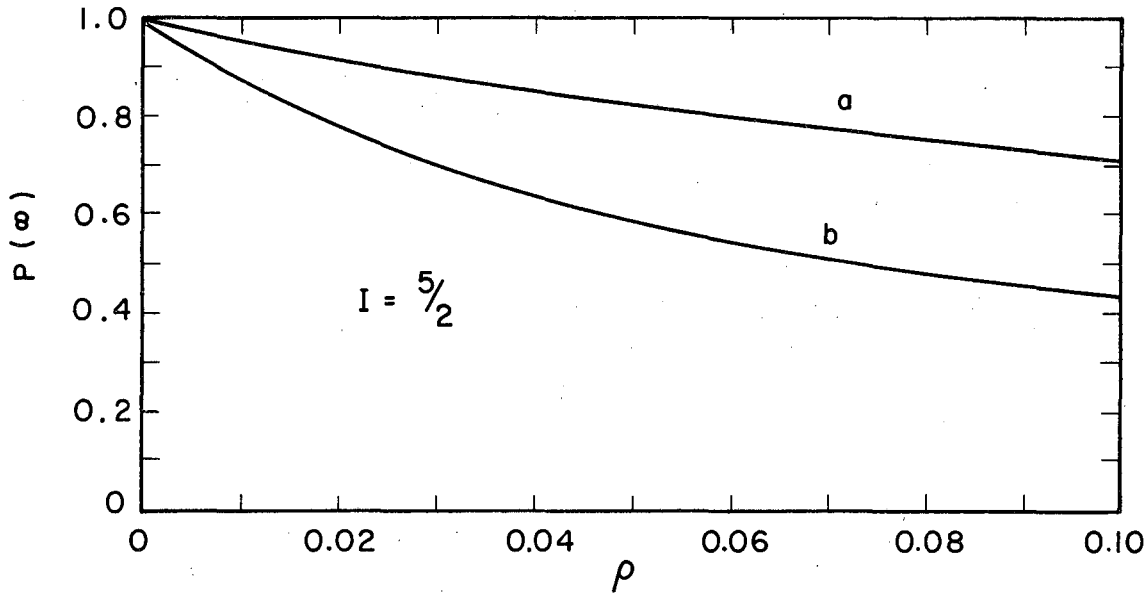

Fig. A-2. Equilibrium polarization of Rb^{85} optically pumped with circularly polarized D_1 light. Curve a, no reorientation in the $P_{1/2}$ state. Curve b, complete mixing in the $P_{1/2}$ state.

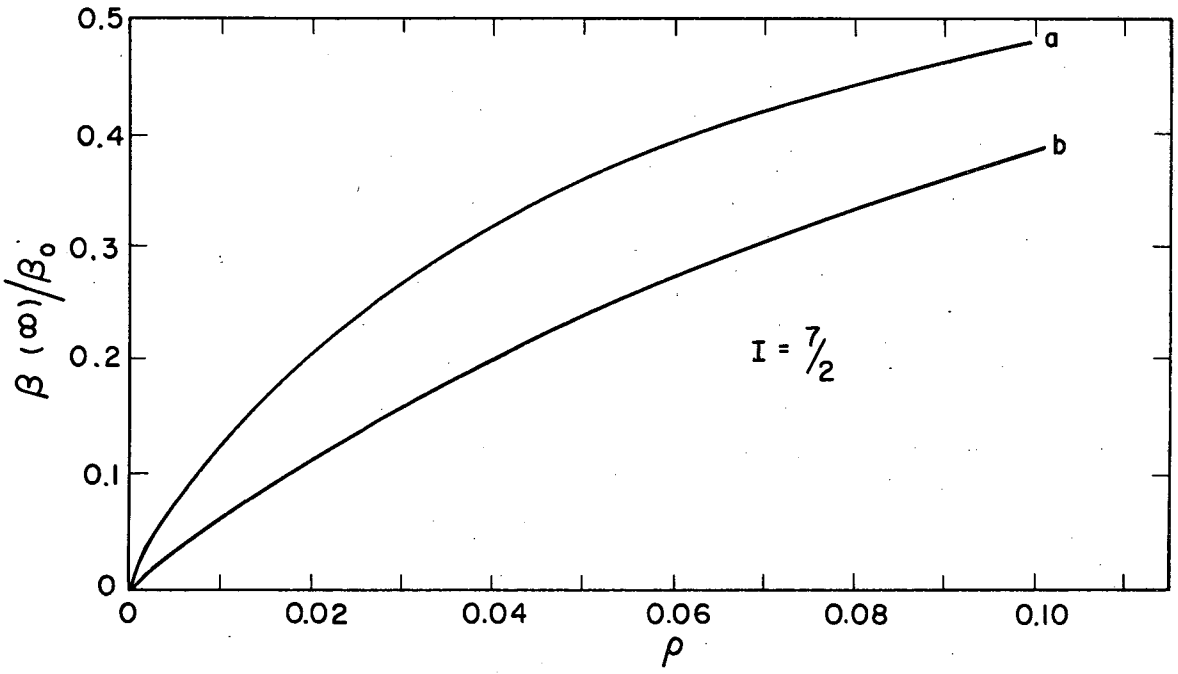

Fig. A-3. Equilibrium absorption probability $\beta(\infty)/\beta_0$ for Cs^{133} optically pumped with circularly polarized D_1 light. Curve a, complete mixing in the $P_{1/2}$ state. Curve b, no mixing in the $P_{1/2}$ state.

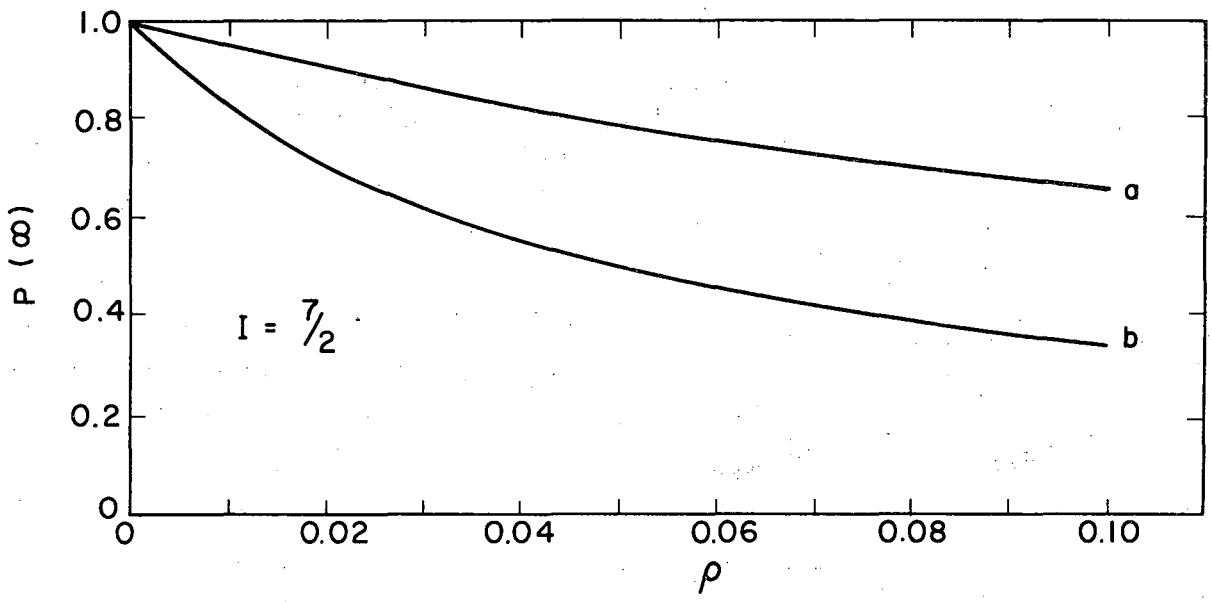

Fig. A-4. Equilibrium polarization of Cs^{133} optically pumped with circularly polarized D_1 light. Curve a, no mixing in the $P_{1/2}$ state. Curve b, complete mixing in the $P_{1/2}$ state.

or since $J = 1/2$,

$$P_{electron} = 2 \sum_{m_F} p(m_F) \sum_{m_J m_I} m_J \left| C(F \tfrac{1}{2} I; m_F m_J m_I) \right|^2 .$$

Similarly

$$P_{nuclear} = [\text{trace}(\rho I_z)]/(m_I)_{max}$$

$$= \sum_{m_F} p(m_F) \sum_{m_J m_I} m_I \left| C(F \tfrac{1}{2} I; m_F m_J m_I) \right|^2 / (m_I)_{max};$$

however, there is no need to calculate both $P_{nuclear}$ and $P_{electron}$ since $\langle F_z \rangle = \langle J_z + I_z \rangle = \langle J_z \rangle + \langle I_z \rangle = (m_J)_{max} P_{electron} + (m_I)_{max} P_{nuclear} = (m_F)_{max} P_{total}$ where $P_{total} = \sum_{m_F} m_F p(m_F)/(m_F)_{max}$. The calculation of the polarization is greatly simplified if we note that $P_{electron} = 1 - \beta$. Electronic and nuclear polarization for Rb^{85} are shown in Fig. B-1.

C. Method of Solution of the Rate Equations

The system to be solved is, in vector form,

$$\dot{\underset{\sim}{p}} + \underset{\approx}{b} \cdot \underset{\sim}{p} = \frac{1}{nT} \underset{\sim}{I}$$

where p_k, $k = 1, 2, \cdots, n$ is the population of the kth state, b_{ij} is the transition rate per unit time via the excited state from state i to state j, T is a relaxation time, and $\underset{\sim}{I}$ is the unit vector ($I_j = 1$, $j = 1, 2, \cdots, n$).

To solve the homogeneous equation we substitute

$$\underset{\sim}{p} = \underset{\sim}{a} e^{-kt},$$

putting

$$-k\underset{\sim}{a}e^{-kt} + \underset{\approx}{b} \cdot \underset{\sim}{a} e^{-kt} = 0 \quad \text{or} \quad (\underset{\approx}{b} - k\underset{\approx}{I}) \cdot \underset{\sim}{a} = 0,$$

where $\underset{\approx}{I}$ is the identity matrix $\underset{\approx}{I}_{ij} = \delta_{ij}$. A nontrivial solution exists if $\det(\underset{\approx}{b} - k\underset{\approx}{I}) = 0$.

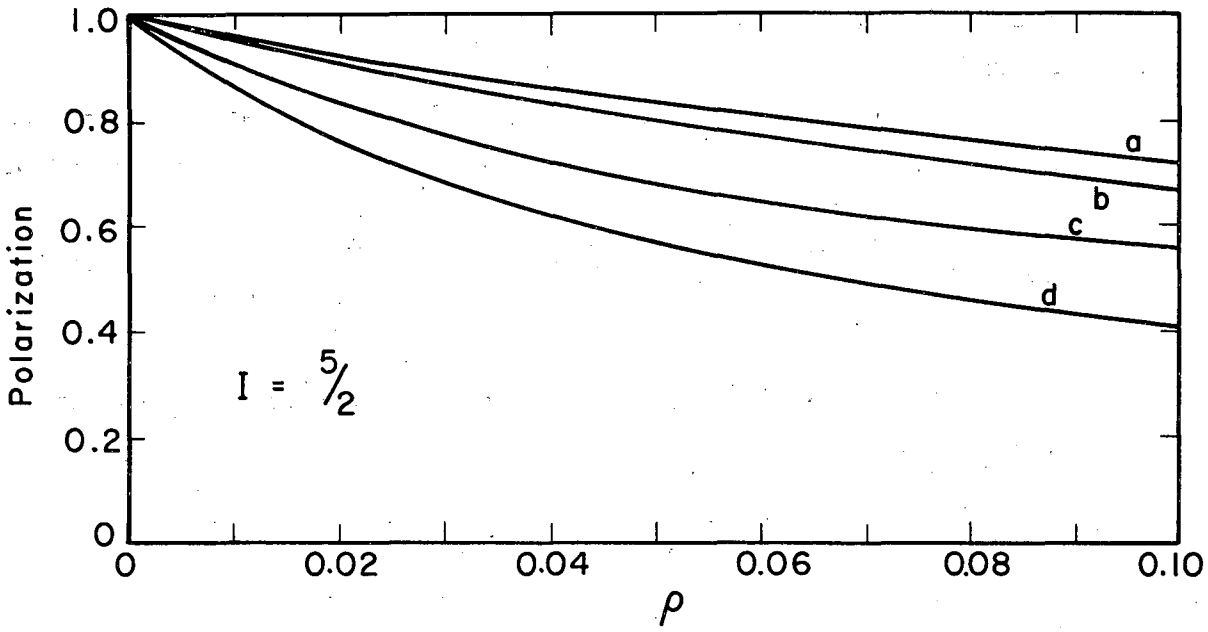

MU-36354

Fig. B-1. Electronic and nuclear polarization for Rb^{85} optically pumped with circularly polarized light. (a) Nuclear polarization with no mixing assumed with the $P_{1/2}$ state. (b) Electronic polarization with no mixing assumed in the $P_{1/2}$ state. (c) Electronic polarization with complete mixing assumed in the $P_{1/2}$ state. (d) Nuclear polarization with complete mixing assumed in the $P_{1/2}$ state.

If the eigenvalues are all distinct the solution of the homogeneous equation will be

$$\underset{\sim}{p} = \sum_{i=1}^{n} a_i \underset{\sim}{a}_i e^{-k_i t}$$

where $\underset{\sim}{a}_i$ is the normalized eigenvector belonging to eigenvalue k_i, and the superposition coefficients a_i are determined by the initial conditions.

If, on the other hand, there is degeneracy among the eigenvalues, eigenvalue k_i having multiplicity γ_i, the solution will be

$$\underset{\sim}{p} = \sum_{i=1}^{\gamma_1} \underset{\sim}{A}_i t^{i-1} e^{-k_1 t} + \sum_{i=1}^{\gamma_2} \underset{\sim}{A}_{i+\gamma_1} t^{i-1} e^{-k_2 t} + \cdots + \sum_{i=1}^{\gamma_n} \underset{\sim}{A}_{i+\gamma_1+\cdots+\gamma_{n-1}} t^{i-1} e^{-k_n t}.$$

For a special solution we make $\underset{\sim}{p}$ = const. = $\underset{\sim}{p}_s$ and upon substitution get

$$\underset{\sim}{\underset{\sim}{b}} \cdot \underset{\sim}{p}_s = \frac{1}{nT} \underset{\sim}{\underset{\sim}{I}} \quad \text{or} \quad \underset{\sim}{p}_s = \frac{1}{nT} \underset{\sim}{\underset{\sim}{b}}^{-1} \cdot \underset{\sim}{\underset{\sim}{I}}.$$

In component form

$$(\underset{\sim}{p}_s)_i = \frac{1}{nT} \sum_{j=1}^{n} b_{ij}^{-1}.$$

The complete solution in which distinct eigenvalues are assumed is then

$$\underset{\sim}{p} = \sum_i a_i \underset{\sim}{a}_i e^{-k_i t} + \frac{1}{nT} \underset{\sim}{\underset{\sim}{b}}^{-1} \cdot \underset{\sim}{\underset{\sim}{I}},$$

and similarly if the eigenvalues are degenerate.

To determine the coefficients a_i we have initially $\underset{\sim}{p}(0) = \frac{1}{n}\underset{\sim}{I}$, hence

$$\frac{1}{8}\underset{\sim}{I} = \sum_i a_i \underline{a}_i = \frac{1}{nT}\,\underset{\sim}{b}^{-1}\cdot\underset{\sim}{I} \qquad \sum_i a_i \underline{a}_i = -\frac{1}{n}\left(\frac{1}{T}\,\underset{\sim}{b}^{-1}\cdot\underset{\sim}{I} - \underset{\sim}{I}\right).$$

If the populations are not equal initially, then

$$\sum_i a_i \underline{a}_i = \underset{\sim}{p}_0 - \frac{1}{nT}\,\underset{\sim}{b}^{-1}\,\underset{\sim}{I}.$$

If a_{ji} denotes the jth component of the ith vector, then

$$\sum_i a_i a_{ji} = \frac{1}{n}\left(1 - \frac{1}{T}\sum_{i=1}^{n} b_{ji}^{-1}\right), \quad j = 1, 2, \cdots, n.$$

The solution of this system is

$$a_i = \frac{\det a^1_{ij}}{\det a}$$

where a^1_{ij} is the matrix formed by replacing the ith column of the matrix a_{ij} by

$$\frac{1}{n}\left(1 - \frac{1}{T}\sum_{j=1}^{n} b_{ij}^{-1}\right), \quad i = 1, 2, \cdots, n.$$

D. Response Time of the Voltage-to-Frequency Converter

We can estimate the effect, on the gross count, of the dead time occurring between application of a voltage and the response of the V-to-f if we assume that the response time τ equals $1/f_{inal}$, where f_{inal} is the final frequency of the V-to-f. If the response of the V-to-f were instantaneous, the gross count between t and $t + \Delta t$ would be

$$\Delta N = \int_t^{t+\Delta t} V(t) f dt = V(t') f \Delta t \quad , \quad t < t' < t + \Delta t.$$

From this we must subtract the count lost in stepping up the voltage from $V(t)$ to $V(t + \Delta t)$. The count lost is

$$\Delta N_L = \left| \int_{\tau(t)}^{\tau(t+\Delta t)} fV(t)\, d\tau \right|$$

and the actual count is $\Delta N_a = \Delta N - \Delta N_L$. Now

$$d\tau = d\left(\frac{1}{fV(t)}\right) = -\frac{dV(t)}{f[V(t)]^2},$$

so

$$\Delta N_L = \left| \int_{V(t)}^{V(t+\Delta t)} \frac{dV(t)}{V(t)} \right| = \left| \frac{\Delta V}{V(t'')} \right|, \quad t < t'' < t + \Delta t$$

and

$$\Delta N/\Delta N_L \approx [V(t')]^2 f/\left(\frac{dV}{dt}\right).$$

It is evident that ΔN_L can become quite large if $V(0) = 0$. In that case $\Delta N_L \to 1$ as $t \to 0$ whereas ΔN itself approaches unity. This is the reason the signal is jacked up on a constant dc voltage V_0, which is a large fraction of the V-to-f range, for then

$$\Delta N_L = \left| \frac{\Delta V}{V_0 + V(t')} \right| << 1.$$

Suppose we are observing a transient $V(t) = V(1-e^{-\lambda t})$ with $\lambda = 1/10$ msec^{-1}, $V = 0.1$, and a sampling time of 1 msec. If $V_0 = 0$, then

$$\frac{\Delta N_L}{\Delta N} \approx \frac{\lambda}{fV} \frac{1}{2(\cosh \lambda t' - 1)} = 10^{-2} \times \frac{1}{2(\cosh t'/10 - 1)},$$

and, for the fifth channel corresponding approximately to 4.5 msec, $\Delta N_L/\Delta N \approx 0.05$ or 5%. The worst case occurs in the first channel where $t' \approx 0.5$ msec; however, there the approximation breaks down because the response time is $\approx 1/10$ sec. The V-to-f is then not able to follow the signal and in all likelihood $\Delta N_L/\Delta N \approx 1$. If instead of $V_0 = 0$ we take $V_0 = 0.9$, then

$$\frac{\Delta N_L}{\Delta N} \approx \frac{V\lambda}{fV_0^2} e^{-\lambda t} \approx 10^{-5} \text{ or } 10^{-3}\%.$$

E. Diffusion Theory of Disorientation

The general features of the relaxation times in optical pumping were accounted for by Franzen on the basis of a diffusion theory. He assumed that disorientation is due to two processes, collisions with the wall and collisions with the buffer gas. Collisions with the wall are inhibited by diffusion and their effect on the polarization is described by a diffusion equation. If n is the number of polarized atoms of Rb^{87}, for example, and D the diffusion coefficient characteristic of the Rb^{87} buffer-gas system, then

$$\frac{\partial n}{\partial t} = D\nabla^2 n$$

if wall collisions alone destroy the polarization. The disorientation due to Rb^{87} buffer-gas collisions is taken into account by adding a sink term $-\sigma N\bar{v}$, where σ is the cross section for disorienting a Rb^{87} atom through collisions with a buffer-gas atom, N is the density of buffer-gas atom, and $\bar{v}$ is the relative mean velocity of the colliding pair. The equation to be solved is then

$$\frac{\partial n}{\partial t} = D\nabla^2 n - \sigma N\bar{v}.$$

Some assumptions must be made about the initial distribution of n and the boundary conditions. It is generally assumed that the density of polarized atoms is uniform initially (when the polarization is in equilibrium due to the action of the pumping light and the relaxation, i.e., before the pumping light is turned off in a Franzen experiment) and that the polarization vanishes at the walls. The last assumption is valid provided the mean free path is very much smaller than the physical dimension of the cell. But the first assumption is strictly true only in an evacuated cell where the diffusion time ($\approx$0.1 msec) is much smaller than the pumping time ($\approx$1 msec), with a conventional pumping source assumed. If a buffer gas is present but the intensity of pumping light is uniform over the cell, the assumption of uniform polarization is still valid. Many experiments reported in the literature involved high alkali densities that resulted in appreciable absorption of the pumping light, in which case the pumping rate becomes a function of the distance through which the light has traveled in the vapor as well as a function of the time, since the transparency of the vapor changes with time. The situation is complex and it is by no means clear that the condition of uniform polarization is satisfied, especially as the diffusion time is on the order of seconds for high buffer-gas pressures. In our experiment low alkali densities are involved (cell temperatures of $\approx 22°C$) and the cross section of the light beam is about the same as that of the cell, so it is possible that both assumptions involved in the solution of the diffusion equation are valid.

In cylindrical coordinates r, ϕ, z, the diffusion equation for a cylindrical cell becomes

$$\frac{\partial n}{\partial t} = D\left(\frac{\partial^2 n}{\partial r^2} + \frac{1}{r}\frac{\partial n}{\partial r} + \frac{\partial^2 n}{\partial z^2}\right) - \sigma N\bar{v},$$

with $n(r, z, 0) = n_0$, $r < a$, $|z| < b$, $n(a, z, t) = 0$, $n(r, \pm b, t) = 0$, where a is the radius of the cylindrical cell and 2b its length L. Separating coordinates, $n(r, z, t) = R(r)Z(z)T(t)$, we get three equations.

$$\frac{1}{T}\frac{dT}{dt} = -\beta^2 = \text{const.}, \qquad \text{(a)}$$

$$\frac{d^2R}{dr^2} + \frac{1}{r}\frac{dR}{dr} + a^2R = 0, \quad a^2 = \text{const.}, \qquad \text{(b)}$$

$$\frac{d^2Z}{dz^2} + \frac{1}{D}(\beta^2 - a^2D - \sigma N\bar{v})Z = 0, \qquad \text{(c)}$$

with $R(r< a)Z(|z| < b)T(0) = n_0$, $R(a)Z(z)T(t) = 0$, and $R(r)Z(\pm b)T(t) = 0$. The solution of (a) is $T(t) = Ae^{-\beta^2 t}$; the solution of (b), which does not vanish on the z axis, is $R(r) = BJ_0(ar)$; and the solution of (c) is $Z(z) = C\cos\sqrt{(\beta^2/D) - a^2 - (\sigma N\bar{v}/D)}\, z$. From the boundary conditions $J(aa)$ equals 0, and $b[\frac{1}{D}(\beta^2 - a^2D - \sigma N\bar{v})]^{-/2}$ equals $(2m-1)\pi/2$, $m = 1, 2, 3, \cdots$. Solving for β^2 and letting $2b = L$, we find that $\beta^2 = D[\{(2m-1)\frac{\pi}{L}\}^2 + a^2] + \sigma N\bar{v}$. The general solution is obtained by summing over m and a,

$$n(r, z, t) = \sum_m \sum_a A_{ma} \exp(-\beta_{ma}^2 t)\, J_0(ar)\cos[2m-1)\,\frac{\pi}{L}z],$$

and A_{ma} is determined from the initial condition. The dominant mode occurs for $m = 1$ and the first zero of the Bessel function $J_0(ar)$. For this mode the polarization decays with a rate

$$\beta_{1a_1}^2 = D[(\frac{\pi}{L})^2 + a_1^2] + \sigma N\bar{v}.$$

Note that D is the diffusion coefficient at buffer-gas density N, and that it is related to the diffusion coefficient at the operating temperature and atmosphere pressure D_0 by $D = D_0(N_0/N)$, where N_0 is the density at the operating temperature and atmosphere pressure. The dependence of the relaxation time $T = 1/\beta_{1a_1}^2$ on buffer-gas density can now be written

$$T = \{D_0N_0[(\frac{\pi}{L})^2 + a_1^2]/N + \sigma N\bar{v}\}^{-1}$$

and some useful relations obtained:

$$T_{max} = \frac{1}{2\sqrt{k D_0 N_0 \bar{\sigma v}}}$$

where $k = (\frac{\pi}{L})^2 + \alpha_1^2$

$$(\Delta N)_{1/2} = 2\sqrt{\frac{3k D_0 N_0}{\bar{\sigma v}}}$$

where $(\Delta N)_{1/2}$ is the width at half maximum of the relaxation curve.

FOOTNOTES AND REFERENCES

1. P. L. Bender, The Effect of Buffer Gas on the Optical Orientation Process in Sodium, (Ph. D. Thesis), Princeton University, 1956 (unpublished).
2. James A. Jordan, Jr., Collision-Induced Mixing in the First Excited States of the Alkalis, (Ph. D. Thesis), University of Michigan, 1964 (unpublished).
3. G. V. Skratskii and T. G. Izyumova, Soviet Physics Usp. (English transl.) 4, 177 (1961).
4. E. U. Condon and G. H. Shortley, The Theory of Atomic Spectra (Cambridge University Press, Cambridge, 1963).
5. For a detailed treatment that takes into account the spectral distribution of the emission line, see W. Heitler, The Quantum Theory of Radiation (Clarendon Press, Oxford, 1954), Sec. 20.
6. W. Franzen, Phys. Rev. 115, 850 (1959).
7. W. Franzen and A. G. Emslie, Phys. Rev. 108, 1453 (1957).
8. This was brought to my attention by Professor W. A. Nierenberg.
9. At the low alkali densities involved in our experiments, the effect of spin exchange on the distribution of the ground-state populations may be ignored.
10. See Allan C. G. Mitchell and Mark W. Zemansky, Resonance Radiation and Excited Atoms (Cambridge University Press, Cambridge, 1934).
11. See Morris Edgar Rose, Elementary Theory of Angular Momentum (John Wiley, New York, 1957), Chapters V and VI.
12. E. R. Andrew, Nuclear Magnetic Resonance (Cambridge University Press, Cambridge, England, 1956).
13. Hans Kopfermann and Hubert Krüger, Z. Physik 103, 485 (1936).
14. The cross section $\sigma_{1/2,\,3/2}$ for Rb in collision with noble gases was recently reported by T. H. Beahn, H. I. Mandelberg, and W. J. Condell, Jr., Bull. Am. Phys. Soc. 10, 459 (1965).

15. The rf is maintained on for longer than the measured relaxation time; however, the $\Delta F = 1$ relaxation rate is not known although there is evidence that it is smaller than the $\Delta F = 0$ relaxation rate.
16. Obtained from S. L. Abbot Company, Los Angeles, California. Paraflint is a saturated hydrocarbon similar to paraffin but having a longer chain and an average molecular weight of 750.
17. H. G. Dehmelt, Phys. Rev. 105, 1487 (1957).
18. For a discussion of the Dehmelt method, see Arnold L. Bloom, Phys. Rev. 118, 664 (1960).
19. The program was adapted by Claudette Rugge of the Lawrence Radiation Laboratory Mathematics and Computing group (Berkeley).
20. Self-spin exchange cannot alter the polarization but does alter the population distribution, in particular, in the limit of $\tau_{exchange} < \tau_{pumping}$, $p_i \sim \exp(-m_i c)$ where c is a constant. See for example L. Wilmer Anderson, Francis M. Pipkin, and James C. Baird, Jr., Phys. Rev. 116, 87 (1959); and L. Wilmer Anderson and Alan T. Ramsey, Phys. Rev. 132, 712 (1963).
21. H. Warren Moos and Richard H. Sands, Phys. Rev. 135, A591 (1964).
22. The vapor pressure of Ba is $<10^{-8}$ mm Hg at 25°C.
23. Varian Associates, Palo Alto, California. See William E. Bell, Arnold L. Bloom, and James Lynch, Rev. Sci. Instr. 32, 688 (1961).
24. The densitometer trace was obtained by John Conway of the Lawrence Radiation Laboratory, Berkeley.
25. The cells were made of three pieces, cylindrical surface and two windows. At the joint between the cylinder and windows the glass was thicker than at other points in the cylinder. The poor conductivity of glass makes this type of construction subject to extreme stress unless great care is taken to heat the cell uniformly. For this reason the cell was not outgassed at as high a temperature as one could attain with a spherical cell limited only by the softening of glass.

26. In practice we find that the Vidar 240A had an inherent noise of about 14 cps, which would limit the sensitivity below the quoted 1μvolt.
27. G. Stephenson, Proc. Phys. Soc. (London) A64, 458 (1951).
28. For an elementary discussion of least squares, see Hugh D. Young, Statistical Treatment of Experimental Data (McGraw-Hill Book Company, Inc., New York, 1962).
29. Ch'en Shang-Yi, Phys. Rev. 58, 1051 (1940).
30. S. M. Jarrett, Phys. Rev. 133, A111 (1964).
31. We should point out here that if the ground state relaxation were by electron randomization then the signal will consist of two exponentials in the limit of zero light intensity. Extrapolation will than yield two relaxation rates which differ by a factor of about 9. This can be seen by noting that the ground state population are governed by the matrix shown in Table II-4 if the relaxation is by electron randomization, where accurate data has been obtained extrapolation of the pumping time has lead to a single relaxation time.
32. Hyatt Gibbs, (Ph. D. Thesis), University of California (Berkeley), 1956 (unpublished).
33. F. A. Franz, Phys. Rev. (to be published), F. A. Franz, Physics Letters 13, 123 (1964).
34. L. Legowski, Journal of Chemical Physics 41, 1313 (1964), and F. A. Franz and E. Liischer, Phys. Rev. 135, A582 (1964).
35. R. Wood and F. Mohler, Phys. Rev. 11, 70 (1918).
36. W. Lochte-Holtgreven, Z. Physik 47, 362 (1928).
37. R. Seiwert, Ann. Physik 17, 371 (1956).
38. G. D. Chapman, L. Krause, and I. H. Brockman, Can. J. Phys. 42, 535 (1964).
39. Except for possible coating of diffusion pump oil.
40. M. A. Bouchiat and J. Brossel, Compt. Rend. 257, 2825 (1963).